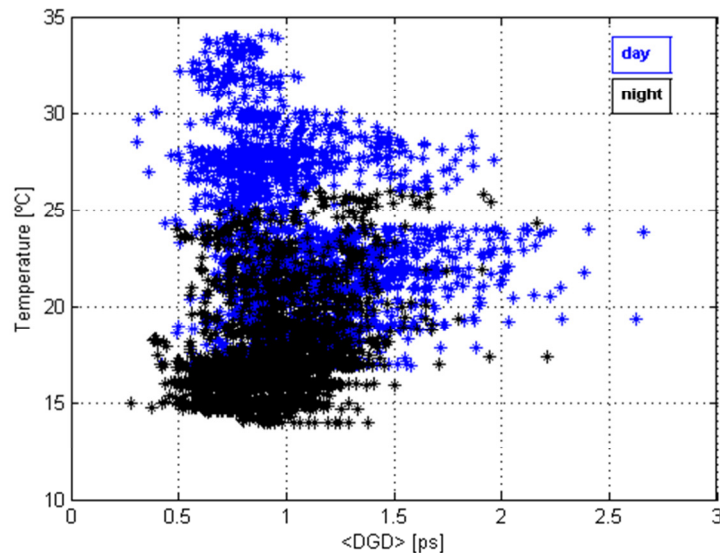


**INSTITUTO SUPERIOR DE ENGENHARIA DE LISBOA**  
**Área Departamental de Engenharia de Electrónica e**  
**Telecomunicações e de Computadores**



## **Ensaaios avançados com fibras ópticas**

### **Advanced characterization of optical fibers**

Alessandro Floris

Licenciado em Engenharia Electrónica

Trabalho Final de Mestrado para Obtenção do Grau de Mestre em Engenharia de  
Electrónica e Telecomunicações

Orientador:

Professor Doutor Manfred Niehus

Júri:

Presidente: Professor Doutor Pedro Renato Tavares de Pinho

Vogais:

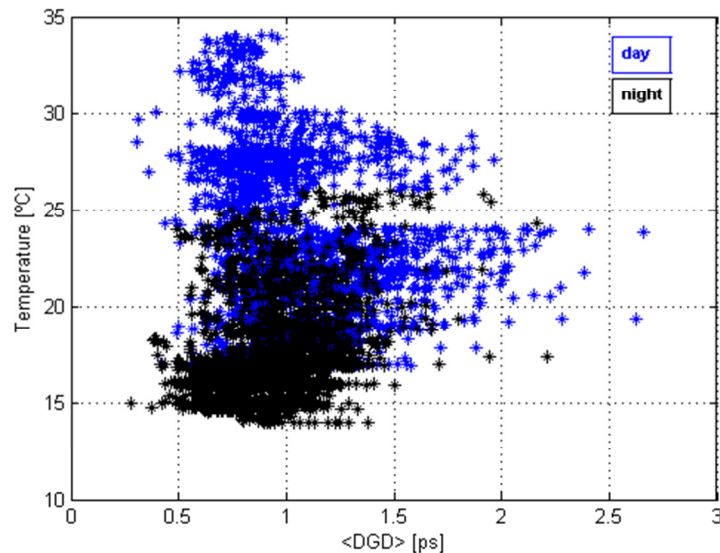
Professor Doutor Paulo Sérgio de Brito André

Professor Doutor Manfred Niehus

**Dezembro de 2014**



**INSTITUTO SUPERIOR DE ENGENHARIA DE LISBOA**  
**Área Departamental de Engenharia de Electrónica e**  
**Telecomunicações e de Computadores**



**Ensaaios avançados com fibras ópticas**  
**Advanced characterization of optical fibers**

Alessandro Floris

Licenciado em Engenharia Electrónica

Trabalho Final de Mestrado para Obtenção do Grau de Mestre em Engenharia de  
Electrónica e Telecomunicações

Orientador:

Professor Doutor Manfred Niehus

Júri:

Presidente: Professor Doutor Pedro Renato Tavares de Pinho

Vogais:

Professor Doutor Paulo Sérgio de Brito André

Professor Doutor Manfred Niehus

Dezembro de 2014



# Abstract

Optical fibers are ubiquitous in the physical layer of modern communication networks, from ultra-long haul transmission to residential access. To cope with the growing bandwidth demand, data rates increase is placing pressure on systems margins. In this scenario, the characterization of optical links calls for advanced measurement methods, in order to properly evaluate overall system performance, capabilities of the network for the current application and for future services upgrades.

In this thesis, we review the methods and technologies adopted for the measurement of spectral attenuation profiles, chromatic dispersion and polarization mode dispersion.

We present results of advanced measurements on single mode optical fibers under laboratory conditions, and fiber links employed under field conditions. For the characterization task, we operate state of the art commercial equipment, implementing the phase shift method for chromatic dispersion measurements, and the fixed analyzer technique for the polarization mode dispersion measurements.

We report and analyse the data collected in deployed optical cables discussing in detail the polarization mode dispersion results, which deviate substantially from the expected maxwellian distribution. We present the so-called “PMD hinge” model, and conclude that this model gives a plausible justification of the observations.

## Keywords

Advanced characterization methods, optical fiber, propagation, attenuation profile, chromatic dispersion, birefringence, polarization mode dispersion, hinge model.

## Resumo

As fibras ópticas estão omnipresentes na camada física das modernas redes de comunicação, desde as transmissões de longo alcance até ao acesso residencial. Para fazer frente ao contínuo aumento das necessidades de largura de banda, o aumento das velocidades de transmissão comprime as margens dos sistemas. Neste cenário, a caracterização das ligações ópticas requer métodos de medida avançados de forma a avaliar devidamente o desempenho do sistema, a capacidade da rede em suportar a aplicação actual ou uma futura actualização de serviços.

Neste trabalho, fazemos uma revisão dos métodos e das tecnologias adoptadas para a medição do perfil de atenuação espectral, da dispersão cromática e da dispersão dos modos de polarização.

Apresentamos os resultados de medidas avançadas em fibras ópticas monomodo em ambiente de laboratório e em ligações utilizadas no campo. Recorrendo a um avançado equipamento comercial, verificamos o perfil de atenuação espectral em cabos ópticos instalados no campo; de acordo com o método do desvio de fase (*phase shift*) medimos a dispersão cromática e, através da técnica do analisador fixo (*fixed analyzer*), avaliamos a dispersão dos modos de polarização.

Reportamos e analisamos os dados recolhidos em cabos ópticos instalados no campo, discutindo em detalhe os resultados referentes à dispersão dos modos de polarização, cuja distribuição de valores se desvia significativamente da esperada distribuição de Maxwell. Apresentamos o modelo de “PMD hinge”, e concluímos que este modelo fornece uma justificação plausível a quanto foi observado.

## Palavras chave

Metodos avançados de caracterização, fibra óptica, propagação, perfil de atenuação, dispersão cromática, birrefringência, dispersão dos modos de polarização, modelo “hinge”.

## **Acknowledgement**

I would like to express my gratitude to Prof. Doc. Manfred Niehus, my supervisor, for all his support and guidance throughout my work.

To have given me plenty of support and collaboration, I also feel indebted to:

Rui Ramos, Marco Besugo and José Nogueira from Espectral Telecomunicações;  
Luís Constantino, Lima Fernandes and Luís Marques from Epoch Telecomsolutions;  
Luís M. Barroca and Rui M. Batista from Portugal Telecom.





# Table of contents

<b>ABSTRACT .....</b>	<b>I</b>
<b>RESUMO.....</b>	<b>II</b>
<b>ACKNOWLEDGEMENT .....</b>	<b>III</b>
<b>TABLE OF CONTENTS .....</b>	<b>V</b>
<b>TABLE OF FIGURES .....</b>	<b>VII</b>
<b>TABLE OF TABLES .....</b>	<b>XI</b>
<b>LIST OF ACRONYMS .....</b>	<b>XIII</b>
<b>LIST OF SYMBOLS.....</b>	<b>XIV</b>
<b>1 INTRODUCTION .....</b>	<b>1</b>
<b>2 SINGLE MODE FIBER PROPERTIES .....</b>	<b>4</b>
2.1 PROPAGATION .....	4
2.2 ATTENUATION AND LOSSES .....	6
2.3 DISPERSION .....	14
2.4 NON-LINEAR EFFECTS .....	22
<b>3 CHARACTERIZATION METHODS.....</b>	<b>24</b>
3.1 ATTENUATION PROFILE.....	24
3.2 CHROMATIC DISPERSION.....	27
3.3 POLARIZATION MODE DISPERSION .....	30
3.4 OPTICAL TIME DOMAIN REFLECTOMETRY.....	35
3.5 MIXED METHODS.....	37
<b>4 CHARACTERIZATION RESULTS.....</b>	<b>41</b>
4.1 OVERVIEW OF MEASUREMENTS .....	41
4.2 CHARACTERIZATION OF ATTENUATION AND LOSSES.....	48
4.3 CHARACTERIZATION OF DISPERSION EFFECTS .....	56
<b>5 DISCUSSION OF RESULTS .....</b>	<b>67</b>
5.1 GENERAL DISCUSSION OF FIELD RESULTS .....	67
5.2 CORRELATION OF PMD AND ENVIRONMENT .....	69
5.3 PMD “HINGE” MODEL .....	77
<b>6 CONCLUSIONS .....</b>	<b>85</b>
<b>APPENDIX .....</b>	<b>87</b>
A. EQUIPMENT LIST.....	87

B. FIBER TYPES (ITU-T STANDARDS).....	88
C. OPTICAL COMMUNICATION STANDARDS.....	91
D. PMD LINK DESIGN VALUE.....	92
E. OPTICAL TELECOM WINDOWS.....	94
<b>BIBLIOGRAPHY.....</b>	<b>95</b>

## Table of figures

Figure 1-1: a) Capacity limit as a function of SNR and b) corresponding maximum spectral efficiency as a function of distance (from [2]).....	2
Figure 2-1: Electric field vectors and intensity profiles of LP modes and conventional modes; intensity profile of transverse electric fields of the same LP mode have the same distribution [8].....	5
Figure 2-2: Wavelength dependency of attenuation coefficient with several physical mechanisms highlighted (after [7]).....	7
Figure 2-3: Fiber designs for reducing bending loss. (a) Reduced MFD design. (b) Depressed cladding design. (c) Trench design. (d) Hole assisted design. (e) Nano-engineered design. (source [12]).....	10
Figure 2-4: Comparison of bending loss characteristics of IBP fibers at 1550 nm (source [12]) .....	11
Figure 2-5: Subscriber Connector (SC) and adapter details (source [14]) .....	12
Figure 2-6: Loss factors in a fiber to fiber connection. (a) Gap between fibers ends; (b) misalignment of tilt; (c) misalignment of offset; (d) mode field mismatch (source [15]) .....	12
Figure 2-7: Loss contribution of a gap between fibers ends.....	14
Figure 2-8: Loss contribution of tilt misalignment.....	14
Figure 2-9: Loss contribution of a misalignment of offset.....	14
Figure 2-10: Loss contribution of fibers' mode field radius mismatch.....	14
Figure 2-11: Total chromatic dispersion D result from material ( $D_m$ ) and waveguide ( $D_w$ ) contributions (source [7]).....	15
Figure 2-12: Time domain effect of birefringence in a short fiber ( [9]) .....	17
Figure 2-13: Graphical representation of the evolution of input SOP $S_0$ in traversing two sections of birefringent fiber (lower inset). After [22] .....	19
Figure 2-14: "Random-walk" of SOP trajectory at a given position z along the link. Locally, the SOP variation with frequency can be described as rotation around vector $\tau$ . .....	20
Figure 2-15: Examples of Maxwellian distributions (left: linear scale; right: logarithm scale).....	21
Figure 3-1: Arrangement for the cut-back method (source [29]) .....	25

Figure 3-2: arrangement for the insertion loss method (source [29]).....	26
Figure 3-3: Setup for the phase shift method (source [20]).....	29
Figure 3-4: Fixed Analyzer setup - (a) tunable laser and power meter combination; (b) wideband source and OSA combination (source [20]).....	31
Figure 3-5: Result of a wavelength scanning and Gaussian fit (source [28]).....	32
Figure 3-6: Arrangement for the Stokes parameter evaluation technique (source [20])	34
Figure 3-7: [left] Interferometric measurement arrangement (source [20]); [right] typical measurement result from a randomly mode coupled fiber (source [31]) .....	34
Figure 3-8: (a) OTDR block diagram (source [20]) and (b) characteristic trace (source [7]) .....	36
Figure 3-9: P-OTDR block diagram (source [35]) .....	40
Figure 4-1: Geographic location of span Lisboa-Setúbal-Lisboa (blue line) .....	43
Figure 4-2: Geographic location of Samora Correia span (exact fiber path is not known) .....	43
Figure 4-3: Geographic location of Alcácer do Sal span (blue line) .....	43
Figure 4-4: Arrangements for: (a) source/module reference; (b) link measurement.....	46
Figure 4-5: Experimental set-up for macrobending losses measurements .....	48
Figure 4-6: Power loss variation according number of wraps around mandrels of different sizes for cabled fibers ( $\lambda = 1550$ nm).....	49
Figure 4-7: Power loss variation according number of wraps around mandrels of different sizes for cabled fibers ( $\lambda = 1490$ nm).....	50
Figure 4-8: Power loss variation according number of wraps around mandrels of different sizes for cabled fibers ( $\lambda = 1310$ nm).....	50
Figure 4-9: Comparison between measured data and ITU-T G.657 specification at 1550 nm .....	51
Figure 4-10: Measurement of connector loss from OTDR trace.....	52
Figure 4-11: Measurement results of SC/APC connector losses at 1310, 1490 and 1550 nm .....	53
Figure 4-12: Attenuation profile (LX link).....	54
Figure 4-13: Attenuation profile (SC link) .....	55
Figure 4-14: Attenuation profile (ALC link).....	56
Figure 4-15: Chromatic Dispersion profile (LX link) .....	57
Figure 4-16: Chromatic Dispersion profile (SC link).....	58
Figure 4-17: Chromatic Dispersion profile (ALC link).....	59

Figure 4-18: Fourier transform result of the PMD measurement of LX link (day 1) as presented in <i>FiberTrace viewer</i> .....	60
Figure 4-19: PMD delay (LX link, day 1) .....	61
Figure 4-20: PMD delay (LX link, day 2) .....	61
Figure 4-21: PMD delay (LX link, day 3) .....	61
Figure 4-22: PMD delay (LX link, whole test) .....	62
Figure 4-23: PMD delay (SC link, day 1) .....	63
Figure 4-24: PMD delay (SC link, day 2) .....	63
Figure 4-25: PMD delay (SC link, day 3) .....	63
Figure 4-26: PMD delay (SC link, day 4) .....	64
Figure 4-27: PMD delay (SC link, day 5) .....	64
Figure 4-28: PMD delay (SC link, whole test).....	65
Figure 4-29: PMD delay (ALC link, day 1) .....	65
Figure 4-30: PMD delay (ALC link, day 2) .....	66
Figure 4-31: PMD delay (ALC link, whole test).....	66
Figure 5-1: AP results for the three measured links .....	68
Figure 5-2: CD results for the three measured links.....	69
Figure 5-3: PMD delay for LX link and temperature reported by Portela and Montijio weather stations .....	71
Figure 5-4: PMD delay for SC link and temperature reported by Montijio weather stations .....	71
Figure 5-5: PMD delay for ALC link and temperature reported by Beja and Montijio weather stations .....	72
Figure 5-6: Relationship between temperature and normalized PMD for LX link.....	72
Figure 5-7: Relationship between temperature and normalized PMD for SC link .....	73
Figure 5-8: Relationship between temperature and normalized PMD for ALC link .....	73
Figure 5-9: Relationship between temperature and PMD for SC link on a day by day basis .....	74
Figure 5-10: Relationship between the variation of PMD and temperature for the LX link .....	75
Figure 5-11: Relationship between the variation of PMD and temperature for the SC link .....	75
Figure 5-12: Relationship between the variation of PMD and temperature for the SC link; details of day 2 .....	76

Figure 5-13: Relationship between the variation of PMD and temperature for the SC link; details of day 3 .....	76
Figure 5-14: Relationship between the variation of PMD and temperature for the ALC link .....	77
Figure 5-15: Histograms of measured PMD for LX, SC and ALC.....	78
Figure 5-16: LX link normalized PMD histograms together with Maxwell and normal distribution fits (linear scale).....	78
Figure 5-17: LX link normalized PMD histograms and Maxwell distribution fit (logarithmic scale).....	79
Figure 5-18: SC normalized PMD histograms together with Maxwell and normal distribution fits (linear scale).....	79
Figure 5-19: SC normalized PMD histograms together with Maxwell distribution fit (logarithmic scale).....	80
Figure 5-20: ALC normalized PMD histogram together with Maxwell and normal distribution fits (linear scale).....	80
Figure 5-21: ALC normalized PMD histograms together with Maxwell distribution fit (logarithmic scale).....	81
Figure 5-22: LX normalized PMD histogram together with Maxwell and Karlsson distribution fits.....	83
Figure 5-23: SC normalized PMD histogram together with Maxwell and Karlsson distribution fits.....	83
Figure 5-24: ALC normalized PMD histogram together with Maxwell and Karlsson distribution fits.....	84
Figure B-1: Dispersion slope for various fiber types .....	89

## Table of tables

Table 2-1: G.657 bend loss specification .....	9
Table 2-2: Commercially available IBP fibers (source [13]) .....	10
Table 2-3: Transmission coefficient relationships for diverse loss mechanism at connector-connector coupling (source [15]).....	13
Table 2-4: Overview of non-linear effects (adapted from [28]).....	23
Table 3-1: Approximation equation according fiber type and spectral region (source [28]) .....	27
Table 3-2: Chromatic dispersion test methods suitability for different link characteristics (adapted from [28]).....	28
Table 3-3: CD-OTDR and Phase shift comparison (source [34]) .....	39
Table 4-1: Links details .....	42
Table 4-2: E8136C OTDR module technical specifications .....	45
Table 4-3: OBS-550 source technical specifications.....	45
Table 4-4: E81MRDISPAP / E81DISPAP AP module specifications.....	46
Table 4-5: E81MRDISPAP /E81DISPAP CD module specifications .....	47
Table 4-6: E81MRDISPAP /E81DISPAP PMD module specifications .....	47
Table 4-7: OBS/ODM characteristics according configuration for each link.....	48
Table 4-8: Attenuation profile, main measured points (LX link).....	54
Table 4-9: Attenuation profile, main measured points (SC link) .....	55
Table 4-10: Attenuation profile, main measured points (ALC link).....	56
Table 4-11: Chromatic dispersion profile, main measured points (LX link) .....	57
Table 4-12: Chromatic dispersion profile, main measured points (SC link).....	58
Table 4-13: Chromatic dispersion profile, Band edges values (ALC link).....	59
Table 4-14: PMD data (LX link, Day 1) .....	61
Table 4-15: PMD data (LX link, Day 2) .....	61
Table 4-16: PMD data (LX link, Day 3) .....	61
Table 4-17: Resume of PMD measurement results (LX link).....	62
Table 4-18: PMD data (SC link, day 1).....	63
Table 4-19: PMD data (SC link, day 2).....	63
Table 4-20: PMD data (SC link, day 3).....	63
Table 4-21: PMD data (SC link, day 4).....	64

Table 4-22: PMD data (SC link, day 5).....	64
Table 4-23: Resume of PMD measurement results (SC link).....	64
Table 4-24: PMD data (ALC link, day 1).....	65
Table 4-25: PMD data (ALC link, day 2).....	66
Table 4-26: Resume of PMD measurement results (ALC link).....	66
Table 5-1: Field measurements resume.....	67
Table 5-2: PMD measurements results resume for the three links.....	77
Table 5-3: Fitting parameters of Normal and Karlsson distributions for the measured data.....	82
Table C-6-1: Optical communications standards, corresponding bit rates and PMD limits.....	91
Table 6-2: Probability associated to the ratio between maximum and mean DGD and corresponding outage probability (adapted from [41]).....	93
Table 6-3: Optical telecom windows.....	94



## List of acronyms

BER	Bit Error Ratio
CATV	Cable TV (Transport)
CD	Chromatic Dispersion
CW	Continuous Wave
CWDM	Coarse Wavelength Division Multiplexing
DGD	Differential Group Delay
DWDM	Dense Wavelength Division Multiplexing
DUT	Device Under Test
FTTx	Fiber To The “X” (Edge, Home, Etc.)
FUT	Fiber Under Test
ITU	International Telecommunications Union
NRZ	Non Return To Zero
ORL	Optical Return Loss
OSA	Optical Spectrum Analyzer
OSNR	Optical Signal To Noise Ratio
PMD	Polarization Mode Dispersion
RZ	Return To Zero
SOPMD	Second Order PMD
WDM	Wavelength Division Multiplexing

## List of symbols

Symbol	Explanation	SI Units
$a$	core radius of a fiber	m
$c$	velocity of light	m/s
$k$	wavenumber	$\text{m}^{-1}$
$n$	refractive index	1
$n_{\text{eff}}$	effective refractive index	1
$r$	radial distance	m
$v_g$	group velocity	m/s
$v_p$	phase velocity	m/s
$A_{\text{eff}}$	effective mode area	$\text{m}^2$
$D_\lambda$	dispersion parameter	ps/(nm km)
$E$	electric field strength	V/m
$L_c$	coherence length	m
NA	numerical aperture	1
$P$	optical power	W
$P_{\text{out}}$	output power	W
$R$	radius of curvature	m
$T$	temperature	K or °C
$T_g$	group delay	s
$V$	normalized frequency	1
$\alpha$	absorption coefficient	$\text{m}^{-1}$
$\beta$	propagation constant	rad/m
$\beta_2$	group velocity dispersion	$\text{s}^2/\text{m}$
$\epsilon_0$	electric permittivity of vacuum	C/Vm
$\epsilon$	relative electric permittivity	1
$\lambda$	optical wavelength	m
$\mu$	relative magnetic permeability	1
$\mu_0$	magnetic permeability of vacuum	$\text{N/A}^2$
$\varphi$	optical phase or phase shift	rad
$\omega$	angular frequency	rad/s, $\text{s}^{-1}$

# 1 Introduction

Optical fiber is the fundamental building block in the physical layer of modern communications networks. The vast majority of worldwide data and voice traffic is transported using optical fibers, interconnected to form a global fiber optic network [1]. The transmission capacity of optical network technology has made dramatic advances over the decades since its introduction in the early 1970s. The later part of the 1990s saw a dramatic increase in system capacity achieved by the introduction of wavelength division multiplexing (WDM), permitting to increase the information carried on a single fiber from a few gigabits per second to over one terabit per second [2].

Shannon determined the capacity  $C$  of memory-less communication channels impaired by additive white Gaussian noise (AWGN); for a given signal-to-noise ratio (SNR) and bit rate  $B$  is:

$$C = B \cdot \log_2\left(1 + \frac{S}{N}\right) \quad (1.1)$$

The application of Shannon's theory to the "optical fiber channel" should hence consider three fundamental physical phenomena in optical fibers: noise, chromatic dispersion, and the Kerr nonlinearity, i.e. the intensity dependence of the refractive index [3]. In the case of the (non-linear) fiber channel, the capacity is limited by noise at low power levels and becomes limited by fiber nonlinearity as power increases [2]. Figure 1-1 shows the theoretical capacity limits, in terms of spectral efficiency, for a standard single mode fiber (S-SMF).

In long-haul optical networks, there has been a great interest and progress in advanced modulation formats for high bit rate systems, to overcome fiber optic communications systems impairments. Beyond dispersion, loss and non-linear effects, it has been found that polarization mode dispersion (PMD) is a major concern for 40 and 100 Gb/s systems [4]. This effect causes pulse broadening because light travels at different velocities depending on its polarization. With a shorter bit duration, 25 ps at 40 Gb/s and 10 ps at 100 Gb/s, compared to 100 ps at 10 Gb/s, the tolerance to PMD decreases by a factor of four and ten, respectively. This is one of the primary motivations for research towards alternative modulations formats beyond conventional on-off keying (OOK), as a means of overcoming the adverse effects of PMD [4].

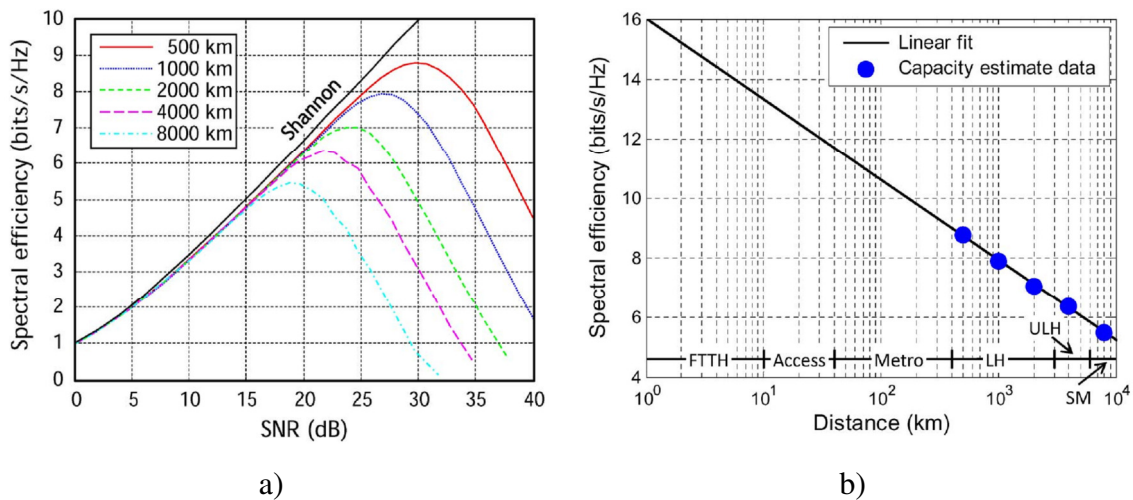


Figure 1-1: a) Capacity limit as a function of SNR and b) corresponding maximum spectral efficiency as a function of distance (from [2])

New developments continue to enhance transmission bit rates (100G is today's reality and field trials have already reported 400G transmission [5]).

However, each step forward in data rates places pressure on system margin. More demand on networks means more demand on optical fiber. At the same time, most operators look to re-utilize the existing fiber infrastructure, and to avoid investing large amounts in new systems. This requires a comprehensive verification of the existing fiber plant and an evaluation of all the fiber impairments, in order to proceed to the data rate upgrade and guarantee reliable operation. Moreover, fiber is enlarging its network footprint, now serving also consumer and businesses. The emergence of Fiber To The Home (FTTH) networks has encouraged the development of fibers showing impressive bending performance, and can handle much harsher environments than the standard ones encountered in long-distance networks.

Careful verification of installed fiber needs to be accomplished in order to verify that the installation is done properly and the services can be turned on. Fiber characterization and in-field measurements turn out to be of vital importance.

Polarization Mode Dispersion (PMD) testing is becoming essential in the fiber characterization process, but still one of the most difficult impairments to evaluate, due to its sensitivity to environmental conditions.

A full set of advanced instruments and techniques is available to help accomplishing network verification tasks.

**Organization of the thesis**

The thesis is organized as follows

The current chapter 1 introduces into and motivates the use of advanced optical fiber characterization techniques.

In chapter 2, fundamental single mode fiber (SMF) characteristics such as optical attenuation and losses sources, chromatic dispersion are presented; particular attention is paid to polarization mode dispersion.

In chapter 3, fiber characterization methods, according to ITU (International Telecommunication Union) recommendations are presented in detail.

Chapter 4 is dedicated to the presentation of the performed measurements; equipment details and link characteristics, together with the presentation of the collected raw data.

In chapter 5, results are then discussed and analyzed in detail.

Chapter 6 is dedicated to the thesis conclusions and suggestions for future work.

## 2 Single mode fiber properties

The low-loss property of optical fibers allows signals to be transmitted over long distances at high data rates before amplification and/or regeneration is required. Nevertheless, optical fibers impose physical limitations that must be taken into account in network design.

Three phenomena mainly determine fiber transmission limits: loss, dispersion, and nonlinear effects.

### 2.1 Propagation

Like all electromagnetic phenomena, light propagation in optical fibers is governed by Maxwell's equations. The propagation is specified describing the evolution of the associated electric and magnetic fields vectors in space and time and is ruled by the frequency domain vector field wave equations (2.1) and (2.2) [6]:

$$\nabla^2 \tilde{\mathbf{E}} + \frac{\omega^2 n^2}{c^2} \tilde{\mathbf{E}} = 0 \quad (2.1)$$

$$\nabla^2 \tilde{\mathbf{H}} + \frac{\omega^2 n^2}{c^2} \tilde{\mathbf{H}} = 0 \quad (2.2)$$

where  $c$  is the speed of light,  $n$  is the refractive index of the material medium supporting the electromagnetic field, and  $\omega$  is the angular frequency of the propagating wave; equation (2.1) and (2.2) actually represents six equations, one for each spatial component of the corresponding field vector. The symbols  $\tilde{\mathbf{E}}$  and  $\tilde{\mathbf{H}}$  represent the Fourier transform of the spatial distribution of the electric and magnetic fields, i.e.

$$\tilde{\mathbf{E}} = \tilde{\mathbf{E}}_{(r,\omega)} = \int_{-\infty}^{\infty} \mathbf{E}_{(r,t)} \exp(i\omega t) dt \quad (2.3)$$

and equivalent for the magnetic field.

In the time domain eq. (2.1) and (2.2) become [7]:

$$\nabla^2 \mathbf{E} + \frac{n^2}{c^2} \frac{\partial^2 \mathbf{E}}{\partial t^2} = 0 \quad (2.4)$$

$$\nabla^2 \mathbf{H} + \frac{n^2}{c^2} \frac{\partial^2 \mathbf{H}}{\partial t^2} = 0 \quad (2.5)$$

The fields in the core and in the cladding must satisfy the wave equations and are related by boundary conditions at the interface; all possible solutions produce a fiber mode. The light energy propagating in the fiber will be divided among the modes supported by the fiber, and since the modes travel at different speeds, the energy in a narrow pulse at the input of a piece of fiber will be spread out at the output. Thus it is desirable to design the structure in a way that it supports only a single mode. Such a fiber is designated single-mode fiber, and the mode that it supports is a  $HE_{11}$  mode referred as the fundamental mode. The notation  $LP_{mn}$  is often used to indicate linearly polarized modes, which are approximate solutions of the wave equation. The fundamental mode  $HE_{11}$  corresponds to the  $LP_{01}$  mode.

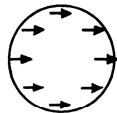



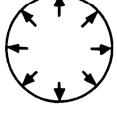



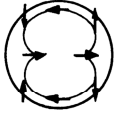

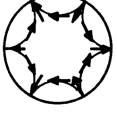

LP-mode designations	Traditional designations	Electric field distribution	Intensity distribution of $E_x$
$LP_{01}$	$HE_{11}$		
$LP_{11}$	$TE_{01}$		
	$TM_{01}$		
	$HE_{21}$		
$LP_{21}$	$EH_{11}$		
	$HE_{31}$		

Figure 2-1: Electric field vectors and intensity profiles of LP modes and conventional modes; intensity profile of transverse electric fields of the same LP mode have the same distribution [8].

In order to obtain single mode propagation, the wavelength  $\lambda$  must satisfy the following condition (valid for step-index profiles)

$$V = \frac{2\pi}{\lambda} a \sqrt{n_{co}^2 - n_{cla}^2} < 2.045 \quad (2.6)$$

where  $a$  is the core radius and  $n_{co}$  and  $n_{cla}$  are the refractive indexes of core and cladding, respectively. The smallest wavelength that satisfies (2.6) sets the boundary between single and multimode propagation, and is referred as cutoff wavelength  $\lambda_c$ .

For S-SMF (G.652), the fiber cutoff wavelength cannot be above 1260 nm.

## 2.2 Attenuation and losses

The amount of losses plays an important role in the power budget in any optical system. The total loss is due to the contribution of all the components included in the system, like the fiber itself and the optical connectors, but can be influenced also by the deployment conditions. The diffusion of optical fiber in the access network and the necessity to reduce equipment space, forces the accommodation of fiber and components into small enclosures; excessive bend results in additional loss due to “leakage” of power out of the fiber core into the cladding.

### Fiber attenuation

The output power  $P_{out}$  of a signal propagating through an optical fiber for a distance  $z$ , is related to the input power  $P_{in}$  by

$$P_{out} = P_{in} e^{-\alpha z} \quad (2.7)$$

the parameter  $\alpha$  represents the fiber attenuation and its dimension are the inverse of distance, typically expressed in  $\text{Neper}\cdot\text{m}^{-1}$ ; when specified in  $\text{dB}\cdot\text{km}^{-1}$ , the value is approximatively 4.343 times the attenuation coefficient in  $\text{Neper}\cdot\text{m}^{-1}$ . The optical power decays exponentially with propagation distance.



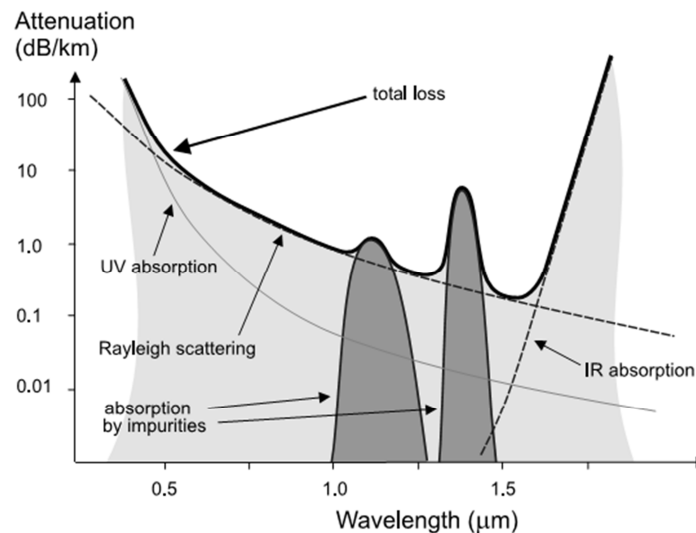


Figure 2-2: Wavelength dependency of attenuation coefficient with several physical mechanisms highlighted (after [7])

Multiple contributions do exist to the overall attenuation coefficient that arise from material properties as well as attenuation mechanisms associated with fiber fabrication (preform development, drawing conditions). Losses are strongly dependent on the optical wavelength as shown in Figure 2-2.

Intrinsic propagation losses in optical fibers have various origins. The material has some intrinsic absorption; silica fibers increasingly absorb light when the wavelength gets longer than approximately 1.7  $\mu\text{m}$ . Absorption peaks can result from impurities, as is the case around 1.24  $\mu\text{m}$  and 1.39  $\mu\text{m}$  if the core material is not water-free. At short wavelengths, Rayleigh scattering becomes important; the contribution of Rayleigh scattering to the attenuation coefficient scales with the inverse fourth power of the wavelength. The third window is in the transition point; close to 1.6  $\mu\text{m}$  the contribution from infrared resonances overtakes the Rayleigh contribution.

Increased scattering losses can result from irregularities of the core/cladding interface. This problem is more severe for fibers with large refractive index contrast (high numerical aperture NA). Therefore, low-loss single-mode fibers for long-haul data transmission are made with relatively small NA, even though a higher NA would provide a more robust guidance.

Typical attenuation coefficient for S-SMF (e.g. Corning SMF-28) is very close to 0.2 dB/km at 1550 nm and 0.30 dB/km at 1310 nm.

## Bending losses

Optical fibers need to be bent for various reasons both when deployed in the field and particularly within equipment; also, accidental excessive bending may occur during installation in harsh environments.

The bend radius of standard single mode fiber must not exceed few centimeters in order to keep the bending loss low. Bending losses are wavelength dependent; attenuation at 1550 nm is higher than at 1310 nm for the same bend radius.

Bend losses are classified in microbends (microscopic bend of the fiber axis) and macrobends (curvature radius large compared to the fiber diameter). While the first are typically related to manufacturing processes, the second are dependent on cable/fiber installation. Typically, macrobend losses are negligibly small under normal conditions, but increase rapidly once a certain critical curvature radius  $R_c$  is reached, so care must be taken during deployment and especially within equipment. The ITU-T standards specify that the additional loss at 1550 nm due to bending must be in the range 0.5-1 dB, depending on the fiber type, for 100 turns of fiber wound with a radius of 37.5 mm. Thus, a bend with a radius of 4 cm results in losses of less than 0.01 dB.

The critical radius is dependent on the particular fiber's design, but can be estimated, for a standard single-mode fiber (S-SMF), as [9]:

$$R_c \cong \frac{20\lambda}{(n_{co} - n_{cla})^2} \left( 2.748 - 0.996 \frac{\lambda}{\lambda_c} \right)^{-3} \quad (2.8)$$

where  $n_{co}$  and  $n_{cla}$  are the refractive indexes of core and cladding,  $\lambda$  is the considered wavelength and  $\lambda_c$  is the cutoff wavelength<sup>1</sup>. For a standard G.652 fiber,  $R_c$  is close to 30 mm.

To address high-density applications and in particular to overcome the harsh laying conditions typical of inside and outside FTTx installations, many manufacturers have introduced improved bend performance (IBP) fibers with enhanced macrobend characteristics. The ITU-T G.657 recommendation identifies two classes of "bending-loss insensitive single-mode optical fibre and cable for the access network". Category A

---

<sup>1</sup> Fiber cut-off wavelength  $\lambda_c$  is measured over 2 meters of uncabled primary-coated fiber, with one loop of 140 mm radius loosely constrained, with the rest of the fiber kept straight [18].

defines bend-improved fibers and their insertion loss requirements for curvature radius down to 7.5 mm (0.5 dB for one turn, subcategory A2), together with the necessity to maintain backward compatibility to G.652.D recommendation. Category B specifies requirements for bending radius down to 5.0 mm (0.15 dB for one turn), but does not require backward compatibility to previous recommendations; also, category B is indicated as appropriate only for short reach distances (less than 1000 m).

ITU-T states that “Although modelling results on various fibre types have been published, no generally applicable bending loss model is available to describe the loss versus bend radius behaviour”.

	radius (mm)	No. of turns	Max. @ 1550 nm [dB]	Max. @ 1625 nm [dB]
G.657.A1	15	10	0.25	1.0
	10	1	0.75	1.5
G.657.A2	15	10	0.03	0.1
	10	1	0.1	0.2
	7.5	1	0.5	1.0
G.657.B2	15	10	0.03	0.1
	10	1	0.1	0.2
	7.5	1	0.5	1.0
G.657.B3	10	1	0.03	0.1
	7.5	1	0.08	0.25
	5	1	0.15	0.45

Table 2-1: G.657 bend loss specification

The simplest way to reduce the bending loss of a fiber is to increase the refractive index difference between the core and the cladding; on the other hand this affects other key optical attributes like mode field diameter<sup>2</sup> (MFD), cut-off wavelength and chromatic dispersion. MFD difference between fibers increases splice and connectors losses. In general, the common feature of bend insensitive fibers (BIFs) profiles is a depressed-index area, or a trench, that is added in the cladding close to the step-index core. The trench confines the tail of the fundamental LP mode without modifying its intrinsic nature; as a consequence, bend losses can be reduced [10].

<sup>2</sup> The mode field diameter is defined as the diameter of the irradiance distribution in a single-mode fiber, measured at the point where the irradiance falls to  $1/e^2$  times the irradiance at the center of the core.

Several fiber structures have been proposed to increase bend resilience while maintaining the necessary S-SMF compatibility; from typical step-index profile, with increased refractive index difference between core and cladding, to more complex structures like trench index-profile and the hole-assisted fiber (HA-SMF), or the recent NanoStructure™ technology [11], all answer to the bending problem with different degrees of performance (Figure 2-4) and compatibility with the previous standards. Figure 2-3 illustrates the mentioned structures. Besides NanoStructure™, all other fiber technologies are commercially available; a list is provided in Table 2-2.

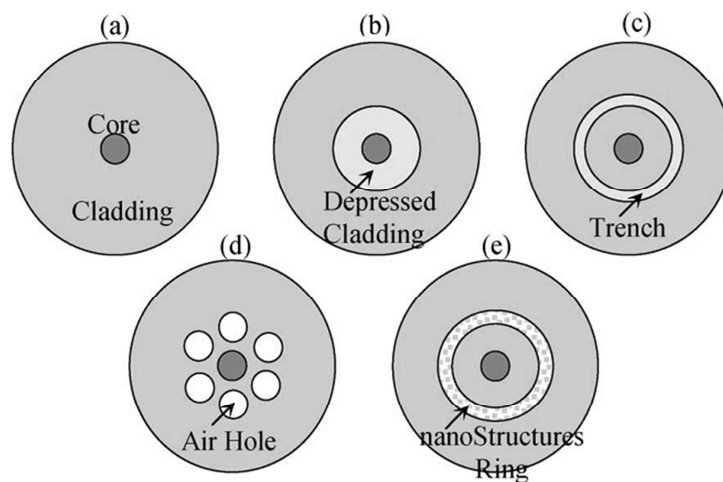


Figure 2-3: Fiber designs for reducing bending loss. (a) Reduced MFD design. (b) Depressed cladding design. (c) Trench design. (d) Hole assisted design. (e) Nano-engineered design. (source [12])

Design	Producer	G657A1	G657A2	G657B2	G657B3
Tall / thin core	Sumitomo	Pure Access			
	Corning	ClearCurve XB			
	OFS	AllWave FLEX			
	Prysmian	CasaLite			
Trench only	Sumitomo				PureAccess-R5
	Draka	Bendbright	Bendbright-XS		Bendbright-Elite
	Corning		ClearCurve LBL		
Trench & ring	Corning				ClearCurve ZBL
	OFS				EZ-Bend
Voids	Prysmian			CasaLite-Plus	CasaLite-Xtreme

Table 2-2: Commercially available IBP fibers (source [13])

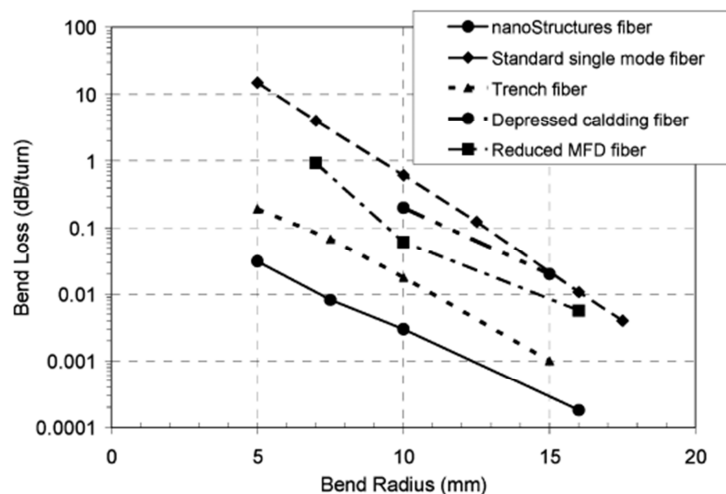


Figure 2-4: Comparison of bending loss characteristics of IBP fibers at 1550 nm (source [12])

## Connector losses

Optical fibers require numerous fiber connections. Although splicing is largely adopted, use of reliable connectors provides numerous advantages in terms of flexibility. Mated connectors, besides offering a stable mechanical joint, must be able to provide a good optical coupling; best coupling is normally achieved by physical contact (PC) of the involved connectors end faces.

Fiber-optic connectors contain a ferrule, which accommodates the fiber end and allows exact positioning. They are attached one to the other by means of a coupler with a sleeve (adapter). A complete connection consists of the combination connector/coupler/connector. The two ferrules, present on the fiber ends, must connect as precisely as possible inside the coupler to minimize loss of light and its reflection (return loss); for this reason they are normally spring-loaded, to keep them pressed together. The extremely small fiber core dimension demands for the highest mechanical and optical precision, requiring tolerances in the order of few tenths of micrometer.

ITU-T L.36 recommendation defines four grades of attenuation performance, with the lowest (Grade D) having a maximum insertion loss of 1.0 dB (0.5 dB typical). Insertion loss is defined as the measurement of the amount of optical power lost through a mated connector pair. L.36 also defines return loss grades, from 1 to 4, being the grades 2, 3 and 4 referred to the PC (non-angled) end face finish, while the grade 1 is referred to angled physical contact (APC) polishing.

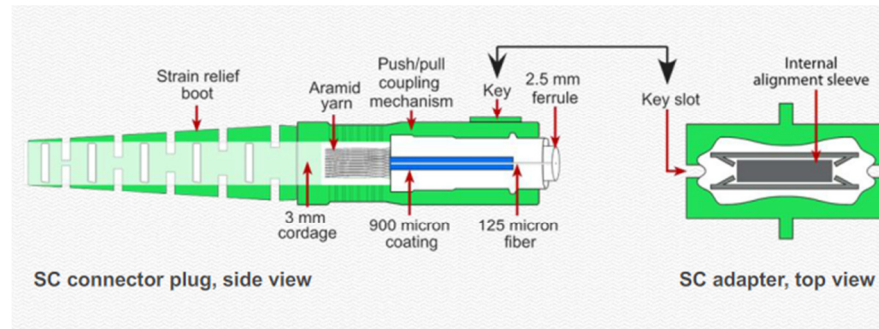


Figure 2-5: Subscriber Connector (SC) and adapter details (source [14])

The loss mechanisms present in a fiber to fiber coupling (e.g. splice) is also detectable at connector-connector coupling. The sources of optical degradation of an optical connection are primarily determined by non-correct alignment of fiber cores, as depicted in Figure 2-6; additionally, incorrect mating (e.g. one or both connectors not properly plugged into the adapter) and contamination (e.g. dust) affect performance in a severe way.

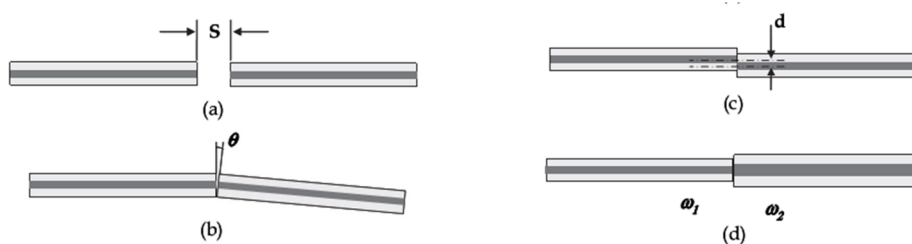


Figure 2-6: Loss factors in a fiber to fiber connection. (a) Gap between fibers ends; (b) misalignment of tilt; (c) misalignment of offset; (d) mode field mismatch (source [15])

The misalignment might be due to a gap  $s$  between fibers, a tilt misalignment  $\theta$ , a lateral offset  $d$  or a MFD mismatch and all their possible combinations. Insertion loss mainly depends on lateral offset between cores and angular offset. Defined a transmission coefficient  $T$ , which is the ratio of transmitted light power to incident light power at the fiber connection [15], transmission loss equations can be defined for each source of loss mechanism as summarized in Table 2-3.

Loss mechanism	Transmission coefficient	Equation reference
gap $S$ between fiber ends	$T_{gap} = \left[ \left( \frac{\lambda S}{2\pi n \omega^2} \right)^2 + 1 \right]^{-1}$	(2.9)
tilt misalignment $\theta$	$T_{\theta} = \exp \left[ \frac{-(\pi n \theta \omega)^2}{\lambda^2} \right]$	(2.10)
offset misalignment $d$	$T_{offset} = \exp \left[ -\frac{d^2}{\omega^2} \right]$	(2.11)
fields mismatch	$T_{\omega} = \left( \frac{2\omega_1\omega_2}{\omega_1^2 + \omega_2^2} \right)^2$	(2.12)

Table 2-3: Transmission coefficient relationships for diverse loss mechanism at connector-connector coupling (source [15])

In the relationships of Table 2-3,  $\omega$  represents the mode field radius,  $n$  is the refractive index of the medium between fiber ends (typically air). The effective mode field radius  $\omega$  (half of the MFD) can be approximated as [16]:

$$\omega \cong a \left( 0.65 + \frac{1.619}{V^{1.5}} + \frac{2.879}{V^6} \right) \quad (2.13)$$

where  $V$  is the normalized spatial frequency.

The contribution of an air gap is showed in Figure 2-7. PC connectors and advances in the end face cleaving and mechanical mechanism inside the connector, normally avoid or reduce air gaps to few micrometers.

In the case of tilt misalignment  $\theta$ , as visible in Figure 2-8, very few degrees of tilt introduce important losses. Ferrule cleaving is of paramount importance to avoid tilt misalignment.

As shown in Figure 2-9, offset misalignment introduces important losses; very small offset compromise connector mating quality.

The MFD tolerance in G.652 fibers is  $\pm 0.6 \mu\text{m}$  [17]; considering a worst case, maximum mode field radius mismatch can reach  $0.6 \mu\text{m}$ . As can be seen from Figure 2-10, the contribution is well below 0.1 dB.

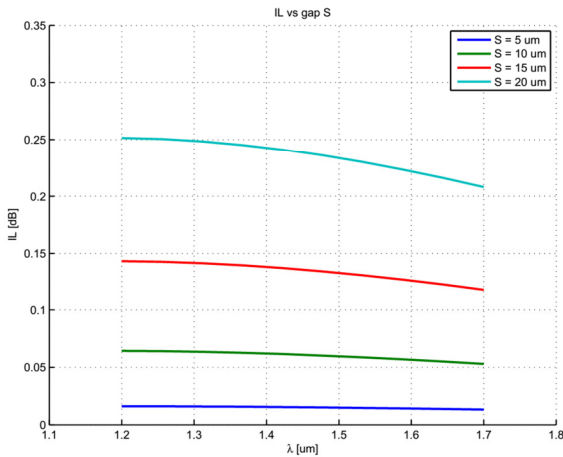


Figure 2-7: Loss contribution of a gap between fibers ends

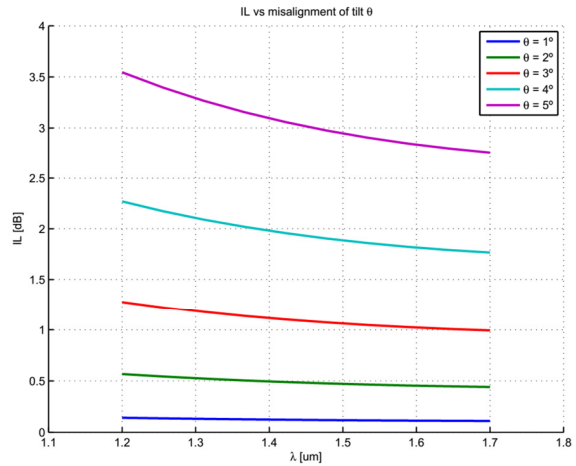


Figure 2-8: Loss contribution of tilt misalignment

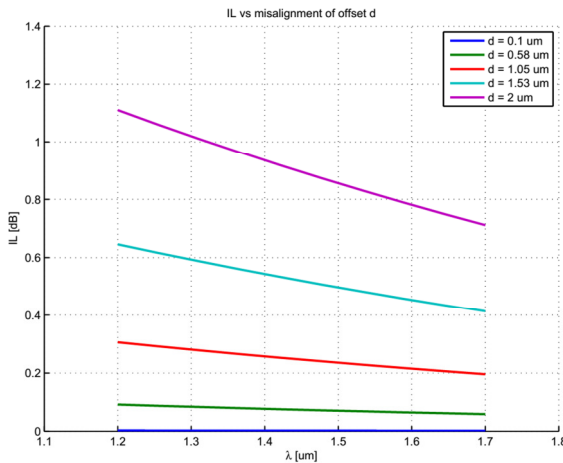


Figure 2-9: Loss contribution of a misalignment of offset

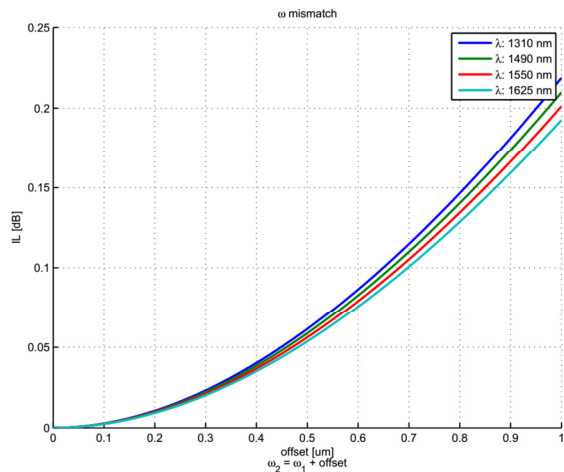


Figure 2-10: Loss contribution of fibers' mode field radius mismatch

## 2.3 Dispersion

Dispersion is the name given to any effect wherein different components of the transmitted signal travel at different velocities in the fiber, arriving at different times at the receiver. Its effect is to broaden light pulses, provoking inter symbol interference, and consequently limiting the maximum bit rate and/or link length.



## Chromatic dispersion

Chromatic (or intramodal) dispersion is determined by the fiber's material composition, structure and design, and by the light source operating wavelength and spectral width. Chromatic dispersion manifests through the frequency dependence of the refractive index  $n_{(\omega)}$  [18], provoking propagation delay differences between the different spectral components of the transmitted signal, travelling at different speeds ( $c/n_{(\omega)}$ ) [18].

The delay difference is the result of two different contributions<sup>3</sup>, namely [19]:

- Material dispersion  $D_m$ : arises directly from the wavelength dependence of the refractive index;
- Waveguide dispersion  $D_w$ : optical power is partitioned between core and cladding, with a wavelength-dependent distribution; as the wavelength is varied, we have a crossover from mostly core index to mostly cladding index, resulting in a contribution to the wavelength dependence of the effective index.

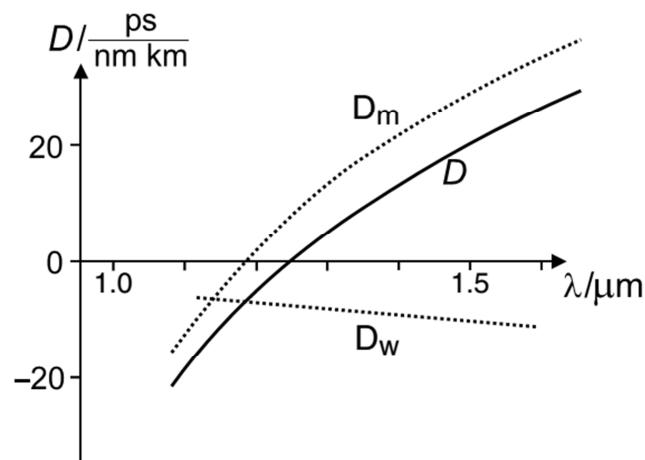


Figure 2-11: Total chromatic dispersion  $D$  result from material ( $D_m$ ) and waveguide ( $D_w$ ) contributions (source [7])

<sup>3</sup> Core and cladding indexes do not vary at the same rate with wavelength, so their difference is also wavelength-dependent. This provokes another contribution which, however, is often much smaller than material and waveguide dispersion [7]

Mathematically, the overall effects of fiber dispersion are accounted for by expanding the mode-propagation constant  $\beta$  in a Taylor series around a central frequency  $\omega_0$  [18].

The first derivative of the propagation constant gives the velocity at which a pulse propagates and is called the group velocity. The key parameter governing the evolution of pulse shape is the second derivative of the propagation constant, which is related to the rate of change of the group velocity with frequency, and is called group velocity dispersion (GVD). It is defined as [19]:

$$\beta_2 = \frac{d^2\beta}{d\omega^2} \quad (2.14)$$

In the absence of chromatic dispersion,  $\beta_2$  is equal to zero, and all pulses would propagate without change in shape. In general  $\beta_2$  is not null.

For most optical fibers, there is a zero-dispersion wavelength, at which the GVD parameter is zero (close to 1300 nm for SSMF); if  $\beta_2$  is positive, the chromatic dispersion is said to be normal, while if  $\beta_2$  is negative is said to be anomalous.

Group velocity dispersion is commonly expressed in terms of the chromatic dispersion parameter  $D$ , measured in  $\text{ps}\cdot\text{nm}^{-1}\cdot\text{km}^{-1}$ , and related to  $\beta_2$  as [19]:

$$D = -\frac{2\pi c}{\lambda^2} \beta_2 \quad (2.15)$$

The relative time delay  $\Delta\tau_g$  between two wavelength components separated by  $\delta\lambda$ , and after a propagation length  $L$ , is [20]:

$$\Delta\tau_g = D \cdot L \cdot \delta\lambda \quad (2.16)$$

In general, different types of fiber have different dispersion characteristics. However, for a standard single-mode fiber, the dispersion parameter over a given band can be described by [17]:

$$D(\lambda) = \lambda \frac{S_0}{4} \left[ 1 - \left( \frac{\lambda_0}{\lambda} \right)^4 \right] \quad (2.17)$$

where  $S_0$  is the dispersion slope and  $\lambda_0$  is the zero-dispersion wavelength. According ITU-T G.652,  $S_0$  should be below  $0.092 \text{ ps/nm}^2\text{-km}$  and  $\lambda_0$  between 1300 and 1324 nm.

## Polarization mode dispersion

The two orthogonally polarized modes of a single-mode fiber are, under ideal conditions, degenerate (i.e., they have identical propagation constant). In practice, mechanical and geometrical distortions break the cylindrical symmetry and result in a difference in the index of refraction seen by the two components, referred as fiber's birefringence [21]. The differential time delay  $\Delta\tau_\omega$  between the slow and fast components (also referred as eigenstates or eigen-polarizations) will depend, at a given frequency  $\omega$ , on the eigenstates phase velocities  $v$  and on the fiber length  $L$  as [22]:

$$\Delta\tau_\omega = \frac{L}{v_x} - \frac{L}{v_y} = \frac{1}{\omega}(\beta_x - \beta_y)L = \frac{\beta}{\omega}L \quad (2.18)$$

where the indexes  $x$  and  $y$  refer to the slow and fast eigen-states. When an arbitrarily polarized optical pulse is injected into a birefringent fiber, its components along the two eigenstates propagate at different group velocity  $v_g$ , and will experience a differential group delay (DGD). At the output, the pulse will consist of two identically shaped and orthogonally polarized replicas of the original pulse, delayed by the quantity  $\Delta\tau_g$ , expressed as [22]:

$$\Delta\tau_g = \frac{L}{v_{gx}} - \frac{L}{v_{gy}} = \frac{\partial\beta}{\partial\omega}L = \beta'L \quad (2.19)$$

The birefringence changes both in strength (the difference between the refractive indexes) and orientation (the eigen-polarizations) along the propagation axis of the optical fiber [21].

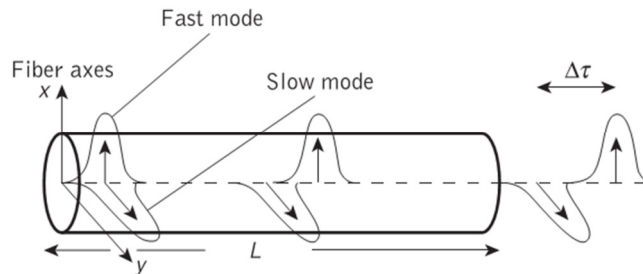


Figure 2-12: Time domain effect of birefringence in a short fiber ( [9])

A vectorial description of the problem can be based on Stokes' parameters and the Poincare sphere, which provide a mapping of both the state of polarization and

birefringence to a three dimensional space, called Stokes space [23]. The birefringence at a given fiber location can be represented by a vector  $\boldsymbol{\beta}$ , whose orientation, by convention, coincides with the slow eigen-polarization axis and whose magnitude ( $\beta$ ) equals the difference between the two eigen-states propagation constants.

Birefringence can be considered constant in a short piece of fiber. The differentiation between short and long-length regime is given by the so-called correlation length ( $L_c$ ), which is defined mathematically as the mean length over which the two polarization modes remain reasonably correlated [18]. When considering the power exchange between the modes, the correlation length is also referred as coupling length, and the short and long regimes are referred as weak and strong regimes. Numerical values of the correlation length for G.652 fibers are reported, for example in [24], to be between 8 and 20 meters. However, due to its dependence on employment conditions, it is not too surprising that values for the correlation length given in literature vary wildly, from centimeters to several hundred meters.

Typical optical transmission distances require fiber lengths much bigger than the correlation length; telecom fibers are usually modeled as a sequence (of N) constant birefringent sections whose birefringence axes are randomly oriented. The total PMD vector  $\boldsymbol{\tau}$  at the end of the fiber can be obtained using the concatenation rule [23]:

$$\vec{\tau} = \vec{\tau}_N + \hat{\beta}_N \vec{\tau}_{N-1} + \hat{\beta}_N \hat{\beta}_{N-1} \vec{\tau}_{N-2} + \cdots + \hat{\beta}_N \hat{\beta}_{N-1} \hat{\beta}_2 \vec{\tau}_1 \quad (2.20)$$

A graphical representation of the evolution of the SOP as wave propagates along different fiber sections is shown in Figure 2-13; the convention used in the figure is that symbol's superscript denotes frequency, and subscript denotes section. Considering the monochromatic case, the input SOP  $\mathbf{S}_0$  (represented by a point on the sphere), rotates about the constant birefringence vector  $\boldsymbol{\beta}_1^0$  by  $\beta_1 L_1$  radians while traversing the first section length  $L_1$ , according eq. (2.18). The resulting SOP  $\mathbf{S}_1^0$  will then enter the second section suffering again a rotation around  $\boldsymbol{\beta}_2^0$  of  $\beta_2 L_2$  radians. Eventually, process will repeat for the successive sections, finally resulting in the output SOP  $\boldsymbol{\beta}_N^0$ .

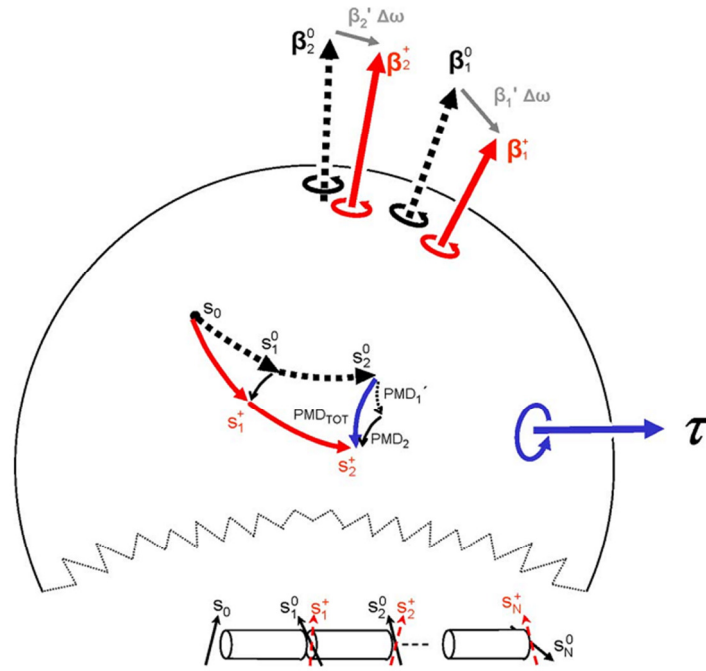


Figure 2-13: Graphical representation of the evolution of input SOP  $S_0$  in traversing two sections of birefringent fiber (lower inset). After [22]

The effect of changing position along a constant birefringence fiber or changing the optical frequency are both reflected through a rotation of the polarization around a birefringence vector [21]. In a non-monochromatic case, and assuming a small increment  $\Delta\omega$  (compared to  $\omega$ ), the signal component will encounter slightly different birefringences  $\beta_i^+$  and will rotate over different arcs. In a first-order approximation,  $\beta_i^+$  can be expressed as [22]:

$$\beta_i^+ = \beta_i^0 + \frac{\partial \beta_i^0}{\partial \omega} \Delta\omega \quad i = 1, 2, \dots, N \quad (2.21)$$

The addendum of eq. (2.21) is a “delay vector”; its magnitude, multiplied by the section length  $L_i$ , will give the rotation angle. For section 1 for example, the additional rotation will take  $S_1^0$  to  $S_1^+$  with rotation around  $\beta_1^+$ , by an angle  $\beta_1^0 \Delta\omega L_1$ , according eq. (2.19).

Locally, and in the vicinity of the optical frequency  $\omega_0$ , the evolution of the SOP can be described as a precession about a vector  $\tau$ , called the PMD vector [21]; its orientation defines the principal states of polarization (PSP) and its magnitude is the differential group delay. Each section has its own PMD vector ( $\beta_1^+ \Delta\omega$  and  $\beta_2^+ \Delta\omega$  in Figure 2-13). The PMD  $\tau$  is not simply the vector sum of each section, since each section has its own PMD vector orientation and suffers a rotation due to all sections preceding it; this is

evident from eq. (2.20). Taking as example the Figure 2-13, the effect of the second section on  $\mathbf{S}_1^+$  can be viewed as a simultaneous rotation by  $\beta_2^0 L_2$  of both  $\mathbf{S}_1^0$  and  $\beta_1' \Delta\omega$  (the result is the arc labelled  $\text{PMD}_1'$ ).

The aforementioned can be resumed mathematically as follows [25]:

$$\frac{\partial \vec{s}}{\partial z} = \vec{\beta} \times \vec{s} \quad (2.22)$$

$$\frac{\partial \vec{s}}{\partial \omega} = \vec{\tau} \times \vec{s} \quad (2.23)$$

$$\frac{\partial \vec{\tau}}{\partial z} = \frac{\partial \vec{\beta}}{\partial \omega} + \vec{\beta} \times \vec{\tau} \quad (2.24)$$

The first equation states that the birefringence  $\beta$  rotates the SOP  $\mathbf{S}$  (at a fixed frequency) as a function of distance  $z$ . Eq. (2.23) states that the PMD  $\tau$  rotates the SOP (at a fixed distance) as a function of frequency. Eq. (2.24) states that PMD grows, as one moves down the fiber through another section, by rotating the existing PMD about the birefringence vector of that section and adding the previous section's PMD [22].

In a long optical fiber, due to the randomness of the birefringence orientation and to the mode coupling, the polarization vector will essentially move (a “random-walk”) all over the Poincare sphere with the change of the signal optical frequency [20].

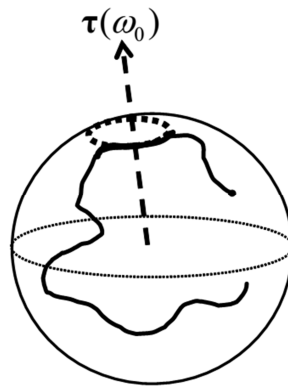


Figure 2-14: “Random-walk” of SOP trajectory at a given position  $z$  along the link. Locally, the SOP variation with frequency can be described as rotation around vector  $\tau$ .

The net effect is also time dependent due to variations on the physical conditions of the link, like mechanical stress or temperature. For all these reasons, the relationship between DGD and PMD is complex and permits only a statistical treatment.

System impairments at a given wavelength are controlled by the instantaneous DGD. The total DGD ( $|\boldsymbol{\tau}|$ ) is a random variable (with independent and identically distributed components [25]) described by a Maxwell distribution [23]. The probability density function, valid for the concatenation model described by eq. (2.20), is [26] :

$$P(\Delta\tau) = \frac{32}{\pi^2} \frac{\Delta\tau^2}{\langle\Delta\tau\rangle^3} \exp\left(-\frac{4 \cdot \Delta\tau^2}{\pi \cdot \langle\Delta\tau\rangle^2}\right) \quad (2.25)$$

An example of such distribution is shown in Figure 2-15. For any optical frequency there exists a small, but finite, probability of having a very large value of DGD depending on the orientation of the independent vectors [23].

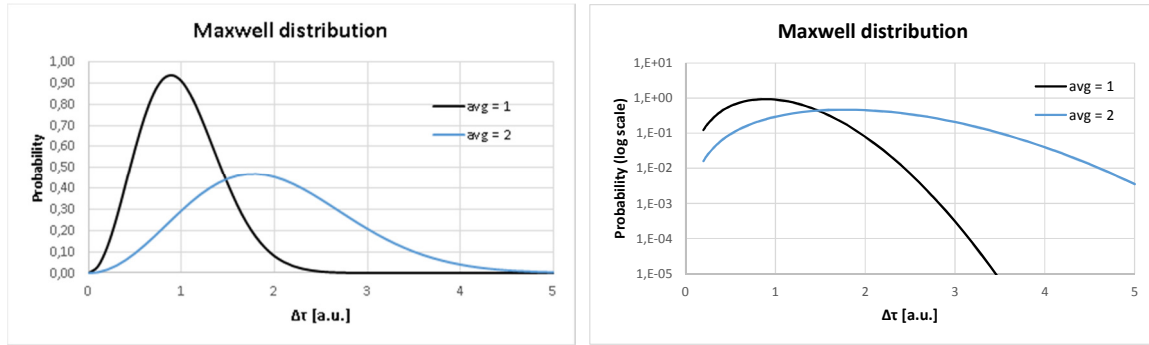


Figure 2-15: Examples of Maxwellian distributions  
(left: linear scale; right: logarithm scale)

The PMD coefficient  $D_{PMD}$ , typically specified for commercial fibers, represents PMD characteristics of one particular length of fiber over a given optical frequency range; it can be used to calculate the expected average DGD, that for long fibers ( $L \gg L_c$ ) scales with the square root of the fiber length as [6]:

$$\langle\Delta\tau\rangle = \langle DGD \rangle = D_{PMD} \cdot \sqrt{L} \quad (2.26)$$

ITU-T requires manufacturers to specify cabled fiber polarization mode dispersion on a statistical basis, and not on an individual fiber basis; fiber datasheet provides the maximum PMD value for the individual fiber, and the (statistical) upper limit for concatenated lengths of fiber, referred as link design value or  $PMD_Q$  (see appendix D).

The DGD is a sensitive function of wavelength and fiber environment, and statistically it follows a Maxwell distribution. Therefore, a single DGD measurement cannot characterize a fiber. Instead a polarization mode dispersion (PMD) measurement is used, an average or root-mean-square (rms) value of DGD over some wavelength range [27].

Polarization maintaining (PM) fibers are special fibers designed to have a strong refractive index difference (high birefringence) between the two principal axis, in order to reduce the power exchange between the degenerate modes (weak polarization mode coupling) [20]. In order to maintain the SOP of an optical signal, the polarization state of input optical signal has to be aligned to either the slow or the fast axis [20].

In PM fibers, DGD scales linearly with the fiber length and is assumed to represent the overall PMD effect. PM fibers are commonly used in applications where preserving polarization is essential, e.g. for the connection between lasers and modulators (when modulator requires polarized light as input), but are rarely used for long-distance transmission, because of their cost and higher attenuation.

## **2.4 Non-linear effects**

At high bit rates and/or at high transmitted power, nonlinear effects may affect transmission quality. In the case of wavelength division multiplexing (WDM) systems, nonlinear effects can become important even at moderate powers and bit rates.

These effects are typically divided in two categories. The first arises due to the interaction of light waves with phonons, and includes stimulated Brillouin scattering (SBS) and stimulated Raman scattering (SRS). The second category is related to the dependence of the refractive index on the optical intensity leading to self-phase modulation (SPM), cross-phase modulation (XPM) and four-wave mixing (FWM). Except for SPM and XPM, all nonlinear effects provide gains to some channel at the cost of absorbing power from other channels. SPM and XPM affect only the phase of signals and can cause spectral broadening, which leads to increased dispersion.

Table 2-4 gives a short overview of these impairments and their effects.



<b>Impairment</b>	<b>Cause</b>	<b>Effect</b>	<b>Possible compensation</b>
Four Wave Mixing (FWM)	Signal interference	<ul style="list-style-type: none"> <li>- Power transfer from original signal to other frequencies</li> <li>- Production of sidebands (harmonics)</li> <li>- Channel crosstalk</li> <li>- Increased bit errors</li> </ul>	Use of S-SMF (compensate CD with compensators); unequal channel spacing
Self-Phase Modulation (SPM) and Cross Phase Modulation (XPM)	Intensity-dependent refractive index	<ul style="list-style-type: none"> <li>- Spectral broadening</li> <li>- Initial pulse compression (in positive CD regimes)</li> <li>- Accelerated pulse broadening (in negative CD regimes)</li> <li>- Channel crosstalk due to “walk-of” effects</li> <li>- Increased bit errors</li> </ul>	Use of fiber with CD Compensators
Stimulated Raman Scattering (SRS)	Interaction of signal with fiber molecular structure	<ul style="list-style-type: none"> <li>- Decreased peak power</li> <li>- Decreased OSNR</li> <li>- Optical crosstalk (especially in bidirectional WDM systems)</li> <li>- Increased bit error</li> </ul>	Careful power design
Stimulated Brillouin Scattering (SBS)	Interaction of signal with acoustic waves	<ul style="list-style-type: none"> <li>- Signal instability</li> <li>- Decreased peak power</li> <li>- Decreased OSNR</li> <li>- Optical crosstalk (especially in bidirectional WDM systems)</li> <li>- Increased bit errors</li> </ul>	Spectral broadening of the light source

Table 2-4: Overview of non-linear effects (adapted from [28])

## 3 Characterization methods

Optical fiber characteristics provide essential information for the optical communication system designer in order to make wise choices of fibers, materials and devices according application requirements. However, although the system designer does not usually need to measure fundamental parameters of the fiber, there is a requirement for field measurements in order to evaluate overall system performance, capabilities of the network for the current application and for future services upgrades.

The International Telecommunication Union (ITU) has recommended several standards for fiber transmission systems and fiber measurements. These are known as Fiber Optic Test Procedures (FOTPs).

In particular, ITU-T G.650.3 defines fiber characterization as "*a comprehensive suite of measurements that is carried out on an optical fibre cable link to determine the key performance attributes of that link which may affect current or future applications that operate over that link. Fibre characterization also allows the quality of the optical fibre cable link to be assessed, including the identification of the type and grade of fibre installed. Full fibre characterization includes connector end face inspection, insertion loss measurements, return loss measurements, OTDR testing, chromatic dispersion testing, polarization mode dispersion measurement, and spectral attenuation*".

The test methods are divided by ITU into reference test methods (RTMs) and alternative test methods (ATMs). An RTM provides a measurement of a particular characteristic strictly according to the definition, which usually gives the highest degree of accuracy and reproducibility, whereas an ATM may be more suitable for practical use but can deviate from the strict definition.

### 3.1 Attenuation profile

With the advent of DWDM and CWDM technologies, the whole spectral portion from 1270 nm to 1630 nm is used. SMFs were not originally designed to be used in the spectrum between 1310 nm and 1550 nm. In old fiber, there is a region of very high attenuation near 1385 nm known as the “water peak”. This portion of the spectrum is now used in CWDM systems. Also, both CWDM and DWDM systems utilize the spectrum up to 1630 nm. This leads to the necessity to evaluate attenuation characteristics over a large spectrum.

The spectral attenuation profile (SAP or AP) provides the fiber attenuation coefficient as a function of the wavelength. ITU-T G.650.1 provides recommendation on the methods and procedures to be followed for accurate measurements. The most common techniques are the cut-back (RTM), the insertion loss and the backscattered method (both ATM).

### Cut-back method

The cut-back method requires first measuring the output power (expressed in dB<sub>m</sub>) at the end of the FUT length  $L$ . Afterwards, only a portion of length  $L_{cut}$  of the FUT (for example, 2 m from the launching point) is left connected (cutting the remaining portion) and the new output power is measured with the same launching conditions. The attenuation coefficient of the (removed length of) FUT is simply:

$$\alpha(\lambda) = \frac{1}{L - L_{cut}} 10 \log \frac{P(\lambda) |@L}{P(\lambda) |@L_{cut}} \quad \left[ \frac{dB}{unit\ length} \right] \quad (3.1)$$

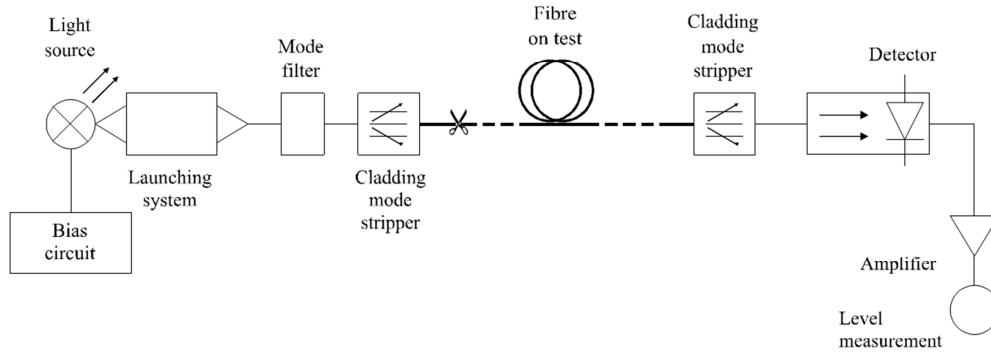


Figure 3-1: Arrangement for the cut-back method (source [29])

Usually mode filters<sup>4</sup>, for the elimination of higher order modes, and cladding mode strippers<sup>5</sup>, which encourages the conversion of cladding modes to radiation modes, are

<sup>4</sup> Mode filtering simulates the effects of long lengths of fiber by attenuating higher-order modes; it is relevant when measuring close to  $\lambda_c$  and in short pieces of fiber.

adopted to optimize the launching and propagation conditions. The factor of coupling loss between light source and fiber is neglected. Therefore, accuracy is dictated by fiber length measurements, stability of launching conditions and coupling to the detector. The cut back method is a destructive and time consuming method, so it is not adopted for field measurements.

## Insertion loss technique

The insertion loss technique consists of the measurement of the power loss due to the insertion of the FUT between a launching and a receiving system that has been previously interconnected for referencing purposes. Whenever the FUT does not allow the propagation to the receiving end of modes other than the fundamental one, filters and strippers can be avoided. The insertion loss technique is less accurate than the cut-back method, due to connector and/or splice loss uncertainty, but has the advantage of being non-destructive for the FUT and for connectors that might exist at fiber ends, being suitable for field use and intended for use with connectorized cables. ITU recommends the use of the insertion loss method as an alternative tests method.

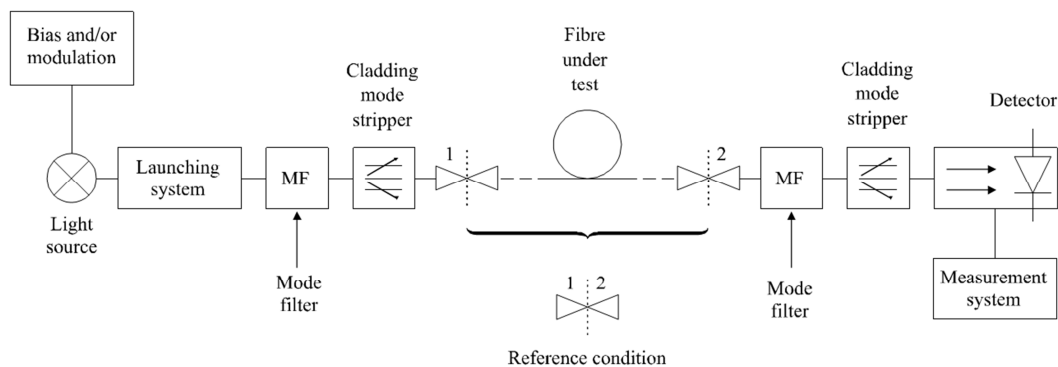


Figure 3-2: arrangement for the insertion loss method (source [29])

## Backscattered method

The backscattered technique is an ATM based on optical time domain reflectometry (OTDR), discussed in detail in section 3.4. ITU suggests bidirectional backscattering

<sup>5</sup> Some light is inevitably launched into fiber's cladding. Though cladding modes dissipate rapidly with fiber length, they can interfere with measurement in short pieces of fiber.

measurements, and relegates unidirectional measurements to particular cases, like verification of the backscatter slope variation in cabled fibers.

## 3.2 Chromatic dispersion

Different techniques exist for the measurement of chromatic dispersion. Most of the methods take delay measurements as a function of wavelength; chromatic dispersion and slope are extrapolated from the derivative of the group delay data (with respect to wavelength). The derivative is usually calculated after fitting data to a mathematical model; different approximations are used according the fiber type and the spectral region, as summarized in Table 3-1. Therefore, the accuracy of the computation of the chromatic dispersion coefficient depends on the amount of measured data.

Fiber type	ITU-T standard	Wavelength range	Approximation
Dispersion un-shifted	G.652	Around 1310 nm	3-term polynomial
		1550 nm region	Quadratic
		1260 – 1640 nm	5-term polynomial
Dispersion shifted	G.653	1550 nm region	Quadratic
		1260 – 1640 nm	5-term polynomial
NZDS	G.655	1550 nm region	Quadratic
		1260 – 1640 nm	5-term polynomial
Wideband NZDS	G.656	1260 – 1640 nm	5-term polynomial
Mixed types including DCF		1550 nm region	Quadratic
		1260 – 1640 nm	5-term polynomial

Table 3-1: Approximation equation according fiber type and spectral region (source [28])

ITU-T G.650.3 recommendation suggests following techniques for chromatic dispersion measurement (TIA/EIA reference is indicated between parenthesis): the RTM is the modulated phase-shift method (FOTP-169); the alternative methods are the

pulse-delay method (FOTP-168) and the differential phase shift method (FOTP-175). Table 3-2 provides applicability of these methods according link characteristics.

Application	Phase shift	Diff. phase shift	Pulse delay
G.652; G.653; G.655	✓	✓	✓
Mix of fiber types	✓	✓	✗
$L > 120$ km	✓	✓	✗
$20 \text{ km} < L < 80$ km	✓	✓	✓
$L < 20$ km	✓	✓	✗
Amplified link	✓	✓	✗

Table 3-2: Chromatic dispersion test methods suitability for different link characteristics (adapted from [28])

## Phase-Shift methods

In the phase-shift method an adjustable light source is modulated with a sinusoidal signal at frequency  $f_m$ . After propagation through the FUT, signal is detected via a photodiode and compared with the sinusoidal reference source, retrieving the phase shift induced by the fiber. The phase measurement is repeated at intervals across the wavelength range of interest. A relative phase delay of  $360^\circ$  between two wavelengths corresponds to a group delay of  $f_m^{-1}$ . The group delay can be expressed as:

$$\Delta\tau_g(\lambda) = \frac{\phi(\lambda)}{2\pi} \frac{1}{f_m} \quad (3.2)$$

where  $\phi$ , dependent on the measured  $\lambda$ , represents the phase difference between the test and the reference signal, i.e. the phase shift.

The value of chromatic dispersion is determined by the derivative of the group delay (its absolute value is not measured directly):

$$D(\lambda) = \frac{1}{L} \frac{d(\Delta\tau_g(\lambda))}{d\lambda} = \frac{1}{2\pi \cdot L \cdot f_m} \frac{d\phi(\lambda)}{d\lambda} \quad (3.3)$$

The reference phase delay and the choice of the reference wavelength are not critical. A high modulation frequency is desirable since it increases the phase sensitivity

of the measurement and reduces uncertainty; sinusoidal, trapezoidal or square wave modulation may be used, typically with a frequency range of 30 to 100 MHz and a very high spectral stability [30]. On the other hand a high frequency may require the measurement system to track the number of full cycles of the phase shift to avoid ambiguities, increasing complexity. Also, the wavelength tuning step needs to be small enough to obtain a sufficient number of phase measurements within each cycle. Consequently, the selection of the modulation frequency depends on the chromatic dispersion value of the specimen and on the wavelength window to be covered.

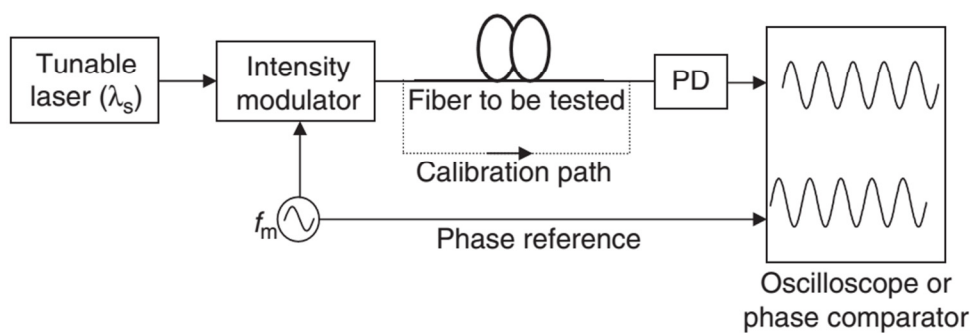


Figure 3-3: Setup for the phase shift method (source [20])

In Figure 3-3, the reference signal is directly connected to the phase detector. This configuration is possible only when source and detector are co-located. For field testing, an optical reference link can be used to carry the reference signal or this can be transmitted directly on the fiber under test.

The phase shift technique presents high accuracy and repeatability [28]; its dynamic range (more than 40 dB) is by far superior to the pulse delay method. Fiber length must be known in advance and this technique does not allow sectionalizing the fiber according to its dispersion characteristics. The phase shift method is a ITU-T and IEC reference test method.

The differential phase shift method is very similar to the phase shift technique. The major difference is that the phase is measured across two closely spaced wavelengths obtaining chromatic dispersion directly, rather than measuring the relative group delay

and calculating the derivation of it. The chromatic dispersion at the mid wavelength<sup>6</sup> is obtained recurring to eq. (3.3), dividing it by the wavelengths spacing  $\Delta\lambda = |\lambda_1 - \lambda_2|$ .

Increasing the wavelength interval between the two modulated signals will increase the accuracy of the delay at one individual wavelength, but will decrease the number of data points that can be acquired to trace the delay curve, leading to a lower accuracy in the dispersion coefficient calculation. The wavelength spacing between the differential phase measurement data is typically in the range of 2 to 20 nm.

## Pulse-Delay method

The pulse delay technique (also known as time-of-flight method) consists in directly measuring the relative time delay experienced by the propagation through a known length of fiber of various optical pulses centered at different wavelengths.

The method may use pulses of light both greater than and less than the zero-CD wavelength. The optical pulses must be of short duration and of sufficient intensity as well as have spatial and temporal stability to obtain quality measurements. The resolution is limited by the shortest time delay that the detector is able to measure. The measured time delays are then differentiated with respect to wavelength to obtain the chromatic dispersion.

Accuracy of the time-of-flight method is not only determined by the number of wavelengths and fitting equation adopted but is also a function of the dispersion, distance, and pulse width. Distances greater than several kilometers are required to cause sufficient time delay between the pulses, and thus this method is not suited particularly well for short fiber lengths (<10 km). Therefore, it is important to use sufficient wavelength spacing and get data from different bands.

## 3.3 Polarization Mode Dispersion

PMD measurement techniques are generally divided into time-domain and frequency domain methods. Time domain methods operate by sensing pulse delays between the modes propagating in the fast and slow axis, whereas the frequency domain

---

<sup>6</sup> If the two measured wavelengths are  $\lambda_1$  and  $\lambda_2$ , the mid wavelength is  $\lambda = \frac{1}{2}(\lambda_1 + \lambda_2)$



methods operate by detecting changes of polarization with frequency. Measurement capabilities of various instruments range from around 1 fs to about 100 ps of DGD. Smaller ranges are needed for the measurement of the instantaneous DGD of optical components or short pieces of fiber, whereas the larger ranges are used to characterize long fiber links. In any PMD test method, the light source window must be as wide as possible in order to obtain a large amount of statistical sampling. This allows the statistical average to be determined with a minimum amount of uncertainty.

ITU-T G.650.2 classifies as RTM the Stokes parameter evaluation technique, also referred as Jones-Matrix-Eigen analysis, and as alternative test methods the State of Polarization (SOP) method, the Interferometric technique and the Fixed Analyzer method.

## Fixed Analyzer Method

Light from a tunable laser or a broadband source is polarized (fixed polarization) and launched into the FUT; at the receiver side a fixed polarizer is followed by an optical power meter or an optical spectrum analyzer (OSA). Typical arrangements are shown in Figure 3-4.

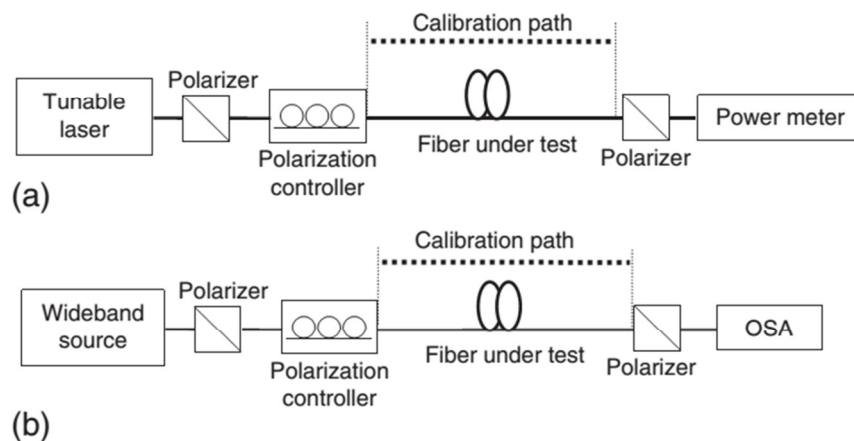


Figure 3-4: Fixed Analyzer setup - (a) tunable laser and power meter combination; (b) wideband source and OSA combination (source [20])

In the arrangement of Figure 3-4 (a), by varying the frequency of the tunable optical source, the signal polarization state at the fiber output changes; the polarizer converts this SOP change into an optical power, which is then detected by the power meter.

In the system of Figure 3-4 (b), different signal frequency components will exhibit different polarization states at the output of the birefringent fiber; the polarizer converts this frequency-dependent polarization rotation into a frequency-dependent optical power spectral density, which can be accurately measured by an OSA.

The received optical power spectrum shows a number of peaks and valleys (extrema) result of polarization variations of the received light, and proportional to the rate of change of the received SOP. Larger PMD will result in a higher density of extrema. The mean DGD in the interval  $\lambda_{start} - \lambda_{stop}$  can be calculated as [31]:

$$\langle DGD \rangle = \frac{k N_e \lambda_{start} \lambda_{stop}}{2c(\lambda_{start} - \lambda_{stop})} \quad (3.4)$$

where  $N_e$  is the number of singular points (peaks and valleys) and  $k$  is constant, which equals 1 for polarization maintaining fibers (no mode coupling) and 0.824 for the generality of standard fibers (which show random mode coupling).

Another data analysis method is to determine the Fourier transform of the transmission spectrum; the mean DGD value is determined (for fiber with strong mode coupling) from the standard deviation of a Gaussian curve fit (Figure 3-5).

The frequency step size  $\delta\lambda$  (or the OSA spectral resolution, if arrangement in Figure 3-4 (b) is implemented) should satisfy, in the 1550 nm window [20]:

$$\delta\lambda_{[nm]} < \frac{1}{\langle \Delta\tau \rangle_{[ps]}} \quad (3.5)$$

The instrument is not sensitive to shock or vibration, assuming that the spectrum analyzer is realized with Fabry-Perot technology.

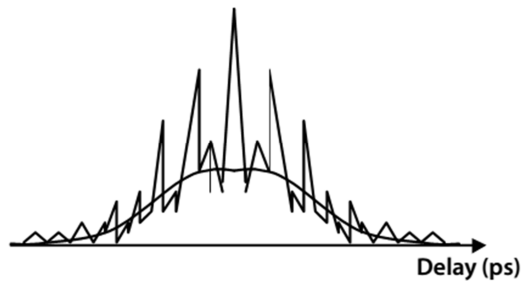


Figure 3-5: Result of a wavelength scanning and Gaussian fit (source [28])

## Jones Matrix Eigen Analysis (JME) Method

The Stokes parameter evaluation technique is the ITU-T G.650.2 reference test method. The change in the output state of polarization in function of wavelength is determined and characterized by the Jones matrix eigen analysis (JME), or by the rotation of the SOP vector on the Poincare Sphere (PS). Jones matrixes are widely used to represent the polarization state of a light wave or the transfer characteristics of a passive optical device. This technique can be applied to both short and long fibers, regardless of the degree of polarization mode coupling.

The key components of the measurement system are shown in Figure 3-6. A tunable laser is stepped through a multitude of optical frequencies; for each of them, the polarization filter is adjusted to three different linearly polarized states (typically 0°, 45° and 90°). On the receiver side, a polarimeter measures the output SOP corresponding to insertion of each of the three polarizers configurations.

The maximum wavelength interval  $\Delta\lambda$  around  $\lambda_0$  over which the measurements is performed depends on the expected DGD, and should satisfy ([32])

$$\Delta\tau_{max} \cdot \Delta\lambda \leq \frac{\lambda_0^2}{2 \cdot c} \quad (3.6)$$

in order to ensure that from one test wavelength to the next, the output SOP rotates less than 180 degrees about the principal states axis of the Poincare sphere. The Stokes parameters obtained are then analyzed with the JME method (or the PS method) to obtain the instantaneous DGD.

Knowing the Jones matrix representation of the fiber at two closely spaced wavelengths allows obtaining the DGD from the following equation [20]:

$$\Delta\tau = \frac{1}{\Delta\omega} \cdot \arg\left(\frac{\lambda_{e1}}{\lambda_{e2}}\right) \quad (3.7)$$

In equation (3.7),  $\lambda_{e1}$  and  $\lambda_{e2}$  are the eigenvalues of the Jones matrix  $T_{\omega+\Delta\omega} \cdot T_{\omega}^{-1}$  and  $\Delta\omega$  is the difference in optical frequency between the two wavelengths at which the Jones matrix is determined. The matrixes  $T_{\omega+\Delta\omega}$  and  $T_{\omega}$  are the Jones matrixes at the frequencies  $\omega+\Delta\omega$  and  $\omega$ . Measuring the DGD over many different wavelengths and averaging them gives the PMD.

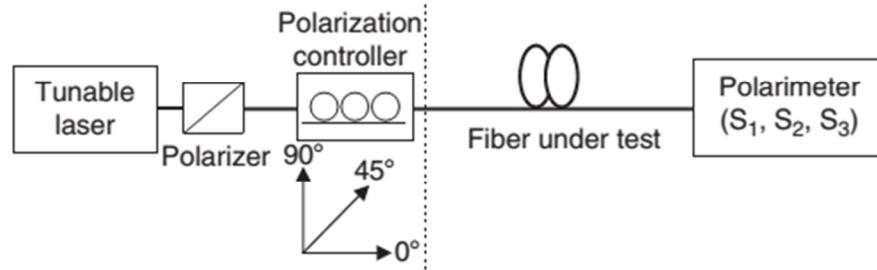


Figure 3-6: Arrangement for the Stokes parameter evaluation technique (source [20])

In order to obtain the correspondent DGD, one acquisition is required for each wavelength, making the measurement method relatively slow but producing the most accurate results in comparison to other methods. Also, acquisition accuracy is affected by movement and/or vibration of the FUT, making it not preferable for field measurement.

## Interferometry

One of the possible arrangements for the interferometric measurement is depicted in Figure 3-7. A filtered broadband source is followed by a polarizer that sets a polarization state. The signal, after propagation in the device under test (DUT), is coupled through a polarization beam splitter to an interferometer; each arm of the interferometer receives only one PSP, horizontal or vertical. Two mirrors are on the interferometer arms, one of which is adjustable; the relative delay of the two beams depends on the position of the moving mirror. The resulting signal of the interfering beams is coupled to a photodetector, and represents the cross-correlation of the two polarizations.

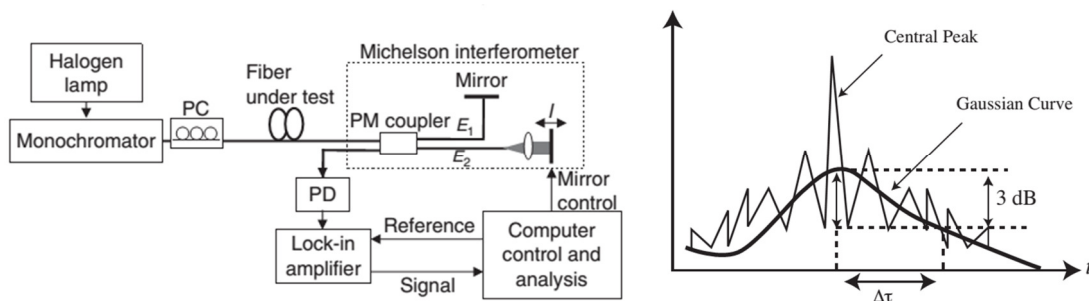


Figure 3-7: [left] Interferometric measurement arrangement (source [20]); [right] typical measurement result from a randomly mode coupled fiber (source [31])

A typical measurement result from a randomly mode coupled fiber is shown in Figure 3-7. The central peak occurs when both paths are at equal lengths, which represents zero DGD. The side peaks located at both sides of the central peak represent the condition where both the moving and fixed paths are not at equal value, representing the PMD existence. Many side peaks are produced while the mirror is adjusted. The Gaussian curve that best fits the pattern, including the central peak, is determined<sup>7</sup>; the mean DGD can be calculated from the curve standard deviation as [20]:

$$\langle \Delta\tau \rangle = \sigma\sqrt{2/\pi} \quad (3.8)$$

The main advantages of this method are [33] its high dynamic range, good absolute uncertainty, the capability to measure low DGD values and the tolerance to movement along the fiber path during the measurement since movement may change the details of the interferogram, but not the overall shape. On the other hand, measurement time may be long since averaging is necessary, and moving parts make this method not well appropriate for field equipment.

### 3.4 Optical time domain reflectometry

The Optical Time Domain Reflectometer (OTDR) is an electro-optical instrument largely used for characterization and troubleshooting of optical fibers and optical links. It allows performing a variety of measurements, like fiber length, splices and connectors related losses as well as locate such discontinuity point along the link.

OTDR operation principle resembles the radar: a signal is launched into the fiber; all light that is reflected or scattered back is collected and evaluated. In more detail, a short pulse carrying a certain amount of energy is injected in the FUT. The time of flight of the pulse (i.e. the time to echo) is precisely calculated, and time is converted into distance according equation (3.9), where the factor 2 counts for the two-way path of the pulse. Knowing the fiber properties (i.e. the refractive index) is it possible to calculate the fiber length  $L$ .

---

<sup>7</sup> When measuring devices without mode coupling, the central peak (correspondent to balanced arms) is ignored; DGD is obtained from the distance between the two side peaks [16]

$$t_{echo} = \frac{2 \cdot n}{c} L \quad (3.9)$$

The block diagram of an OTDR instrument is shown in Figure 3-8. An electrical pulse generator drives the laser source, producing a train of short optical pulses. A photodiode is used to detect the backscattered optical power from the FUT through a directional coupler. The received optical signal is conditioned and analyzed by a digital-signal processor (DSP). The DSP needs to be precisely synchronized with the pulse generator in order to obtain an accurate calculation of the propagation delay of each backscattered pulse.

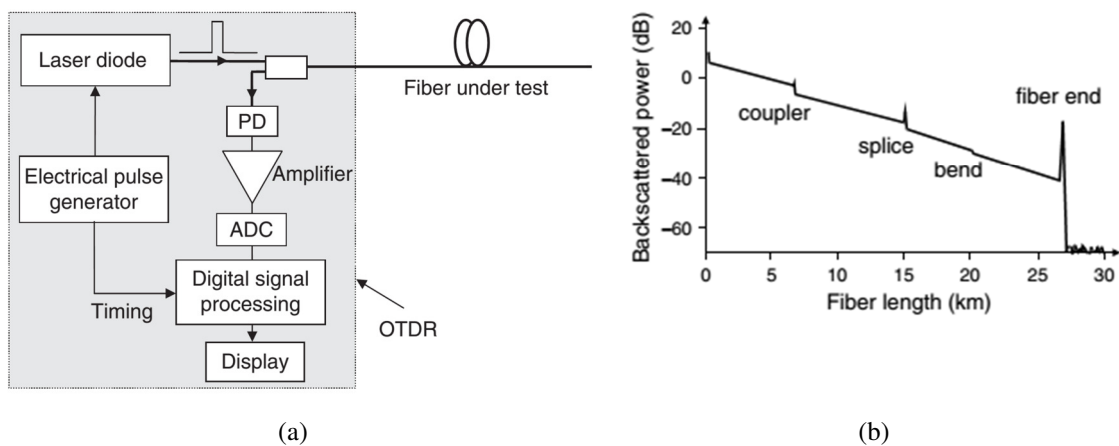


Figure 3-8: (a) OTDR block diagram (source [20]) and (b) characteristic trace (source [7])

OTDR's DSP perform extensive signal processing to calculate distance, loss and reflection of each event, link length, loss, and fiber attenuation; due to the low power levels involved, many acquisitions are performed and averaged in order to improve noise rejection. The result is the fiber's characteristic trace, or profile (a plot of attenuation versus distance, as shown in Figure 3-8). One of the main advantages of using an OTDR is that it performs a single-ended measurement, requiring access to only one end of the fiber/link.

OTDRs base their operation on Rayleigh scattering and Fresnel reflections.

Any pulse sent down a fiber will suffer omnidirectional scattering along the entire fiber length; some of the light is (back)scattered towards the source. Since Rayleigh backscattering is a linear process, the magnitude of the backscattered optical power is linearly proportional to the optical power at that location.

---

Whenever light traveling in a material encounters a different density material, some of the light is reflected towards the light source. Changes in material density occur at fiber ends, at breaks, and sometimes at splice joints or connectors; the amount of reflected light depends on the magnitude of change in material density. This type of returned light is called a Fresnel reflection and gives to the OTDR the capability of locate discontinuities along the fiber (e.g. breaks).

Fresnel reflections lead to an important OTDR limitation known as “dead zone”. There are two types of dead zones: event and attenuation. A dead zone is defined as the length of time during which the detector is temporary blinded by a high amount of reflected light.

The event dead zone is the minimum distance after a Fresnel reflection where an OTDR can detect another event; in other words, it is the minimum length of fiber needed between two reflective events that guarantee detection of both. Closely spaced events might still be detected, but will be probably displayed overlapped or, in the worst case, presented as a single one (merged). Similarly, the attenuation dead zone is the minimum distance after a Fresnel reflection where an OTDR can accurately measure the loss of a subsequent event. Dead zones are influenced by the pulse width. Short pulses carry less energy, minimizing dead zones; but on the other hand they reduce the backscattering level and may result in the incapacity to reach the fiber end.

### **3.5 Mixed methods**

Field measurements require the necessity to transport test equipment to the different measurement locations; clearly, it is desirable to minimize the number of different equipment to be carried along to accomplish the characterization tasks. OTDRs are a very good example of “multi-measurement” equipment. Moreover, one of the big advantages of OTDR is its capability to reveal the location, along the fiber, of the particular event detected; it would be desirable to have distance measurements also for other fiber characteristic beyond those typically revealed by a standard OTDR.

Two existing examples of such “consolidation” and feature-set extension are the CD-OTDR and P-OTDR.

## CD-OTDR

An OTDR measures the distance at different wavelengths, based on the delay experienced by the launched pulses; in fact it measures a delay versus wavelength, so can be used to determine chromatic dispersion, in the same way as in the phase shift method.

A CD-OTDR operates very similarly to a standard OTDR launching multiple laser pulses into one end of the fiber under test. Chromatic dispersion is computed using the difference in distance to the last event. The accuracy of the measurement depends on the ability to measure the last reflection. APC connectors reduce the effectiveness of the method, and might require the installation of a reflective termination to correctly locate the end of the fiber (turning the measure in a two-ended method). Clearly, method is not compatible with non-bidirectional components (such as EDFAs).

The dispersion coefficient is obtained using the best-fit values of the appropriate Sellmeier coefficients. The fit equation recommended for any type of fiber and in a broad spectrum ( $> 300$  nm) is a 5-term Sellmeier equation, which requires at least five points to be resolved. Due to the fiber spectral attenuation, some wavelengths (e.g. in the 1310 nm band and/or close to the water peak) will be almost undetectable after 70 to 80 km, leaving only three points for the fitting.

The measurement uncertainty depends on the shape and the width of the pulses and the number of different lasers (wavelengths) available. Short pulses will spread and get distorted as they propagate, making determination of exact arrival time difficult. It is therefore needed to use more wavelengths, increasing instrument cost.

When some wavelengths disappear, other readings are masked by the noise at the end of the trace. The average time required to obtain an acceptable repeatability (i.e. to improve the OSNR, not the accuracy), will increase rapidly depending on the length of the fiber; acquisition time may reach up to ten minutes per trace. The limiting distance may then be estimated as 70 km. On the other hand, short distances difficult the measurement. In fact, an OTDR shows strong limitations due to its clock, synchronization and pulse repeatability; the minimum distance can be estimated to be around 10 km.



	Phase Shift	CD-OTDR
Application	Long-haul	Metro and Access
Measurement	Two-ended	Single-ended
Accuracy	Good	<5% with a 6- $\lambda$ OTDR

Table 3-3: CD-OTDR and Phase shift comparison (source [34])

The industry standards IEC60793-1-42 states: “*Investigations have shown that in practice the approximation coefficient will be small over the wavelength range 1200 nm to 1600 nm. Therefore, a simplified four term fit can also be used*” and “*The measurement wavelengths shall span the zero dispersion wavelength,  $\lambda_0$ , or contain at least one point within 100 nm of  $\lambda_0$  to use these data for calculation of  $\lambda_0$* ”.

Consequently, the use of the OTDR with four wavelengths, including one in the 1310 nm region, is well adapted for G.652 fiber CD measurement and determination of the zero wavelength value. Using the pulse delay method within the C-band only will prevent measuring the  $\lambda_0$  around 1310 nm with confidence.

DWDM networks employ Raman amplification; fiber type must be known at system design and optimization stages to optimize Raman gain. An effective way to achieve this is using a CD-OTDR, automatically obtaining fiber length and CD coefficient.

## P-OTDR

When upgrading old fiber links to higher bit-rate, working with a mix of newer and older fibers means, it might be encountered large PMD variations in a given link span.

High PMD on old links is mostly caused by one or few bad sections. This can be traced back to the fabrication process of old fibers, where PMD was not even measured. Sections with very high PMD were therefore unknowingly introduced in cables.

Network operators are looking for ways to locate the high-PMD sections, in order to replace them when upgrading their systems.

A polarization optical time-domain reflectometer (P-OTDR), also known as distributed PMD analyzer, measures the degree of polarization of the backscattered light as a function of distance [35], allowing to sectionalize the fiber based on its PMD characteristics.

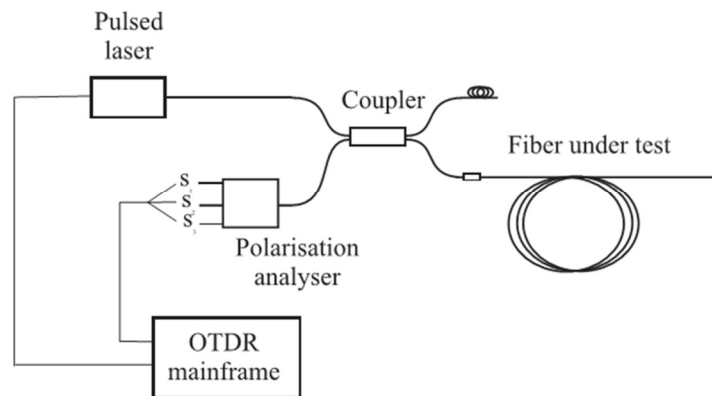


Figure 3-9: P-OTDR block diagram (source [35])

The basic setup for a P-OTDR is shown in Figure 3-9. A pulsed laser source emits short polarized pulses, which are sent to the FUT through a coupler. Back reflected light is routed to a polarization analyzer, which extracts Stokes components as a function of time. This allows obtaining the SOP of the backscattered light as a function of the distance of the scattering point.

---

## 4 Characterization results

The data collected along this work is divided in laboratory and field data.

The laboratory data was acquired in ISEL ADEETC Telecom laboratory and in EPOCH TELECOMSOLUTIONS training center in Linda-a-Velha – Oeiras, Portugal.

The field data was gathered through measurements carried out on deployed communication cables, located in the region of ‘Lisboa e Vale do Tejo’, Portugal, part of PORTUGAL TELECOM (PT) optical network infrastructure.

Equipment list is available in appendix A; main specifications are provided along next paragraph; most of the equipment has been kindly provided by ESPECTRAL TELECOMUNICAÇÕES which is Portugal’s sale representative of the manufacturer JDSU.

### 4.1 Overview of measurements

Laboratory tests had the scope not only to collect some data, but also to make first experiences and learn how to correctly operate the sophisticated equipment that would have been later used in field measurements.

In laboratory tests the main objective was to study and collect data related to connectors and bend insensitive fibers loss characteristics. Due to the short fiber lengths available, and the favorable ambient conditions, impairments such as PMD could not be effectively evaluated without the aid of extra resources (e.g. a thermal chamber, for the verification of temperature effects). Nevertheless AP, CD and PMD measurements were performed on an available piece of 12-fiber G.652 optical cable, still wounded in the reel, splicing together several fibers of the cable and obtaining a total length of roughly 38.5 km. Cable is of recent manufacture (approximately 10 years old). Results did not show any deviation from the expected or any peculiarity, they were completely according to specification. Worth to mention only that the PMD measurement showed a low and very stable value along a 48 hour test, with an average PMD coefficient below  $0.1 \text{ ps/km}^{1/2}$  and a standard deviation in the order of  $10^{-3} \text{ ps/km}^{1/2}$ . Instrument used was the 81MRDISPAP, whose characteristics will be presented in the next paragraphs. The measured PMD values can be considered realistic, considering that we are utilizing a relative new cable, still wrapped around the reel and located in a very stable thermal environment (EPOCH laboratory).

Regarding the field measurements, a short description of the three deployed optical fiber characteristic and locations is provided here; the three links are build *ad-hoc* from dark fibers (not carrying traffic) for the sole purpose of these measurements.

First span consists of two G.652 type fibers (from same cable), laid mostly in conduit, going from Lisbon to Setúbal. Cable crosses the Tagus River over the “25 Abril” Bridge and follows A2/IP7 highway till Setúbal; in Setúbal, the two fibers are spliced making a single span with both ends accessible at PT Picoas central where the test equipment is connected. This span will be referred in short as “LX”.

Second span consists of G.652 fiber, deployed mostly into aerial cable, located in the proximity of Samora Correia. Link is built over four fibers of the same cable, connected together two by two, in one of the extremities via connectors. In Samora Correia PT central, the four fibers are accessible and connectorized; two fibers are connected together by means of a patch cord, making a single span with both ends available in the central, where the measurement equipment is connected. This span will be referred in short as “SC”.

Third span consists again of G.652 fiber, deployed mostly into aerial cable, located in the proximity of Alcácer do Sal. Link is built over four cables that connect PT centrals in Carvalhal and Torrão, passing through Comporta, Alcácer do Sal and Casa Branca do Sado; extremities are connected together making a single span with both ends accessible in Alcácer do Sal central. This span will be referred in short as “ALC”.

A resume of link details is shown in Table 4-1. All the fibers are G.652 with a mix of A and D type; fiber vintage covers at least two decades, but exact dates are unknown.

Short name	Access location	Length	Plant type	Fiber type	Description
LX	Lisboa	115.35 km	Mostly conduit	G.652 A & D	Loop between Lisbon and Setúbal
SC	Samora Correia	106.00 km	Mostly aerial	G.652 A & D	Loop in the proximity of Samora Correia
ALC	Alcácer do Sal	155.00 km	Mostly aerial	G.652 A & D	Loop between Carvalhal and Torrão, with access point in Alcácer do Sal

Table 4-1: Links details

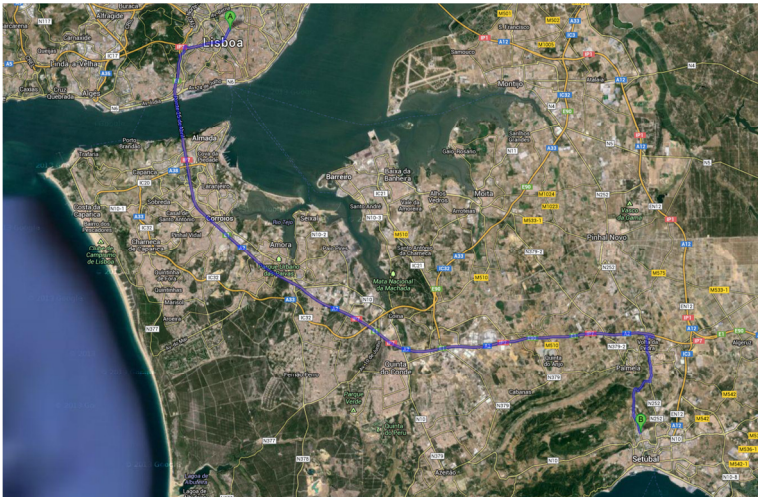


Figure 4-1: Geographic location of span Lisboa-Setúbal-Lisboa (blue line)

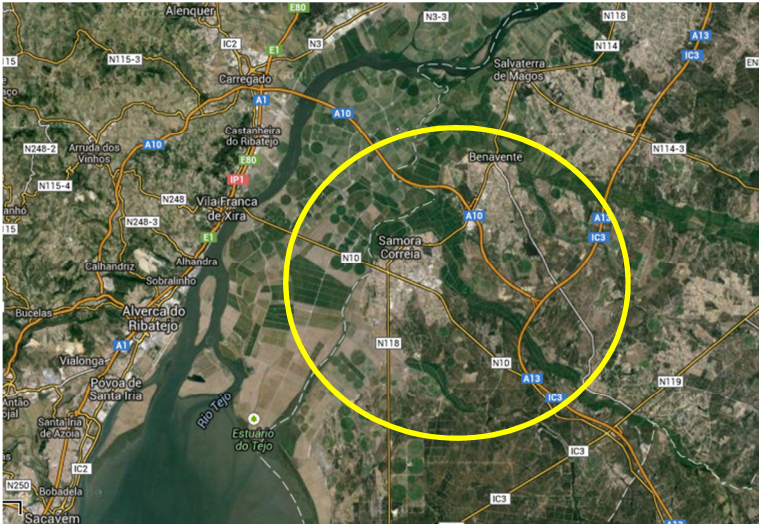


Figure 4-2: Geographic location of Samora Correia span (exact fiber path is not known)

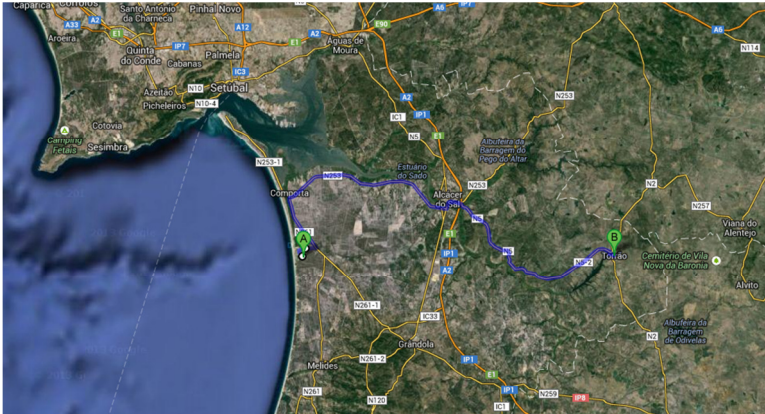


Figure 4-3: Geographic location of Alcácer do Sal span (blue line)

Only a subset of the measurements defined in ITU-T G.650.3 has been performed over the mentioned links; namely: optical time domain reflectometry (solely as pre-verification), attenuation profile, chromatic dispersion, and polarization mode dispersion. The accessible connectors are carefully cleaned before connecting any equipment; but due to the unavailability of magnifier instruments, no visual inspection is performed to assess cleanness.

Measurements are performed recurring to the JDSU Platform 6000A, which is a handheld modular platform that can be configured with pluggable modules, according to test needs. The modules equipped to perform the desired measurements are the following:

- E8136C module, which implements the OTDR functionality;
- Optical Dispersion Measurement (ODM) module E81DISPAP (or 81MRDISPAP), which combines spectral attenuation profile, chromatic dispersion, and polarization mode dispersion testing capabilities;
- OBS-5550 optical broadband source (for AP, CD and PMD measurements).

JDSU instruments allow save data into a file for long term storage, post visualization and post processing; files can be visualized directly in the Platform 6000A or in a personal computer recurring to the software *FiberTrace Viewer*, freely available for download on the JDSU website.

All the links have been kindly prepared and verified by Portugal Telecom staff, so expected attenuation and length were known at the time of our measurements. OTDR measurements were nevertheless performed prior to the start of our characterization with the sole purpose of verify the presence of any break and cross check the reported length.

## **OTDR**

Reflectometry verification is performed using JDSU E8136C module, whose main characteristics are presented in Table 4-2. Verification is performed as unidirectional measurement; an 800 m launch cable (G.652.D fiber) is used.

Central wavelength	1310/1550 $\pm$ 20 nm 1625 $\pm$ 10 nm
Dynamic range	45/45/44 dB
Pulse width	2 ns to 20 $\mu$ s
Event dead zone	0.6 m
Attenuation dead zone	2 m

Table 4-2: E8136C OTDR module technical specifications

### Light source

The optical broadband source used is an OBS-550 which combines, in a single device, the functionalities needed (in terms of light source) to perform the AP, CD and PMD measurements. The optical source contains an EDFA that can be enabled setting device to “High Dynamic Mode”, providing higher emitted spectral power density at the cost of a reduced optical band coverage; this functionality has been used for the LX link, since the available ODM module was of Medium Range (MR) type and for the ALC link due to its total attenuation. Table 4-3 resumes OBS main characteristics.

Wavelength range	1460 to 1640 nm (C+L) <sup>(1)</sup> 1525 to 1570 nm <sup>(2)</sup>
Output power level	> 8 dBm <sup>(1)</sup> > 16 dBm <sup>(2)</sup>
Spectral power density	> -30 dBm/0.1 nm <sup>(1)</sup> > -46 dBm/0.1 nm <sup>(2)</sup>
State of polarization	Polarized (PMD func.) and non-polarized

<sup>(1)</sup> Broadband mode

<sup>(2)</sup> High Dynamic Mode

Table 4-3: OBS-550 source technical specifications

### Attenuation profile module

The attenuation profile measurement is obtained from JDSU ODM module E81DISPAP (E81MRDISPAP for LX link), coupled with a broadband source OBS-550. ODM module embeds a tunable filter, for the selection of desired wavelength, and a broadband power meter; the spectrum analyzer compares the broadband source reference signal to the resulting signal at the end of the fiber under test, retrieving attenuation characteristics.

ODM AP main specifications are reported in Table 4-4 (E81MRDISPAP presents similar characteristic with main difference being in the dynamic range, reduced to 45 dB). As specified in instrument's manual, it is necessary to previously reference the source to the measurement instrument as shown in Figure 4-4 (a). Measurement is possible in the OBS-550 supported band, in 1 nm steps. Connection of source and measurement instrument to the FUT is depicted in Figure 4-4 (b).

	E81MRDISPAP	E81DISPAP
Wavelength uncertainty	$\pm 0.1$ nm	$\pm 0.1$ nm
Measurement time	3 s	6 s
Measurement uncertainty	0.003 dB/km @ 1550 nm 0.004 dB/km @ 1625 nm	0.003 dB/km @ 1550 nm 0.004 dB/km @ 1625 nm
Dynamic range	45 dB	55/60* dB *with source in high dynamic mode

Table 4-4: E81MRDISPAP / E81DISPAP AP module specifications

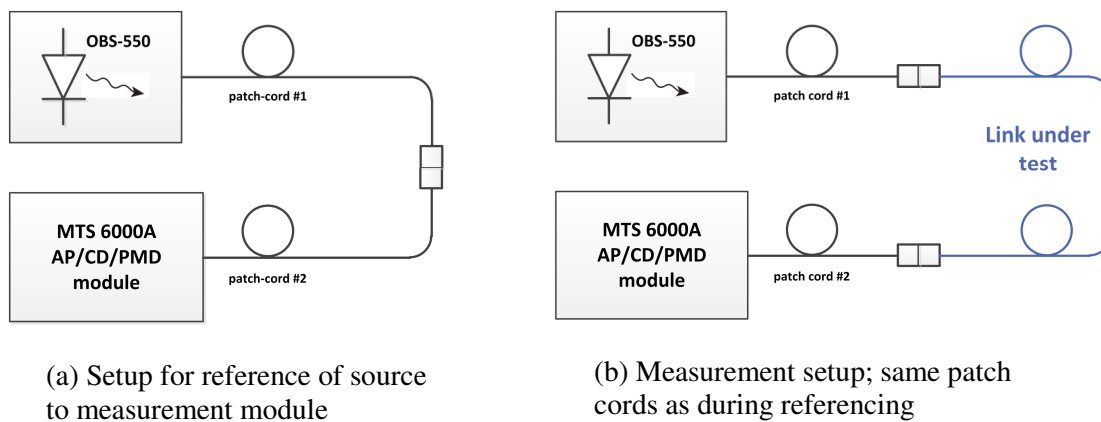


Figure 4-4: Arrangements for: (a) source/module reference;  
(b) link measurement

## Chromatic dispersion module

Also chromatic dispersion measurement is obtained from the same JDSU ODM module E81DISPAP (E81MRDISPAP for LX link), coupled with the broadband source OBS-550. The measurement method is based on the Phase Shift method. The group delay is measured at selected wavelengths, while the delay for other wavelengths, not directly measured, is interpolated by a numerical fitting algorithm (type quadratic, as recommended in user manual for our measurement conditions). The phase measurement



is performed over the entire wavelength range of the broadband source. It is required to reference the measurement instrument to the source (same arrangement as for AP referencing, shown in Figure 4-4 (a)). Connection of equipment to the optical link is as for AP measurement, and depicted in Figure 4-4 (b).

	E81MRDISPAP	E81DISPAP
Wavelength range	1260 – 1640 nm	1260 – 1640 nm
Wavelength uncertainty	±0.1 nm	±0.1 nm
Minimum length	1 km	1 km
Dynamic range	33 dB	45/55* dB * with source in high dynamic mode
Zero disp. uncertainty	n/a	±1.5 nm For 80 km of G.652
Dispersion uncertainty	±0.06 ps/nm/km For 80 km of G.652 over 1530 to 1570 nm	±0.05 ps/nm/km For 80 km of G.652 over 1530 to 1570 nm
Measurement time	10 to 30 s	40 to 80 s

Table 4-5: E81MRDISPAP /E81DISPAP CD module specifications

### Polarization mode dispersion module

Also polarization mode dispersion measurement is integrated in the ODM module E81DISPAP (E81MRDISPAP for LX link), and again the broadband source OBS-550 is used. The measurement is based on the fixed analyzer technique with Fourier transform. Measurements are taken over the C and L bands, in strong coupling mode. No calibration between source and instrument is necessary. Connection of equipment to optical span is as for AP measurement, and depicted in Figure 4-4 (b).

	E81MRDISPAP	E81DISPAP
Measurement range	0.08 to 130 ps	0.08 to 60 ps
Absolute uncertainty	±0.02 ps ±2% PMD	±0.02 ps ±2% PMD
Measurement time (min)	8 s	16 s
Dynamic range	45 dB	58/65* dB *with source in high dynamic mode

Table 4-6: E81MRDISPAP /E81DISPAP PMD module specifications

## Source and module joint characteristics

The following table maps, for each link, OBS source and ODM module configurations and characteristics:

		LX	SC	ALC
OBS		1525 - 1570 nm (C-Band)	1460 - 1640 nm (C+L-Band)	1525 - 1570 nm (C-Band)
		High Dyn. Mode	Broadband Mode	High Dyn. Mode
Module type		E81MRDISPAP	E81DISPAP	E81DISPAP
ODM	AP Dyn. Range	45 dB	55 dB	55 dB
	CD Dyn. Range	33 dB	45 dB	45 dB
	PMD Dyn. Range	45 dB	58 dB	58 dB

Table 4-7: OBS/ODM characteristics according configuration for each link

## 4.2 Characterization of attenuation and losses

### Bending losses

The analysis of macro-bending induced losses has been conducted over Corning ClearCurve© XB optical fiber; according supplier, fiber exceeds ITU-T recommendation G.657.A1.

The fiber<sup>8</sup> is wrapped around different metallic mandrel of various sizes and the induced losses are measured; injected optical signal is obtained from a Grandway© F2H series laser source, covering typical FTTx wavelengths (1310, 1490 and 1550 nm). Output power is measured with a Grandway© FHP3P01 optical power meter. Arrangement is depicted in Figure 4-5.

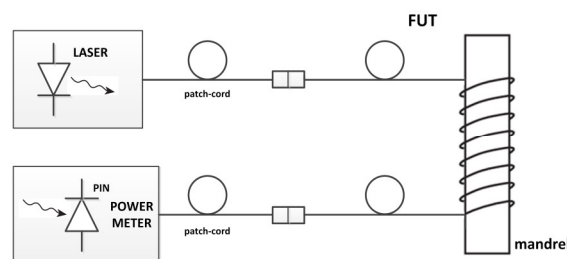


Figure 4-5: Experimental set-up for macrobending losses measurements

<sup>8</sup> Bare fiber, with exposed coating

Fiber performance (loss) is influenced by the mechanical stress applied. The FUT is wrapped manually around the mandrel, keeping in attention to maintain a good adherence and obtain an exact curvature, but without any control on the applied force. Same tests have been performed also with a cabled fiber; the cable structure (jacket and strengthening layer) strongly counteracts the winding making the operation not easy and provoking cable twirl; this fact introduces more uncertainty on the measurement.

Insertion loss measured with FUT in straight position is taken as reference point (IL = 0 dB); successively, fiber is wind around the mandrel and cumulative insertion loss is measured for each complete turn. Measurements are taken for 1310, 1490 and 1550 nm wavelengths, and for mandrel diameter of 16, 12, 10 and 8 mm. Different injected power levels, in the range -2 to -7 dBm, are tested without any noteworthy change on the resultant insertion loss.

Figures 4-6 – 4-8 show the results obtained with the cabled fibers; two specimens, indicated as FUT1 and FUT2, are verified. Notice that measurements with 8 mm mandrel is reported only for 1310 nm wavelength since, for longer wavelengths and after first wrap, losses became extremely high; also, no losses are observed for the 1310 nm wavelength with mandrel diameter above 10 mm width, so results are omitted.

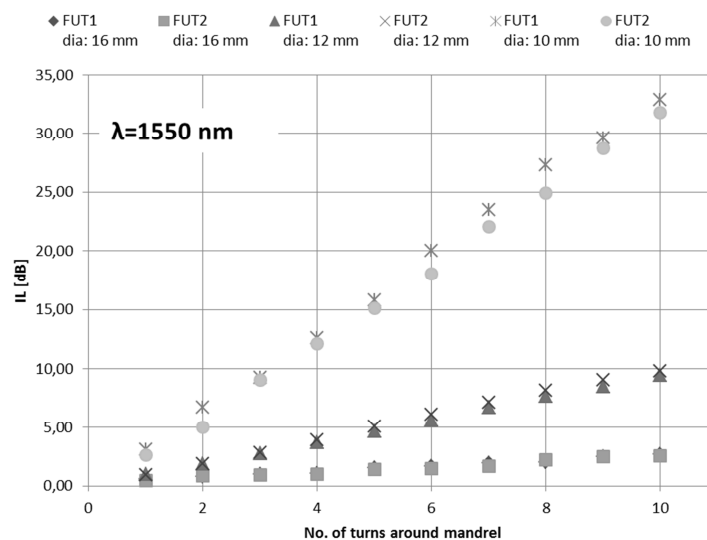


Figure 4-6: Power loss variation according number of wraps around mandrels of different sizes for cabled fibers ( $\lambda = 1550$  nm)

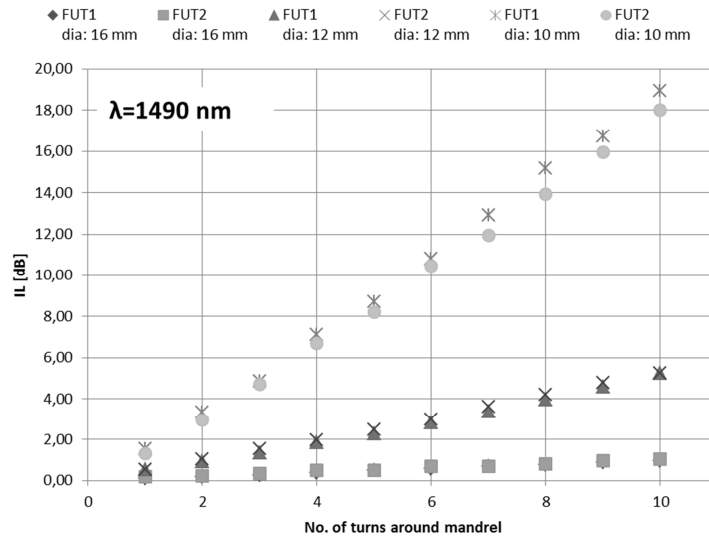


Figure 4-7: Power loss variation according number of wraps around mandrels of different sizes for cabled fibers ( $\lambda = 1490$  nm)

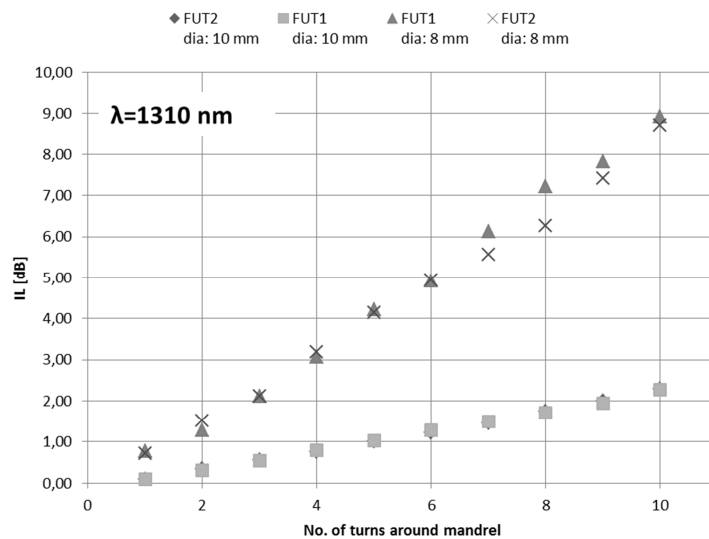


Figure 4-8: Power loss variation according number of wraps around mandrels of different sizes for cabled fibers ( $\lambda = 1310$  nm)

The obtained results show linear behavior between loss and number of turns, with a slope dependent on the radius of curvature. Fiber performance, not only exceeds ITU-T G.657.A1 specification, but stays below G.657.B2 limits, as shown in Figure 4-9.

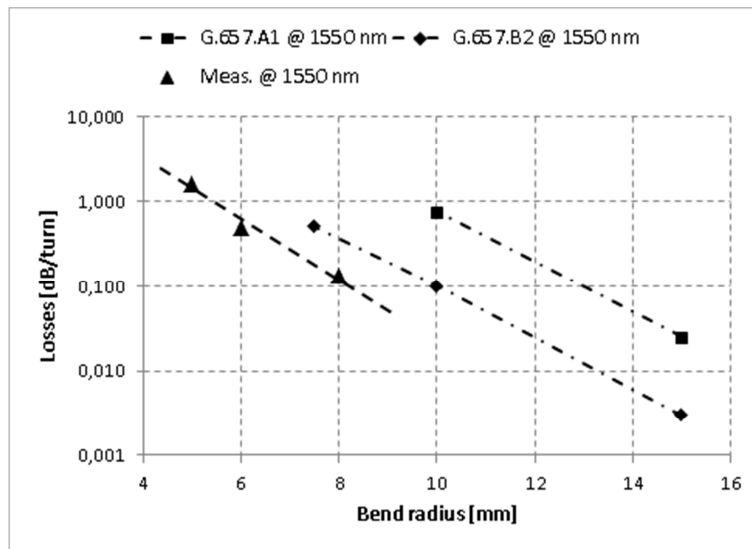


Figure 4-9: Comparison between measured data and ITU-T G.657 specification at 1550 nm

## Connector losses

Connectors' insertion losses were obtained from OTDR traces.

Connectors were placed at extremities of several cables of different lengths, ranging from tens of meters to some kilometers. To perform the desired measurements, OTDR settings were configured according to the different links characteristics. Acquisition time was set to its maximum (5 minutes). All the connectors were factory installed<sup>9</sup>. To assess the repeatability of the measurement and the connection quality, some samples were measured several times, after disconnecting and reconnecting the connectors. No noteworthy variation of the insertion losses was noticed.

An example of the measurement of connector loss at 1550 nm from the OTDR trace, is shown in Figure 4-10; in this case loss is 0.359 dB and return loss is approximately -63.0 dB.

<sup>9</sup> Connectors that have been applied to the fiber and/or cable in a controlled factory environment, as opposed to so called "field installable" connectors, that are applied to the fiber by an installer in field conditions.

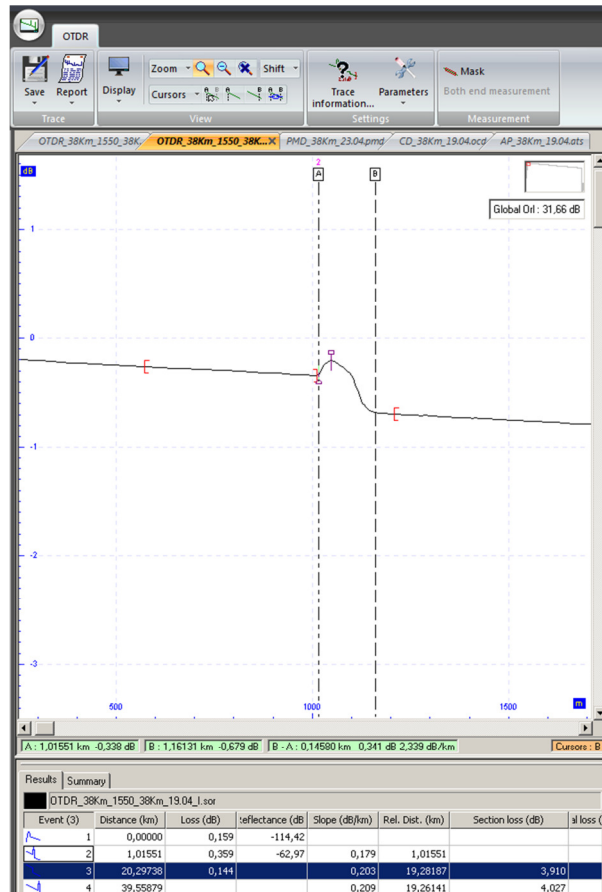


Figure 4-10: Measurement of connector loss from OTDR trace

The tested connectors were all SC/APC type. The SC type is largely diffused in PON implementations because of its design, which provide robustness and allows dense packaging; additionally, angled terminations are preferred for networks carrying RF video overlay which are typically very sensitive to Fresnel reflections.

Connector losses (10 different samples) have been measured for 1310, 1550 and 1625 nm wavelengths. Obtained results are depicted in Figure 4-11.

Results are according ITU recommendation L.36, for grade D connectors. Also optical return loss was verified, and been found always below -60 dB as required by the same ITU recommendation for the APC type. This confirms the correct measurement and the quality of the connectors.

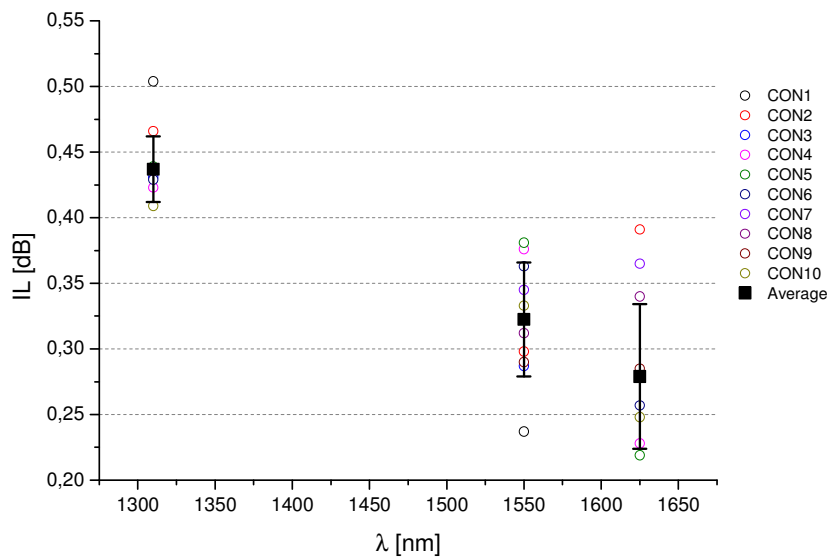


Figure 4-11: Measurement results of SC/APC connector losses at 1310, 1490 and 1550 nm

### Spectral attenuation

Spectral attenuation has been measured on the three field links: LX, SC and ALC. Resulting curves and resuming tables are following presented.

As previously mentioned, module used for the LX span is a medium range (MR) type, with reduced dynamic range in comparison to the 81DISPAP; for this reason source is configured for high dynamic mode. This combination permits to cover only the C-band; the exact range that the source (in high dynamic mode) allows is 1525 to 1570 nm. Some points are still measured outside this range; while the measurements results above 1570 nm are still inside maximum attenuation specification for G.652 cable, below 1525 nm results are violating limits and should not be considered valid. In the spectrum shown in Figure 4-12, dashed curves set G.652 maximum and minimum allowed loss coefficients [36], and vertical bars indicate source spectral range; Table 4-8 resumes measurements in main points.

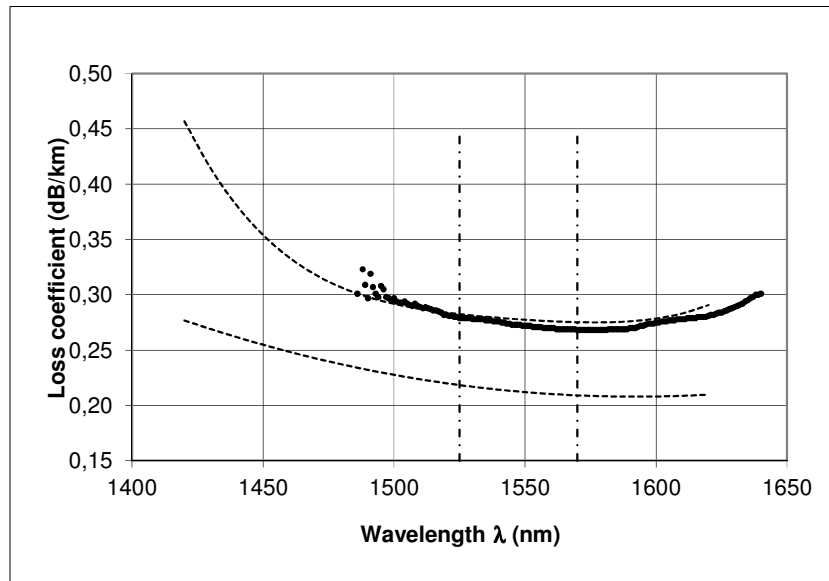


Figure 4-12: Attenuation profile (LX link)

Dashed curves show G.652 maximum and minimum loss coefficient; vertical bars indicate source spectral range when amplifier is enabled

Wavelength (nm)	Profile Attenuation (dB/km)	Span Total Loss (dB)	Comment
1486.00	0.301	34.73	First measured point*
1525.00	0.261	27.63	First valid point
1530.00	0.278	32.07	C-Band edge
1550.00	0.272	31.39	-
1565.00	0.269	31.01	L-Band edge
1570.00	0.268	30.97	Last valid point
1575.00	0.268	30.92	Attenuation minimum**
1625.00	0.284	32.73	U-Band edge*
1640.00	0.301	34.71	Last measured point*

\* outside source spectral range

\*\* considered in correspondence of minimum span total loss; due to approximation, the same attenuation coefficient value is obtained also for other wavelengths

Table 4-8: Attenuation profile, main measured points (LX link)

For the SC link, the module provides a higher dynamic range compared to the module used in LX measurements, allowing use of source in broadband mode. This combination permits to fully cover, beside C and L-band, also S and (partially) U-band. Some points are still measured outside the lower S-Band limit but are to be considered not accurate, even if they are mostly inside maximum G.652 specification. The attenuation profile is according G.652 recommendation.



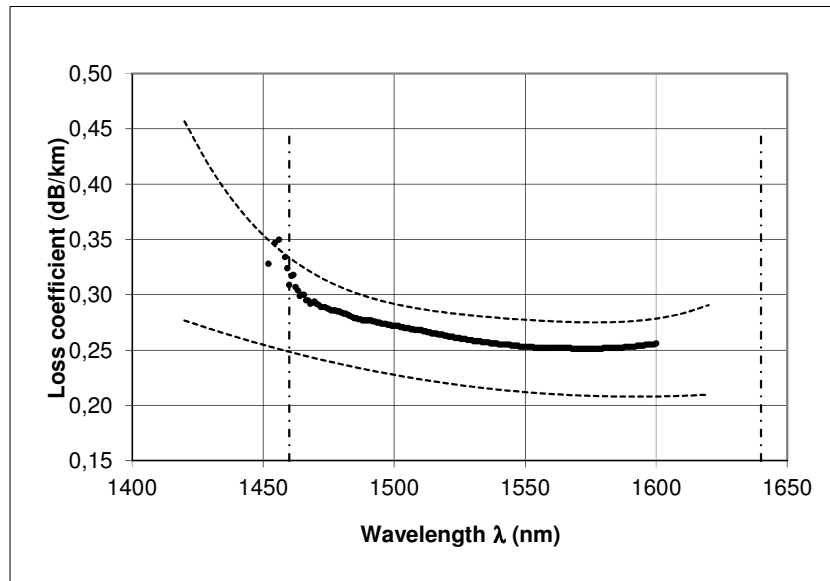


Figure 4-13: Attenuation profile (SC link)  
 Dashed curves show G.652 maximum and minimum loss coefficient; vertical bars indicate source spectral range

Wavelength (nm)	Profile Attenuation (dB/km)	Span Total Loss (dB)	comment
1452.00	0.328	34.78	First measured point*
1460.00	0.309	32.79	S-Band edge
1530.00	0.259	27.42	C-Band edge
1550.00	0.253	26.81	-
1565.00	0.252	26.67	L-Band edge
1572.80	0.251	26.63	Attenuation minimum
1624.80	0.270	28.57	U-Band edge
1640.00	0.285	30.22	Last measured point

\* outside source spectral range

Table 4-9: Attenuation profile, main measured points (SC link)

Last measured span is the ALC link; due to its long length, source is set to high dynamic mode, so same restrictions as for LX measurements apply. Also in this case measurements above 1575 nm seem accurate. The attenuation profile is according G.652 recommendation.

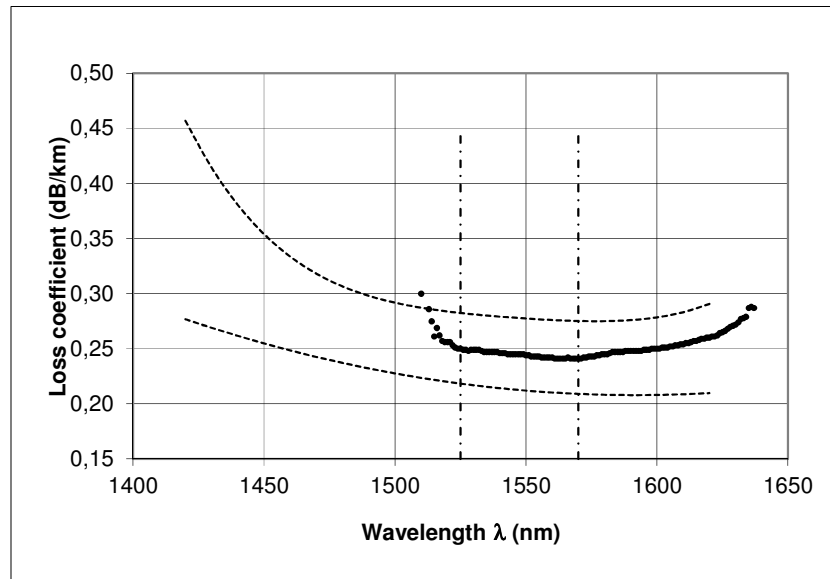


Figure 4-14: Attenuation profile (ALC link)  
Dashed curves show G.652 maximum and minimum loss coefficient; vertical bars indicate source spectral range

Wavelength (nm)	Profile Attenuation (dB/km)	Span Total Loss (dB)	comment
1510.00	0.300	46.55	First measured point*
1525.00	0.250	38.83	First valid point
1530.00	0.249	38.60	C-Band edge
1550.00	0.244	37.85	-
1562.00	0.241	37.36	Attenuation minimum**
1565.00	0.241	37.42	L-Band edge
1570.00	0.241	37.40	Last valid point
1625.00	0.265	41.08	U-Band edge*
1637.00	0.287	44.49	Last measured point*

\* outside source spectral range

\*\* considered in correspondence of minimum span total loss; due to approximation, the same attenuation coefficient value is obtained also for other wavelengths

Table 4-10: Attenuation profile, main measured points (ALC link)

### 4.3 Characterization of dispersion effects

Here are first presented the results of chromatic dispersion measurements, followed by the polarization mode dispersion results.

## Chromatic dispersion characterization

Chromatic dispersion has been measured on the three links: LX, SC and ALC. Resulting curves and resuming tables are following presented.

For the LX link, the instrument reports the relative phase delay for the wavelength range 1527 to 1570 nm; spectrum is shown in Figure 4-15 , where dashed curves show typical G.652 maximum dispersion coefficient [36]; Table 4-11 resumes main measured points. Slope is 0.041 ps/nm<sup>2</sup>-km, below the maximum value of 0.092 ps/nm<sup>2</sup>-km specified in G.652;  $\lambda_0$  is not reported.

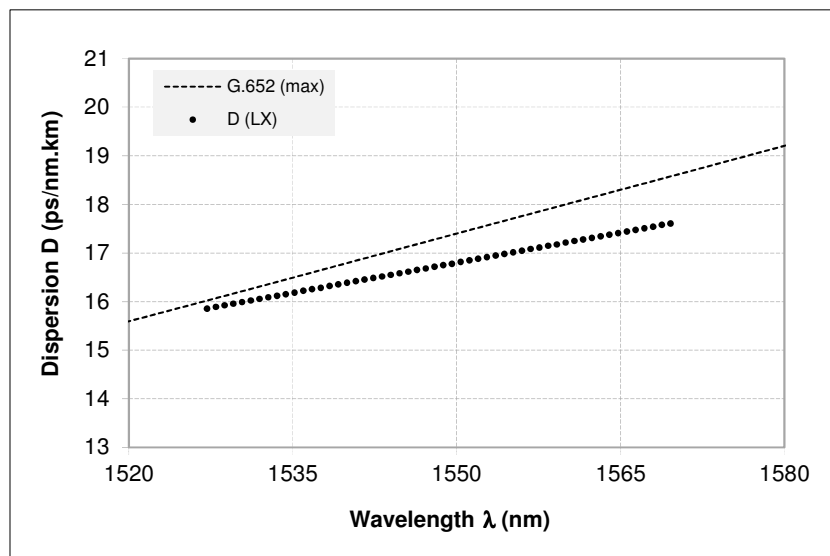


Figure 4-15: Chromatic Dispersion profile (LX link)  
Dashed curve show G.652 maximum dispersion coefficient

Lambda (nm)	Delay (ps/km)	Disp. (ps/nm)	Coef. Disp. (ps/nm.km)	comment
1527	-378.83	1828.32	15.85	First measured point
1530	-340.66	1839.73	15.95	C-Band edge
1550	-13.35	1935.03	16.76	-
1565	247.26	2007.69	17.40	L-Band edge
1570	330.35	2030.34	17.60	Last measured point
S = 0.041 ps/nm <sup>2</sup> /km				

Table 4-11: Chromatic dispersion profile, main measured points (LX link)

For the SC link the measured range is also from 1528 to 1570 nm. The chromatic dispersion coefficient spectrum is shown in Figure 4-16; Table 4-12 resumes main measured points. Reported slope is  $0.055 \text{ ps/nm}^2\text{-km}$ ;  $\lambda_0$  is not reported.

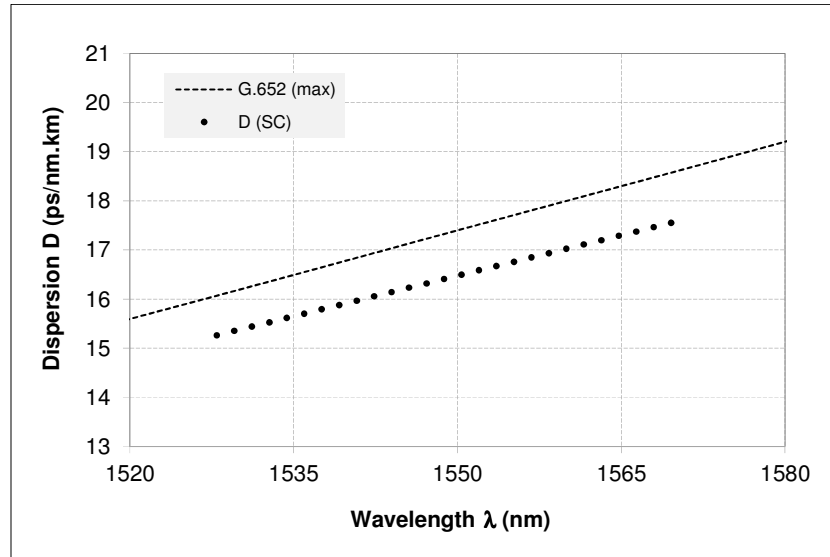


Figure 4-16: Chromatic Dispersion profile (SC link)  
Dashed curve show G.652 maximum dispersion coefficient

Lambda (nm)	Delay (ps/km)	Disp. (ps/nm)	Coef. Disp. (ps/nm.km)	comment
1528	-353.33	1617.33	15.29	First measured point
1530	-327.85	1626.66	15.35	C-Band edge
1550	3.25	1749.99	16.49	-
1564	246.42	1831.99	17.28	L-Band edge
1570	330.01	1859.99	17.55	Last measured point
$S = 0.055 \text{ ps/km/nm}^2$				

Table 4-12: Chromatic dispersion profile, main measured points (SC link)

ALC results are in all similar to previous results; spectrum is shown in Figure 4-17 and Table 4-13 resumes main measured points. Measured range is slightly inferior to the previous cases. Reported slope is  $0.052 \text{ ps/nm}^2\text{-km}$ .

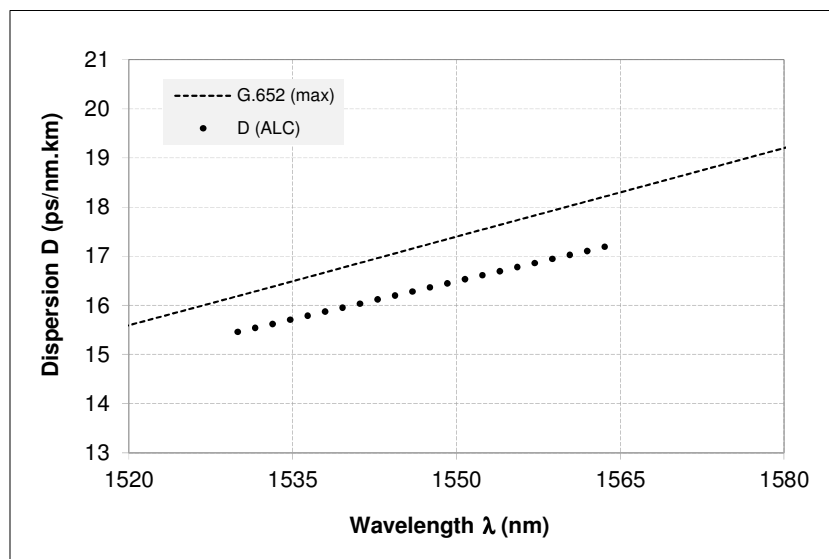


Figure 4-17: Chromatic Dispersion profile (ALC link)  
Dashed curve show G.652 maximum dispersion coefficient

Lambda (nm)	Delay (ps/km)	Disp. (ps/nm)	Coef. Disp. (ps/nm.km)	comment
1530	-322.28	2395.35	15.45	C-Band edge and first measured point
1550	-2.88	2555.08	16.48	-
1564	226.10	2664.00	17.26	Last measured point
$S = 0.052 \text{ ps/km/nm}^2$				

Table 4-13: Chromatic dispersion profile, Band edges values (ALC link)

## Polarization mode dispersion characterization

Polarization mode dispersion has been measured on the three links: LX, SC and ALC. Resulting curves and resuming tables are following presented. The measurements are performed along several days. For each link, day by day results are shown together with a merge of the data into a single plot.

The JDSU module 81DISPAP (or 81MRDISPAP) reports the mean DGD value, also designated as ‘PMD value’, adopting the fixed analyzer method with Fourier transform. The instrument measures the PMD delay at intervals of roughly two minutes in the wavelength range 1530 to 1624 nm; only the PMD value is reported, and not the mean DGD per wavelength. The other reported parameters (dispersion coefficient and SOPMD) are calculated. An example of the Fourier transform, together with its Gaussian fit, is shown in Figure 4-18. The image (view from *FiberTrace Viewer*

software) refers to the first measurement day of the LX link; the corresponding PMD value variation with time is shown in Figure 4-19.

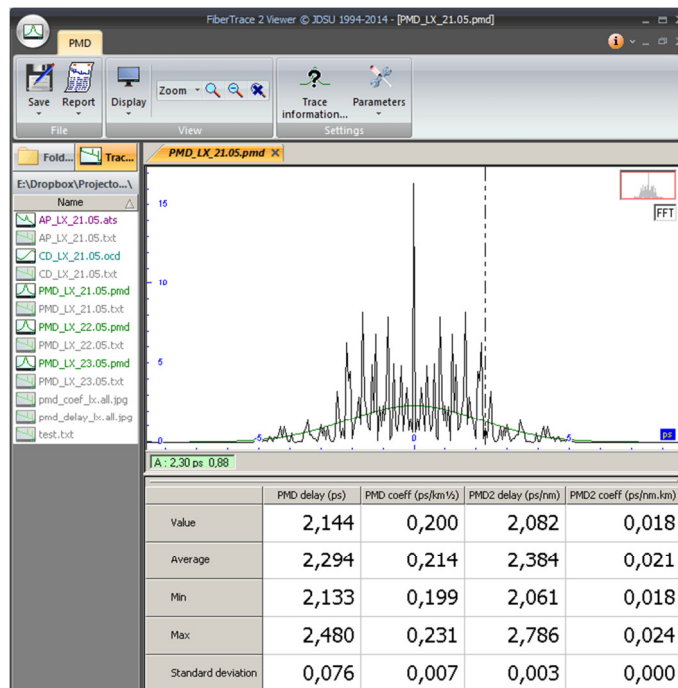


Figure 4-18: Fourier transform result of the PMD measurement of LX link (day 1) as presented in *FiberTrace viewer*

Images 4-19 to 4-21 show the PMD delay results for the LX link on a daily basis, together with the statistics reported by the instrument. Figure 4-22 shows the whole measurements over LX link in a single plot; 2069 points were taken during the test, resulting in an average PMD delay of 2.22 ps. In the image, an increment of 500 samples corresponds to approximately 13h 30m test duration; the whole test last approximately 54h, with two short interruptions in between; Table 4-17 summarizes the whole result. The average PMD calculated over the whole tests days is roughly 2.2 ps.

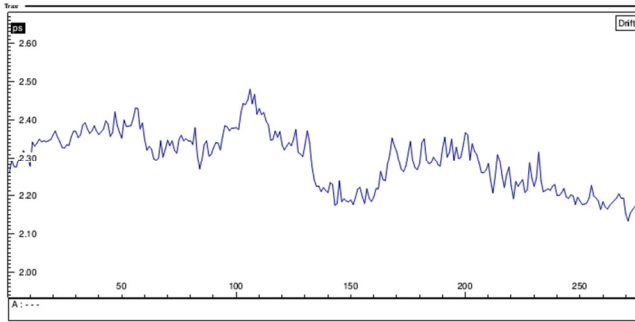


Figure 4-19: PMD delay (LX link, day 1)

	PMD Delay (ps)	PMD Coef (ps/km <sup>1/2</sup> )	SOPMD Delay (ps/nm)	SOPMD Coef (ps/nm/km)
Avg	2.294	0.213	2.383	0.020
Min	2.133	0.198	2.061	0.017
Max	2.480	0.230	2.786	0.023
Sdev	0.076	0.007	0.002	0.000
Number of acquisitions		276	Duration 7h 20m	

Table 4-14: PMD data (LX link, Day 1)

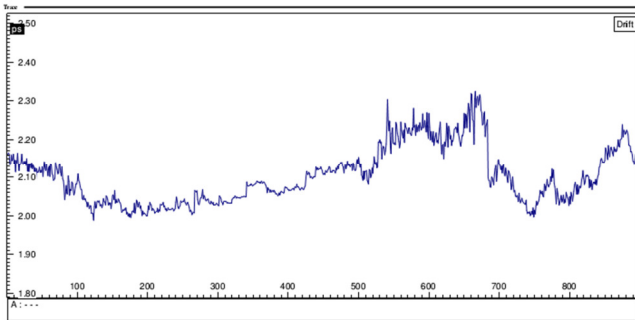


Figure 4-20: PMD delay (LX link, day 2)

	PMD Delay (ps)	PMD Coef (ps/km <sup>1/2</sup> )	SOPMD Delay (ps/nm)	SOPMD Coef (ps/nm/km)
Avg	2.104	0.195	2.005	0.017
Min	1.989	0.185	1.792	0.015
Max	2.325	0.216	2.448	0.021
Sdev	0.072	0.006	0.002	0.000
Number of acquisitions		898	Duration 23h 53m	

Table 4-15: PMD data (LX link, Day 2)

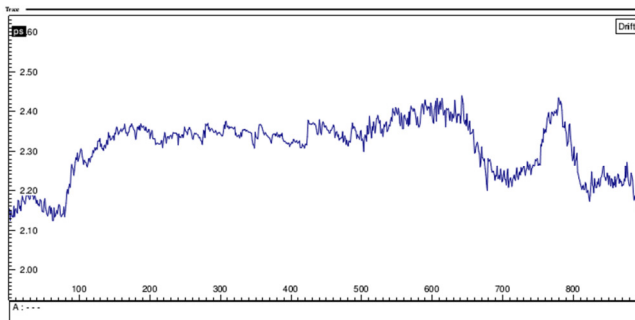


Figure 4-21: PMD delay (LX link, day 3)

	PMD Delay (ps)	PMD Coef (ps/km <sup>1/2</sup> )	SOPMD Delay (ps/nm)	SOPMD Coef (ps/nm/km)
Avg	2.309	0.214	2.415	0.020
Min	2.124	0.197	2.043	0.017
Max	2.440	0.227	2.696	0.023
Sdev	0.073	0.006	0.002	0.000
Number of acquisitions		895	Duration 23h 51m	

Table 4-16: PMD data (LX link, Day 3)

	PMD Delay (ps)	PMD Coef. (ps/km <sup>1/2</sup> )	SOPMD Delay (ps/nm)	SOPMD Coef. (ps/nm/km)
Avg	2.218	0.206	2.236	0.019
Min	1.989	0.185	1.792	0.015
Max	2.480	0.230	2.786	0.023
Sdev	0.124	0.012	0.249	0.002

Table 4-17: Resume of PMD measurement results (LX link)

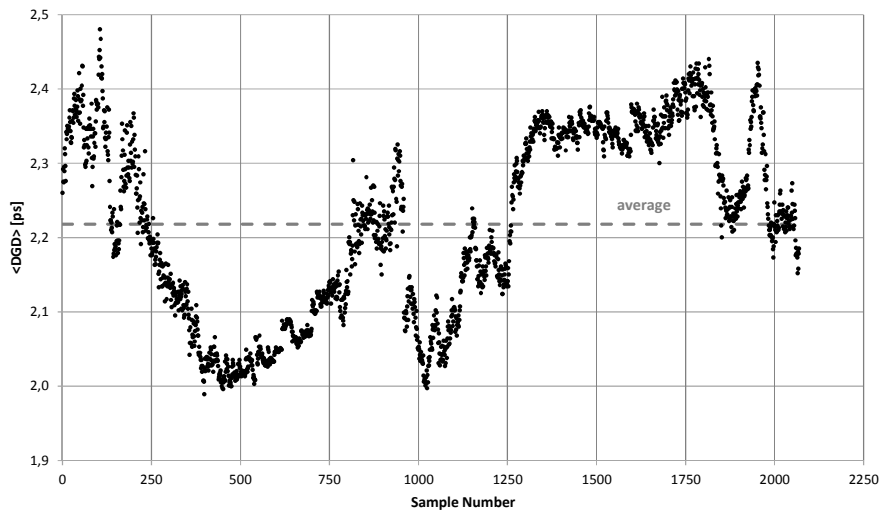


Figure 4-22: PMD delay (LX link, whole test)

Images 4-23 to 4-27 refer to the SC link. The combined result is shown in Figure 4-28; 4621 points were taken during the test, resulting in an average PMD delay of 0.54 ps. In the image, an increment of 500 samples corresponds to approximately 13h 20m test duration; the whole test last approximately 123h, with a long interruption<sup>10</sup> (around 22h), after the first day and other three short interruptions in the order of few minutes. Table 4-23 summarizes the combined results.

<sup>10</sup> This interruption, happening between sample points 1000 and 1001, is not visible in Figure 4-28



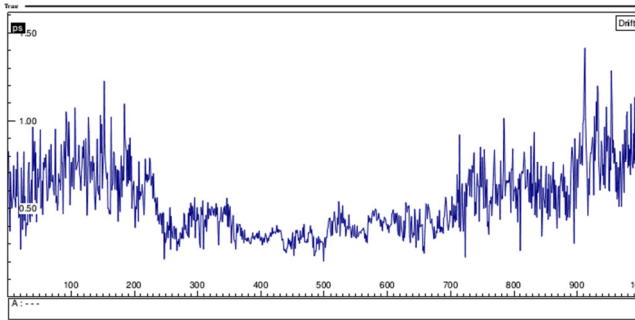


Figure 4-23: PMD delay (SC link, day 1)

	PMD Delay (ps)	PMD Coef (ps/km <sup>1/2</sup> )	SOPMD Delay (ps/nm)	SOPMD Coef (ps/nm/km)
Avg	0.542	0.052	0.133	0.001
Min	0.204	0.019	0.018	0.000
Max	1.414	0.137	0.905	0.008
Sdev	0.195	0.018	0.017	0.000

Number of acq. 1000      Duration 26h 37m

Table 4-18: PMD data (SC link, day 1)

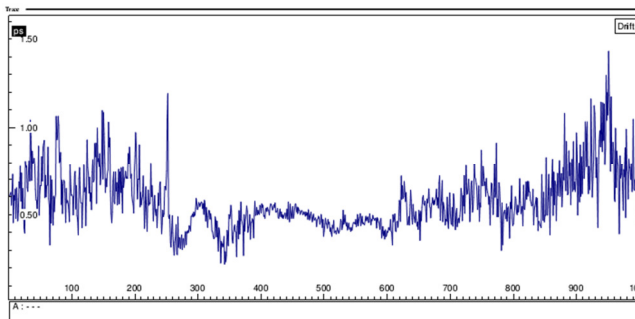


Figure 4-24: PMD delay (SC link, day 2)

	PMD Delay (ps)	PMD Coef (ps/km <sup>1/2</sup> )	SOPMD Delay (ps/nm)	SOPMD Coef (ps/nm/km)
Avg	0.582	0.056	0.153	0.001
Min	0.223	0.021	0.022	0.000
Max	1.433	0.139	0.930	0.008
Sdev	0.165	0.016	0.012	0.000

Number of acq. 1000      Duration 26h 37m

Table 4-19: PMD data (SC link, day 2)

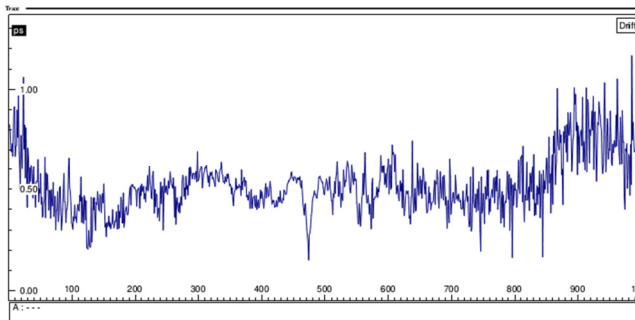


Figure 4-25: PMD delay (SC link, day 3)

	PMD Delay (ps)	PMD Coef (ps/km <sup>1/2</sup> )	SOPMD Delay (ps/nm)	SOPMD Coef (ps/nm/km)
Avg	0.524	0.050	0.124	0.001
Min	0.152	0.014	0.010	0.000
Max	1.167	0.113	0.616	0.005
Sdev	0.140	0.013	0.008	0.000

Number of acq. 1000      Duration 26h 37m

Table 4-20: PMD data (SC link, day 3)

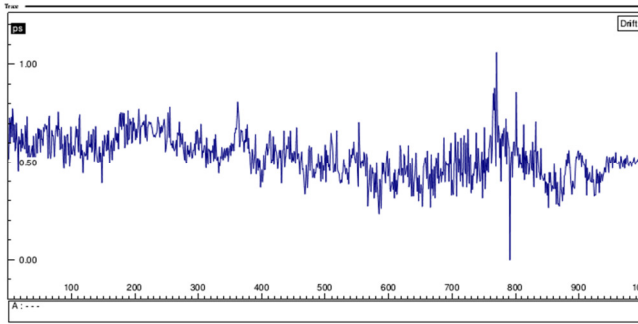


Figure 4-26: PMD delay (SC link, day 4)

	PMD Delay (ps)	PMD Coef (ps/km <sup>1/2</sup> )	SOPMD Delay (ps/nm)	SOPMD Coef (ps/nm/km)
Avg	0.531	0.051	0.128	0.001
Min	< 0.1	-	-	-
Max	1.061	0.103	0.509	0.004
Sdev	0.106	0.010	0.005	0.000

Number of acq. 1000 Duration 26h 37m

Table 4-21: PMD data (SC link, day 4)

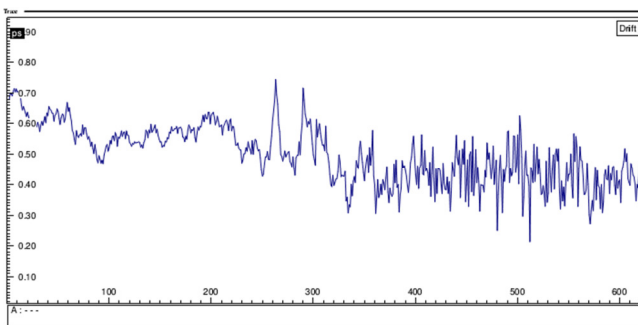


Figure 4-27: PMD delay (SC link, day 5)

	PMD Delay (ps)	PMD Coef (ps/km <sup>1/2</sup> )	SOPMD Delay (ps/nm)	SOPMD Coef (ps/nm/km)
Avg	0.500	0.048	0.113	0.001
Min	0.214	0.020	0.020	0.000
Max	0.745	0.072	0.251	0.002
Sdev	0.093	0.009	0.003	0.000

Number of acq. 621 Duration 16h 31m

Table 4-22: PMD data (SC link, day 5)

	PMD Delay (ps)	PMD Coef. (ps/km <sup>1/2</sup> )	SOPMD Delay (ps/nm)	SOPMD Coef. (ps/nm/km)
Avg	0.539	0.052	0.142	0.001
Min	0.152	0.014	0.010	0.000
Max	1.433	0.139	0.930	0.008
Sdev	0.151	0.015	0.086	0.001

Table 4-23: Resume of PMD measurement results (SC link)

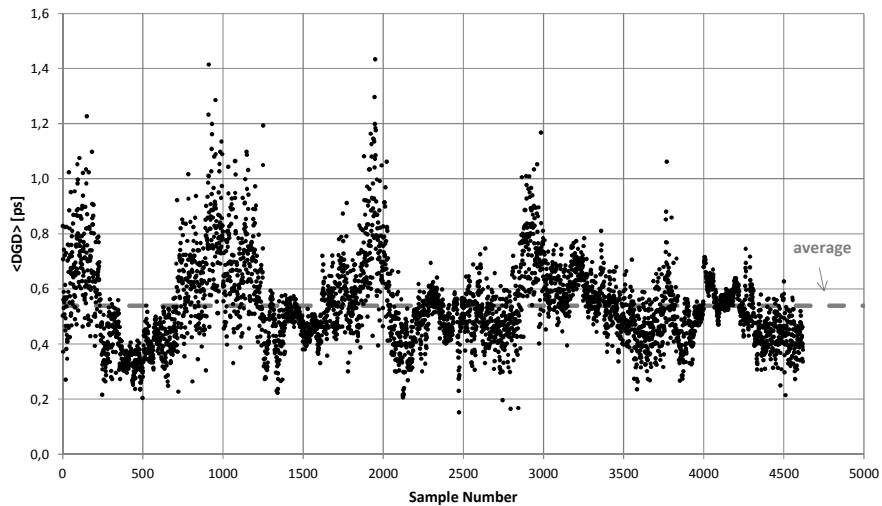


Figure 4-28: PMD delay (SC link, whole test)

Images 4-29 and 4-30 resume the measurements over the ALC link. Combined results in a single plot is shown in Figure 4-31; 2000 points were taken during the test, resulting in an average PMD delay of 1.83 ps. In the image, an increment of 500 samples corresponds to approximately 13h 20m test duration; the whole test last approximately 53h, with a long interruption<sup>11</sup> (around 18h), between the two measurements. Table 4-26 summarizes the results.

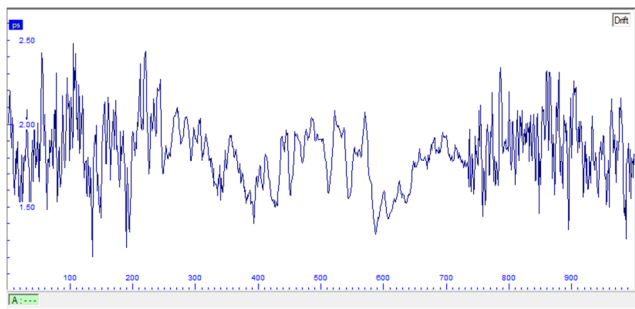


Figure 4-29: PMD delay (ALC link, day 1)

	PMD Delay (ps)	PMD Coef (ps/km <sup>1/2</sup> )	SOPMD Delay (ps/nm)	SOPMD Coef (ps/nm/km)
Avg	1.823	0.146	1.505	0.009
Min	1.206	0.096	0.658	0.004
Max	2.481	0.199	2.788	0.017
Sdev	0.196	0.015	0.017	0.000

Number of acq. 1000      Duration 26h 37m

Table 4-24: PMD data (ALC link, day 1)

<sup>11</sup> This interruption, happening between sample points 1000 and 1001, is not visible in Figure 4-31

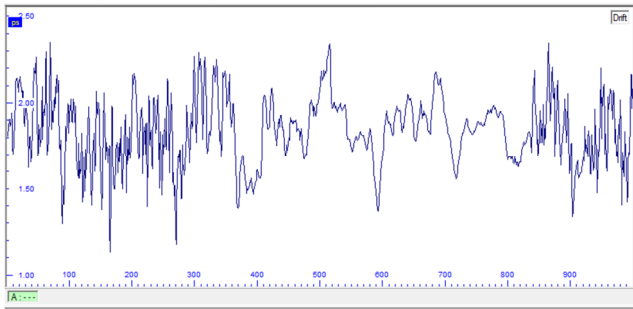


Figure 4-30: PMD delay (ALC link, day 2)

	PMD Delay (ps)	PMD Coef (ps/km <sup>1/2</sup> )	SOPMD Delay (ps/nm)	SOPMD Coef (ps/nm/km)
Avg	1.840	0.147	1.533	0.009
Min	1.133	0.091	0.581	0.003
Max	2.353	0.188	2.508	0.016
Sdev	0.193	0.015	0.016	0.000

Number of acq. 1000      Duration 26h 37m

Table 4-25: PMD data (ALC link, day 2)

	PMD Delay (ps)	PMD Coef. (ps/km <sup>1/2</sup> )	SOPMD Delay (ps/nm)	SOPMD Coef. (ps/nm/km)
Avg	1.832	0.147	1.537	0.009
Min	1.133	0.091	0.581	0.003
Max	2.481	0.199	2.788	0.017
Sdev	0.195	0.016	0.324	0.002

Table 4-26: Resume of PMD measurement results (ALC link)

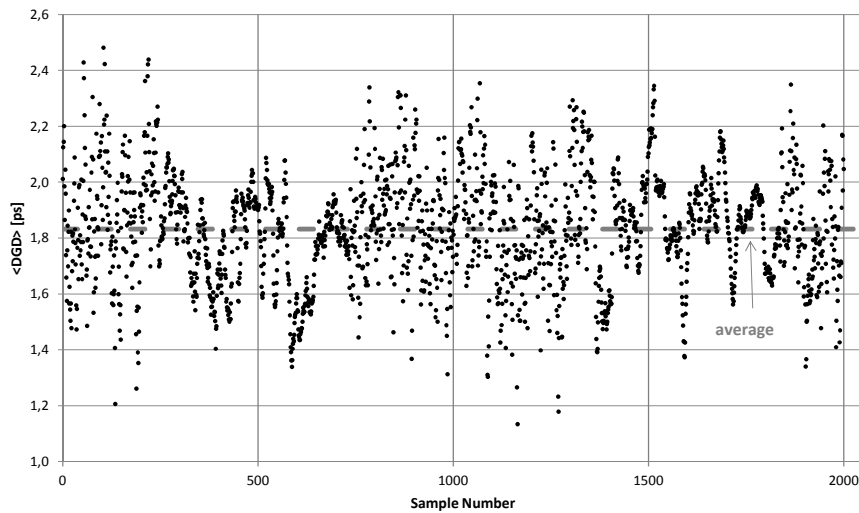


Figure 4-31: PMD delay (ALC link, whole test)

## 5 Discussion of results

### 5.1 General discussion of field results

Field results of each of the analyzed links are discussed here; Table 5-1 summarizes main measured parameters.

Short name	Length	Attenuation at 1550 nm	CD Delay at 1550 nm	PMD Delay
LX	115.35 km	31.39 dB (0.272 dB/km)	718 ps (-6.22 ps/km)	2.218 ps (0.206 ps/km <sup>1/2</sup> )
SC	106.00 km	26.81 dB (0.253 dB/km)	353 ps (-3.33 ps/km)	0.539 ps (0.052 ps/km <sup>1/2</sup> )
ALC	155.00 km	37.85 dB (0.244 dB/km)	464 ps (-2.99 ps/km)	1.832 ps (0.147 ps/km <sup>1/2</sup> )

Table 5-1: Field measurements resume

Regarding the spectral attenuation in the LX link, measured span shows 0.272 dB/km at 1550 nm. This result is in accordance with a G.652 (cabled) fiber, which sets maximum attenuation to 0.3 dB/km at 1550 nm; also the attenuation behavior in the remaining measured portion of the spectrum (excluding few sample outside the spectral range of the source) is according predictions, remaining below 0.4 dB/km in the range 1310 to 1625 nm as required by ITU-T G.652 recommendation for a cabled fiber, even if very close to typical maximum values for non-cabled fibers. Also for the SC link the AP profile is consistent with G.652 fiber type. Total losses measured by the OTDR in the 1550 nm wavelength are around 1 dB higher than that reported by the ODM module; for the 1625 nm wavelength, OTDR reports losses 0.2 dB lower. Differences have little relevance, but in any case AP measurement is to be considered more accurate. For the ALC link situation is similar; measured span shows 0.244 dB/km at 1550 nm; results are in accordance with ITU-T G.652. Total attenuation measured by the OTDR (results provided by PT) for the 1550 nm wavelength is around 1 dB higher than that reported by the ODM module; again, AP measurement is to be considered more accurate.

Note that the reported total attenuation obtained contains also the excess losses (bend, splices and connector losses), that add to the overall fiber attenuation. As example, let assume a 100 km link with 2 dB excess losses; excess losses contribute with 0.02 dB/km to the overall attenuation coefficient. If a splice is defective and adds

an extra dB of losses, we have an ulterior increase of just 0.01 dB/km; in a spectral attenuation measurement a defective splice is simply masked in the overall link loss. Bad splices, dirty connectors or bends can “silently” affect power margins. This example explain the success that the OTDR gained among the measurement and troubleshooting optical equipment, because of its ability to detect (and localize) such high loss events along the link.

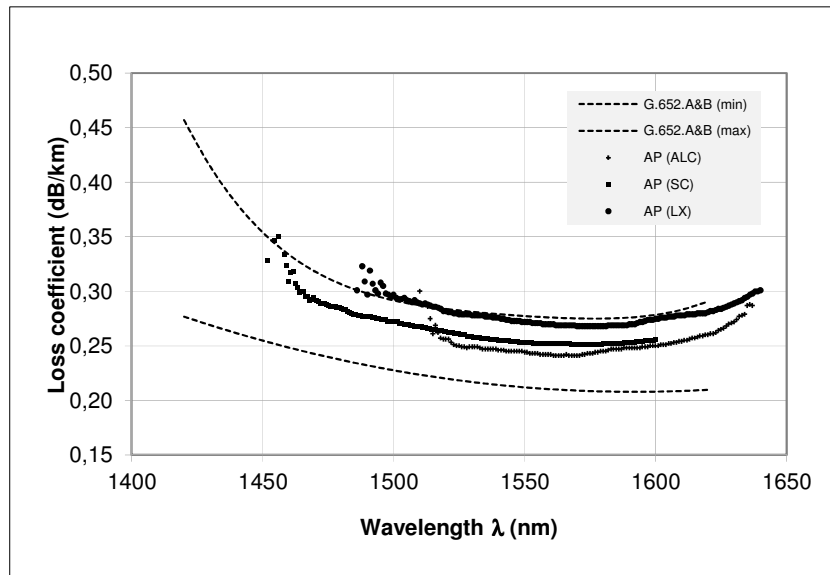


Figure 5-1: AP results for the three measured links

Also chromatic dispersion behavior matches a G.652 fiber. For all the measured links the dispersion value at 1550 nm is very close to the typical 17 ps/nm/km, and slope is below the maximum ITU-T limit of 0.092 ps/(nm<sup>2</sup> km). ITU-T requires at least one measurement close to the 1310 nm for proper approximation curve fit, this is due to the reduced accuracy that Sellmeier equation fitting (quadratic fitting) can provide outside de 1550 nm band; zero dispersion wavelength cannot be correctly calculated from measured data.

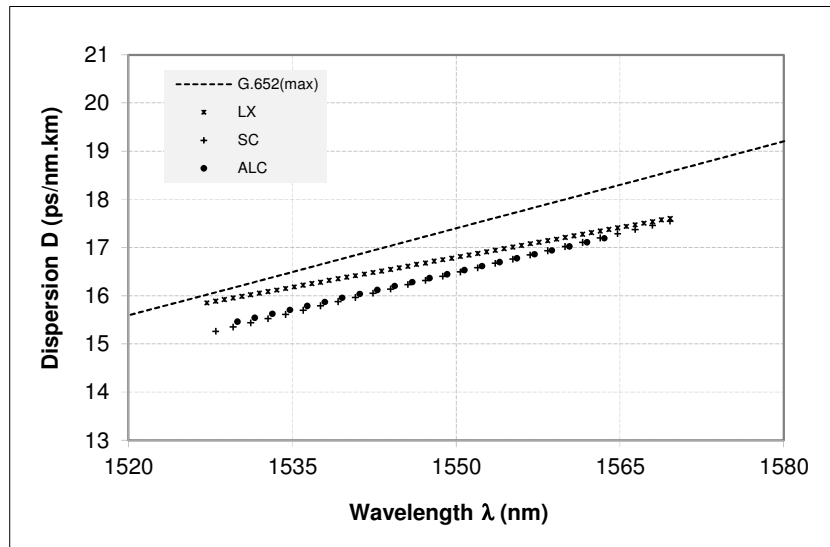


Figure 5-2: CD results for the three measured links

Unlike system impairments caused by chromatic dispersion, signal distortion caused by PMD has a stochastic nature and is dependent on “environmental” conditions to which cable is subjected, like temperature and/or applied mechanical stress.

The three links show an average dispersion coefficient well below a G.652.A fiber, which requires  $0.5 \text{ dB/km}^{1/2}$  maximum; actually PMD value satisfies G.652.B specification ( $0.2 \text{ dB/km}^{1/2}$  maximum) excluding LX links, which shows a value slightly above. Surprisingly low is the mean value for the SC link, that reads  $0.05 \text{ dB/km}^{1/2}$ ; this value make think that cable is probably quite new.

Histograms of the PMD distributions are presented in Figure 5-15. Further investigations over possible correlation between polarization mode dispersion and environment and analysis of the PMD distributions will be conducted on next sections.

## 5.2 Correlation of PMD and environment

Instantaneous DGD value is influenced by the environment conditions. The sources of these changes are variations in the magnitude and/or orientation of the birefringence vector over time caused by perturbations such as temperature, pressure, stress, cabling orientation, bending, aging, etc. [22].

An increase in the fiber's ambient temperature results in a change in the fiber length due to thermal expansion. Moreover, the different thermal expansion characteristics of the coating and buffer materials result in internal stress on the fiber. Also, temperature

affects the fiber material modifying the refractive index. It is then expectable that temperature has influence on fiber dispersion.

Several works investigated the correlation between polarization impairments and temperature. In [27], Cameron et al. demonstrates the fiber PMD is sensitive to changes in temperature and that the rate of PMD change depends on the rate of temperature change. Experiment was conducted on a spooled fiber and temperature was increased at a rate of 0.5 °C/min; a change of roughly 50% was observed for a thermal variation of 40 °C. Authors also tested a buried link, observing no more than 10% relative changes in PMD for a temperature in the range of 19 to 9 °C and decreasing at a rate of 0.02 °C/min. On measurement over an aerial cable, Cameron et al. reported a relative change of around 20% when temperature increased at 0.02 °C/min. Observed variation is understandable since an aerial cable is subject to larger and faster temperature change than a buried one.

Also Galtarossa et al. [37] have shown large variations of PMD in buried links (in which some fiber connectors were located in cabinets above the ground) again related to the fast changes in ambient temperature; authors reported a relative variation in Stokes parameter of 100% in a period of 20 minutes with temperature increasing at a rate of 0.5 °C/min. In addition, authors referred an “irreversible” behavior, meaning that temperature changing in the opposite direction did not reestablish previous status. The strongest fluctuations in DGD occurred at sunrise and sunset.

In order to investigate the correlation with temperature collected data is analyzed against temperature measured by nearby weather stations. It would be hard to obtain detailed temperature distribution and its dynamics along long links, so temperature data should be considered with the deserved caution and as indicative information.

For the LX link, temperature is obtained from weather stations of Lisboa/Portela and Montijo (located around 30 km from both Setúbal and Lisboa); temperature variation is shown in Figure 5-3. In the analysis that will follow, the average temperature between the two stations is considered. In the LX link, there was the suspect that traffic over “25th Abril” bridge (provoking vibration of the bridge structure, and consequently of the cable) might had influence over the PMD value. However, considering traffic peak hours, no correlation seems visible.



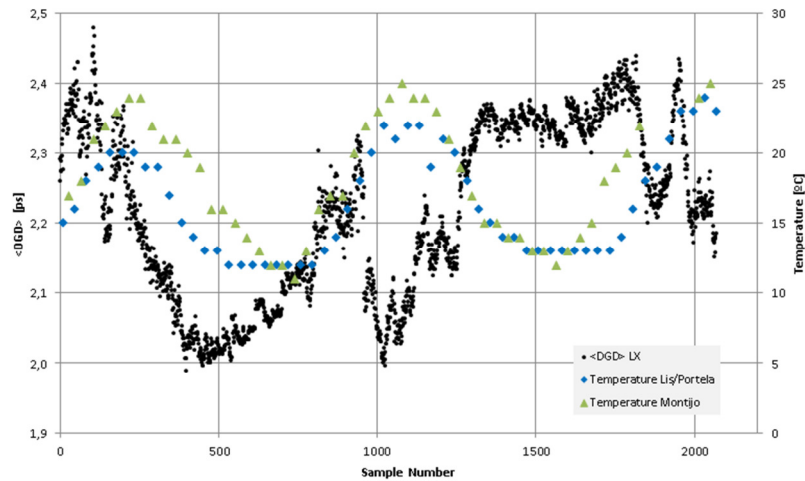


Figure 5-3: PMD delay for LX link and temperature reported by Portela and Montijio weather stations

Figure 5-4 shows the temperature recorded by the weather stations of Montijio (around 30 km at South of Samora Correia) together with mean DGD measured in the SC link.

Finally, temperature recorded by the weather stations of Montijio (around 60 km at North West of Alcácer do Sal) and Beja (around 60 km at South East of Alcácer do Sal) is shown in Figure 5-5 together with ALC PMD results. In the analysis that will follow, the average temperature between the two stations is considered.

A summary visual inspection of these images does not clearly reveal a simple relation between temperature and measurement.

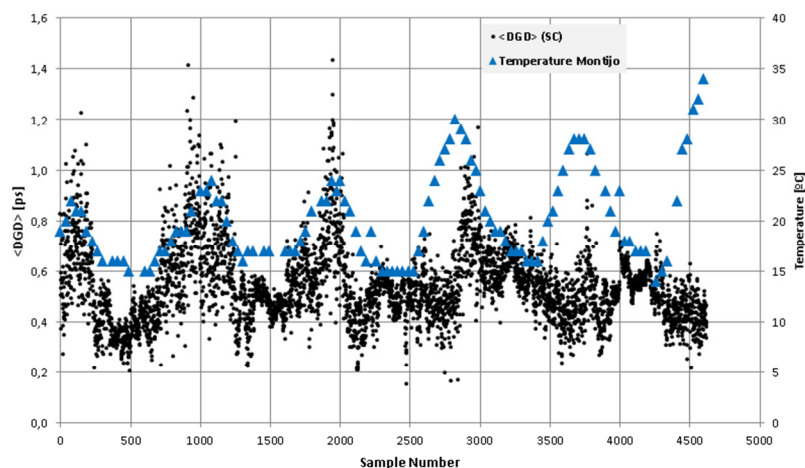


Figure 5-4: PMD delay for SC link and temperature reported by Montijio weather stations

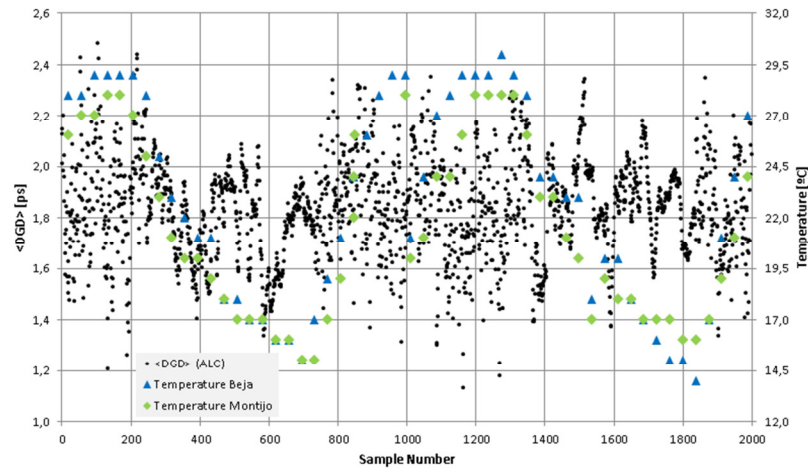


Figure 5-5: PMD delay for ALC link and temperature reported by Beja and Montijio weather stations

Normalized mean DGD in function of temperature is shown in Figure 5-6, Figure 5-7 and 13 for the three links; blue dots represent daylight behavior (considered between 9:00 AM and 7:00 PM) while black dots represent night time (from 7:00 PM to 9:00 AM). Images show clearly that high values of  $\langle \text{DGD} \rangle$  are not necessarily related to high temperatures and are distributed over the whole temperature excursion. Nevertheless, a little higher density of high PMD values seems to occur at higher temperatures and during daylight time. From the images is also clear the dynamic range of the PMD; while for LX link PMD relative variation is roughly  $\pm 10\%$  around mean value, percentage raises to  $\pm 30\%$  for ALC link and reaches high fluctuations in the SC link, exceeding 100% and with few peaks over 150% relative to the mean PMD value.

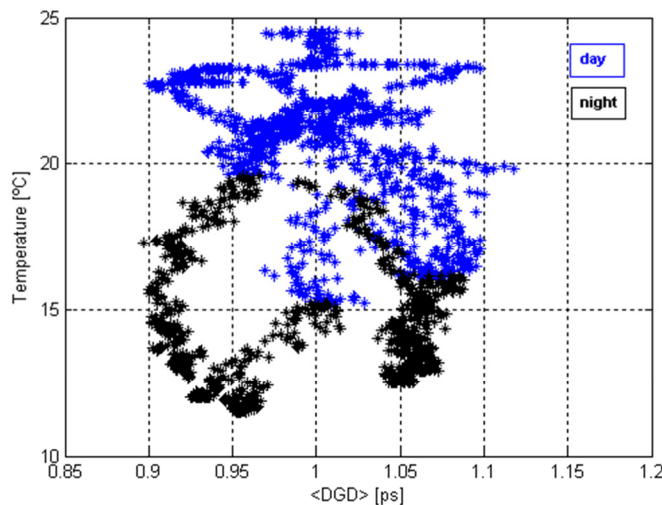


Figure 5-6: Relationship between temperature and normalized PMD for LX link (Day: 9:00 AM to 7:00 PM; Night: 7:00 PM to 9:00 AM)

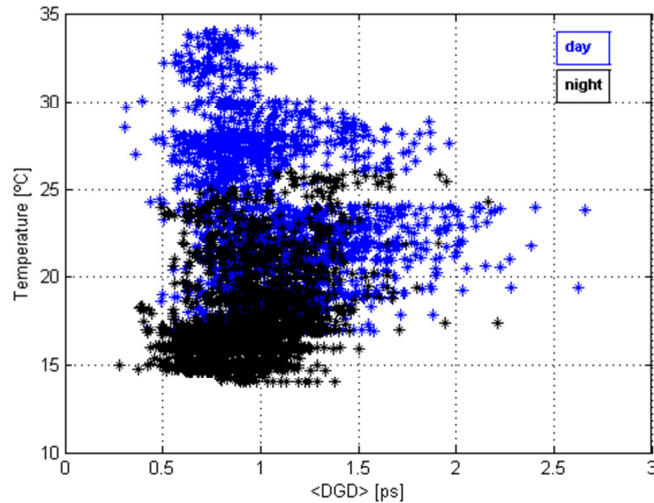


Figure 5-7: Relationship between temperature and normalized PMD for SC link  
(Day: 9:00 AM to 7:00 PM; Night: 7:00 PM to 9:00 AM)

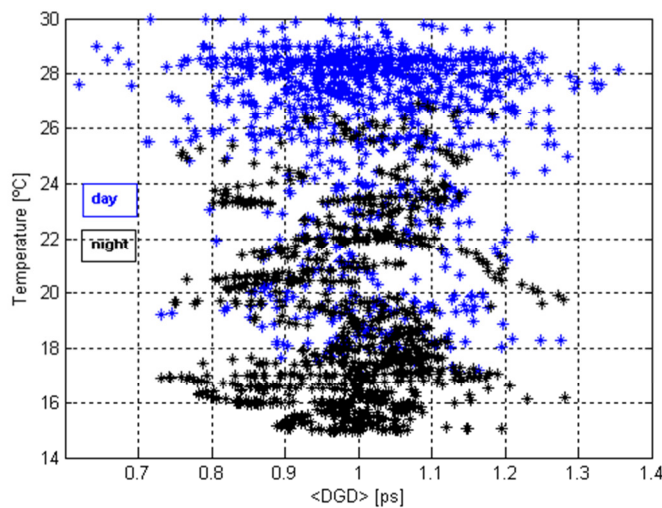


Figure 5-8: Relationship between temperature and normalized PMD for ALC link  
(Day: 9:00 AM to 7:00 PM; Night: 7:00 PM to 9:00 AM)

The daily behavior (roughly 26h 30m of data) of PMD against temperature is shown in Figure 5-9 for the SC link. Not substantial difference in the PMD behavior is appreciable between the different days. The first three days are similar in terms of PMD relative excursion, even if temperature in day 3 differs more than five degrees Celsius, confirming that absolute temperature is not the sole reason of PMD variation. In the last day the relative PMD excursion is lower, but still in the order of  $\pm 50\%$ . The daily behavior for the other two links (not shown) also does not show any noticeable trend. Curiously, the LX daily behavior can be obtained from Figure 5-6, being the first day

pretty much the image slice between 0.9 and 1 ps relative  $\langle \text{DGD} \rangle$ , and the second day being the remaining portion between 1 and 1.1 ps. LX link data was collected during a little more than two days.

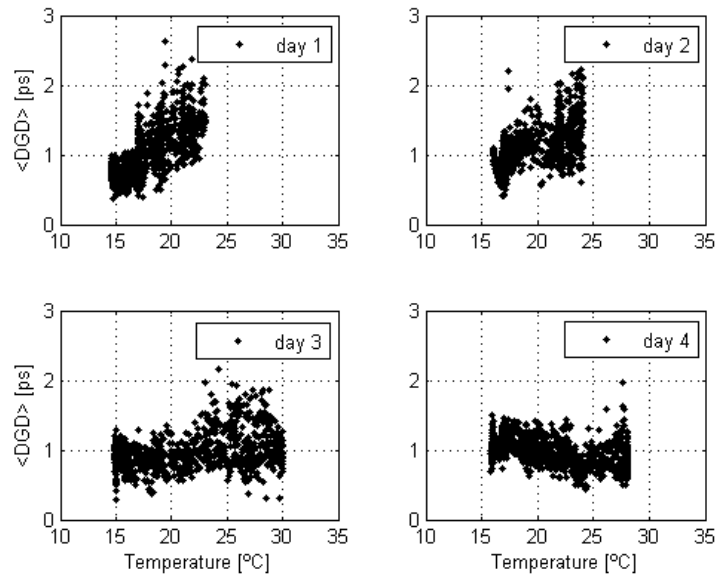


Figure 5-9: Relationship between temperature and PMD for SC link on a day by day basis

Variation of PMD with respect to variation of temperature are shown in figures 5-10 to 5-14; it is perceptible the increase of PMD spread in correspondence of temperature variations. This is clearer in figures 5-12 and 5-13 which show the details of day 2 and 3 of SC link measurements, together with the time of the day.

Results obtained are in agreement with the results obtained from the similar studies previously mentioned.

Larger relative variations of PMD are observed in the two aerial links (SC and ALC); these links, suffer temperature changes in a “more direct” way in comparison to the buried cable (LX), and are also submitted to the mechanical stress provoked on the cable and its support structure by wind conditions. These two concurrently environment conditions might be the reason of the large PMD fluctuations observed. However, the lack of information about wind conditions during the measurements days, does not allow drawing a possible correlation. Anyway, this supposition might also justify the relative stability of the PMD value of the buried link.

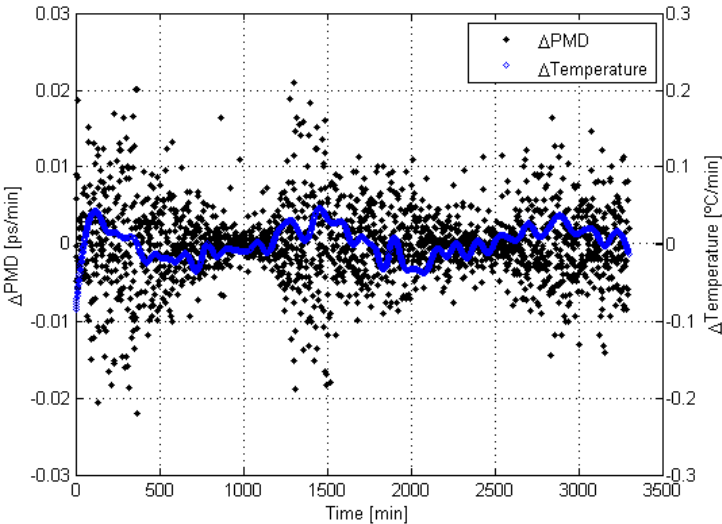


Figure 5-10: Relationship between the variation of PMD and temperature for the LX link

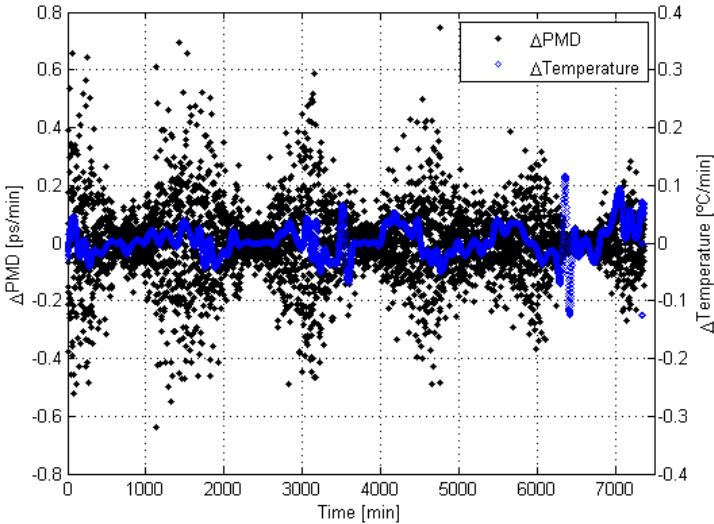


Figure 5-11: Relationship between the variation of PMD and temperature for the SC link

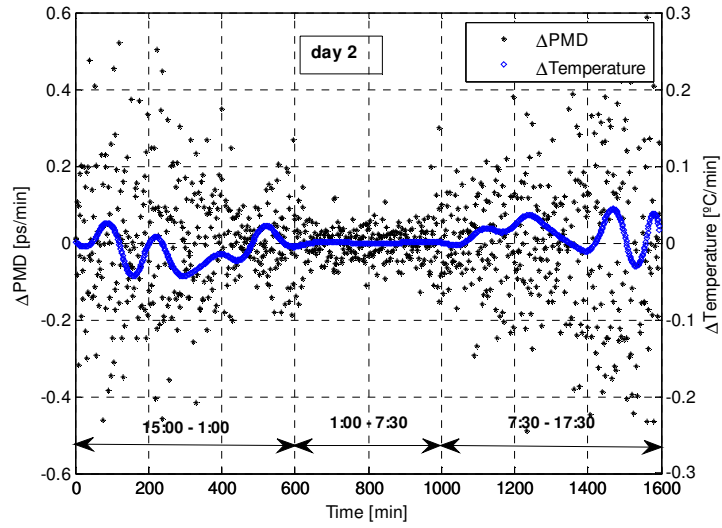


Figure 5-12: Relationship between the variation of PMD and temperature for the SC link; details of day 2

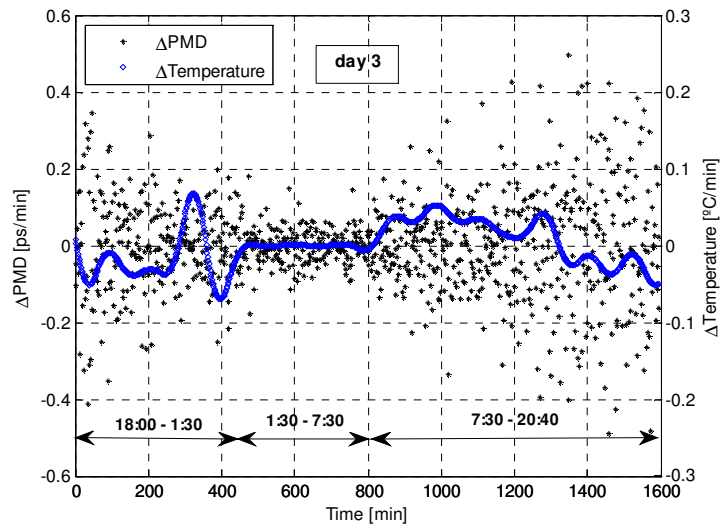


Figure 5-13: Relationship between the variation of PMD and temperature for the SC link; details of day 3

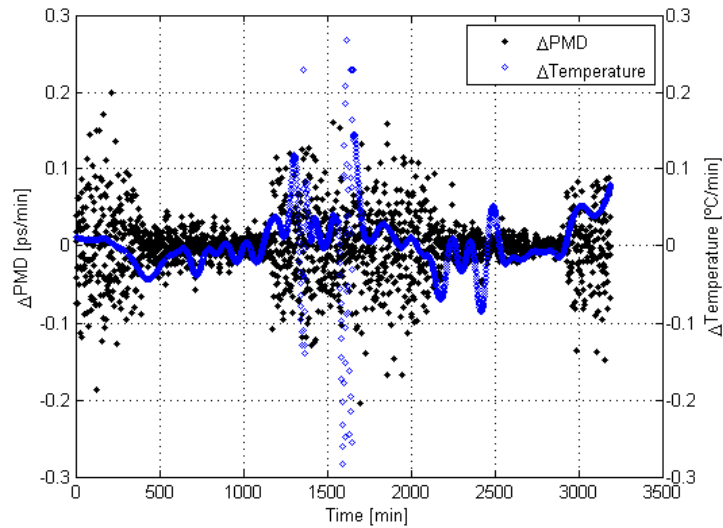


Figure 5-14: Relationship between the variation of PMD and temperature for the ALC link

### 5.3 PMD “hinge” model

The PMD-vector is a random function of the carrier wavelength and might also drift randomly with time; it is therefore a stochastic phenomenon naturally requiring statistical analysis. The most common approach is to use the approximation of first-order PMD, and consider a Maxwellian probability density function (pdf) [26]. Table 5-2 resumes the PMD results for each of the measured links; corresponding histograms are shown in Figure 5-15.

Short name	Length	PMD Delay [ps]	PMD Coeff [ps/km <sup>1/2</sup> ]	CD Delay at 1550 nm
LX	115.35 km	2.218 ps	(0.206 ps/km <sup>1/2</sup> )	718 ps (-6.22 ps/km)
SC	106.00 km	0.539 ps	0.052 ps/km <sup>1/2</sup>	353 ps (-3.33 ps/km)
ALC	155.00 km	1.832 ps	0.147 ps/km <sup>1/2</sup>	464 ps (-2.99 ps/km)

Table 5-2: PMD measurements results resume for the three links

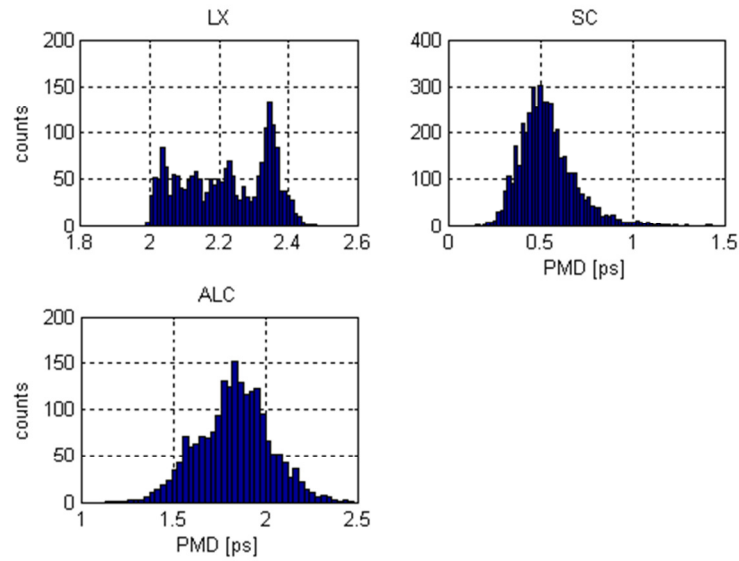


Figure 5-15: Histograms of measured PMD for LX, SC and ALC

Normalized PMD data distributions are shown in figures 5-16 to 5-21 together with corresponding fitted maxwellian and normal distributions. Qualitatively, maxwellian distributions represent a poor fit of the data in disagreement to what predicted by theory ([21]) and obtained in many experimental results (e.g. [27], [37]). A somewhat better result is obtained in the case of SC link; nevertheless data seems better fitted by a normal distribution.

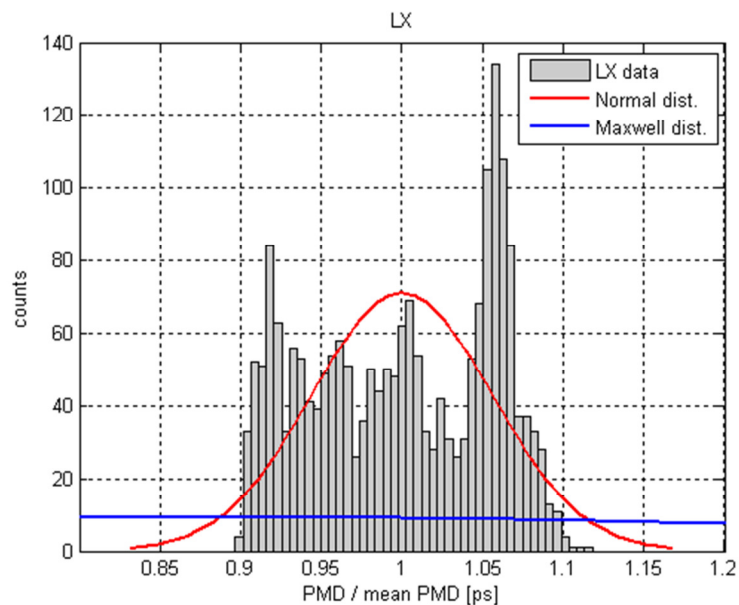


Figure 5-16: LX link normalized PMD histograms together with Maxwell and normal distribution fits (linear scale)



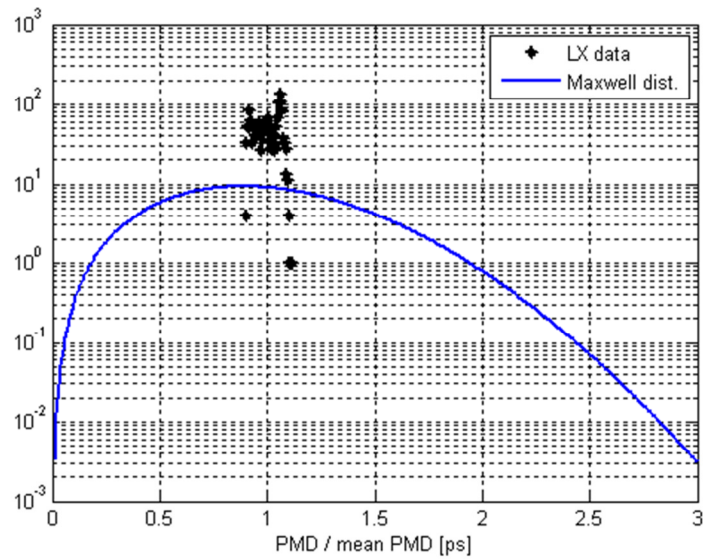


Figure 5-17: LX link normalized PMD histograms and Maxwell distribution fit (logarithmic scale)

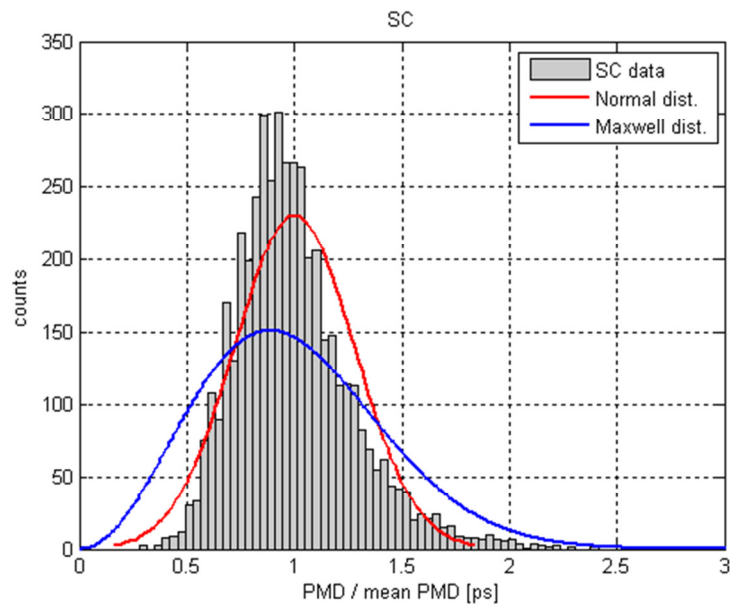


Figure 5-18: SC normalized PMD histograms together with Maxwell and normal distribution fits (linear scale)

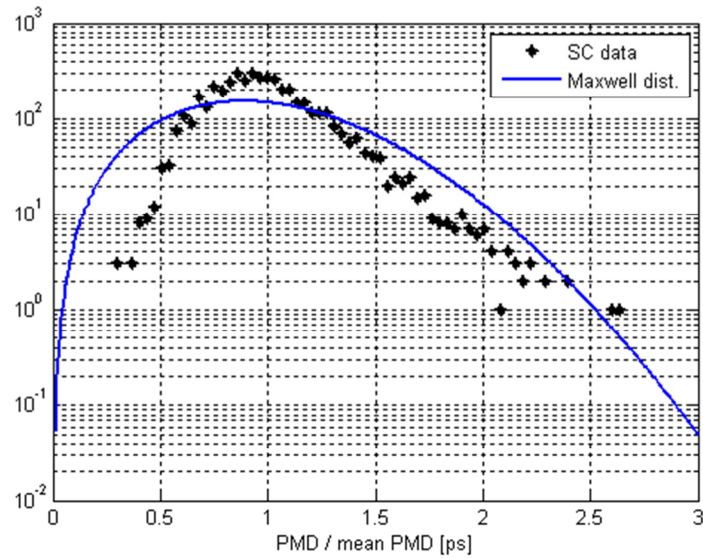


Figure 5-19: SC normalized PMD histograms together with Maxwell distribution fit (logarithmic scale)

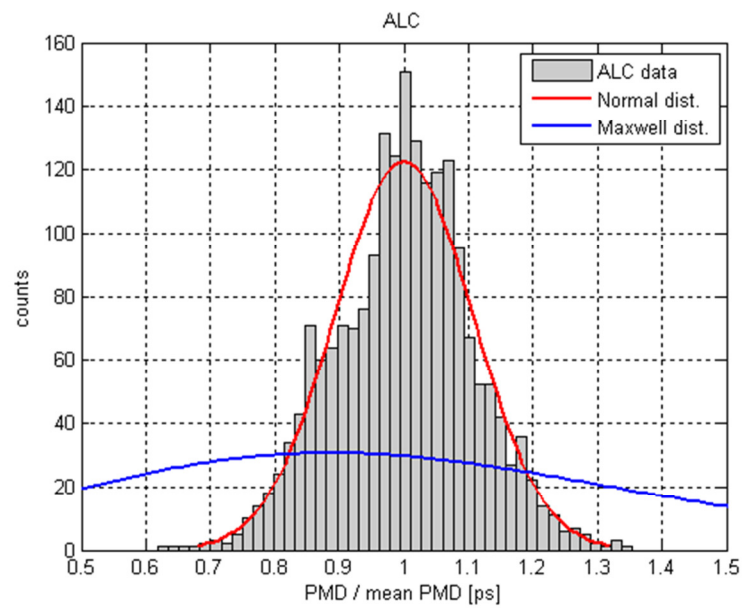


Figure 5-20: ALC normalized PMD histogram together with Maxwell and normal distribution fits (linear scale)

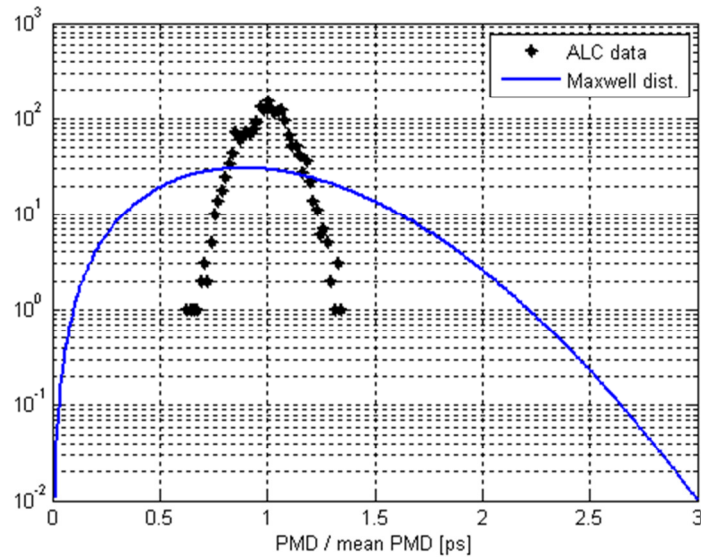


Figure 5-21: ALC normalized PMD histograms together with Maxwell distribution fit (logarithmic scale)

Various experimental reports conclude that behavior of buried links can be assumed constant over large time scales, that range from more than 20 minutes [27] up to months [22]; on the other hand, other studies show that this behavior is often violated [38] and DGD statistics is observed to follow a “truncated” maxwellian distribution [39]. According Karlsson, do exist cases for which the commonly used Maxwellian pdf is only approximate, like in PMD emulators or in systems with components having large deterministic PMD (e.g. isolators, couplers, etc.) [26]; these components have birefringence that is approximatively constant with wavelength and drift time. DGD of such elements is a delta function, centered at the DGD value of the component. According [23], most of the temporal PMD changes that are observed in installed routes arise primarily from a relatively small number of such “hot spots” along the route that are exposed to ambient environment; these hot spots act as random polarization rotators driven by temperature variations and mechanical vibrations [39]. Among these sensitive elements are referred ‘exposed portions of the cable’ and ‘patch cords in the switching offices’ [39], which are all elements present in all the three links that we analyzed.

Karlsson, in [26], provides a pdf for the concatenation of one random section (with PMD  $\tau_{\text{ran}}$ ) and a deterministic element (with PMD  $\tau_{\text{det}}$ ), that reads:

$$P_{(|\tau|)} = P_{Mxw|\tau_{ran}} \exp\left(-\frac{4|\tau_{det}|^2}{\pi|\tau_{ran}|^2}\right) \operatorname{sinhc}\left(\frac{8\tau|\tau_{det}|}{\pi|\tau_{ran}|^2}\right) \quad (5.1)$$

where  $\operatorname{sinch}(x) = \sinh(x)/x$ , and  $P_{Mxw}$  is the Maxwell distribution with average  $|\tau_{ran}|$ . This distribution is of interest in system measurements of the DGD, as it adds one degree of freedom to the Maxwellian distribution and hence improves the agreement with, and interpretation of, measured PMD [37]. In the limit  $|\tau_{det}|=0$ , Eq. (5.1) resumes to the Maxwell distribution; for  $|\tau_{det}| \gg |\tau_{ran}|$  it approaches a Gaussian distribution.

Fit parameters of (5.1) and normal distributions applied to our data are resumed in Table 5-3 (we are considering normalized data). We note that for the LX and ALC case, eq. (5.1) predicts a very large deterministic element; for the SC data the random and deterministic element have an equivalent magnitude.

	Normal dist.		Karlsson dist.	
	$\mu$ [ps]	$\sigma^2$	$ \tau_{ran} $ [ps]	$ \tau_{det} $ [ps]
LX	1	$15.4 \cdot 10^{-3}$	0.13	0.90
SC	1	$22.7 \cdot 10^{-3}$	0.55	0.55
ALC	1	$38.0 \cdot 10^{-3}$	0.17	0.97

Table 5-3: Fitting parameters of Normal and Karlsson distributions for the measured data

The fits of Karlsson distribution to our data resemble a normal distribution, as is evident in Figure 5-23 and Figure 5-24. Nevertheless, for the LX case, Karlsson fit shows a lower peak and poorer tails approximation than the Gaussian shape (Figure 5-22).

We conclude that the parts of the links exposed to the environment act as the main contributors to the PMD temporal variation. These exposed parts are acting as polarization rotators and provoke the variation of the direction of the PMD vector.

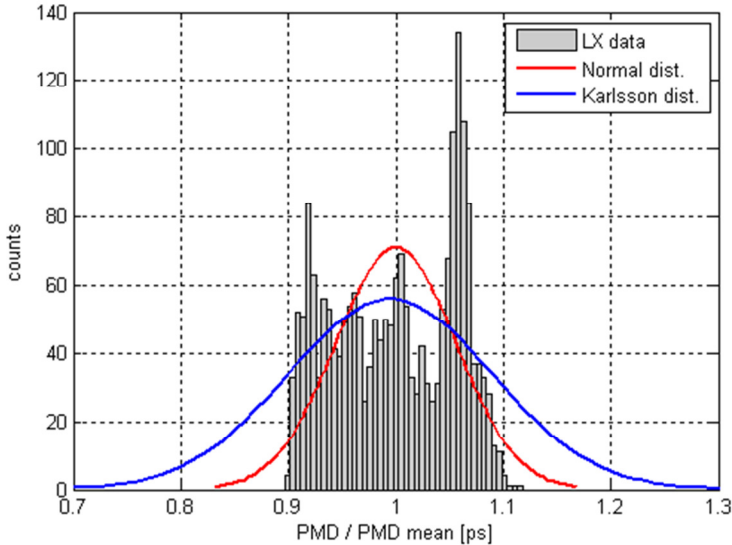


Figure 5-22: LX normalized PMD histogram together with Maxwell and Karlsson distribution fits

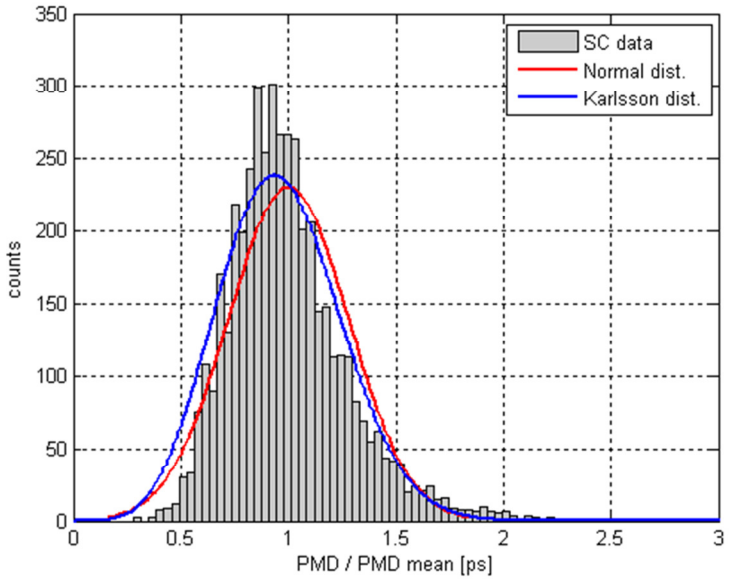


Figure 5-23: SC normalized PMD histogram together with Maxwell and Karlsson distribution fits

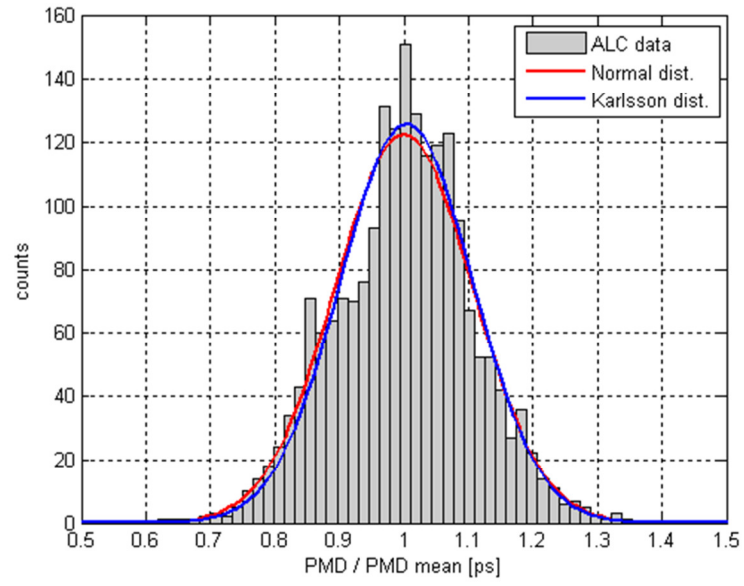


Figure 5-24: ALC normalized PMD histogram together with Maxwell and Karlsson distribution fits

---

## 6 Conclusions

To keep pace with the constant data traffic increase, transmission networks need to be upgraded to higher data rates (e.g. 40/100 Gbps). But there are several issues to consider; what is the impact over existing infrastructure? Is it needed to deploy a new dedicated network? What should be done to the existing fiber plant?

Increasing bit rate turn the transmission intrinsically more sensitive to fiber impairments. One of the main parameters that need to be evaluated is polarization mode dispersion, which can limit the application distance or affect the bit error rate (BER). High PMD is generally associated with old fiber plant, typically deployed before 1999 when fiber manufacturing processes were of lower quality; but also installations subjected to temperature fluctuations or mechanical stress, such as aerial links, may suffer PMD increase and fluctuations. In order to compensate PMD, or estimate the associated outage probability, it is essential to know its statistical characteristics.

Recurring to the fixed analyzer technique we measured the PMD of three optical links, all built with G.652 fiber and with lengths in the order of 100 km; one of the links was mostly laid into conduit, while the other two were constituted largely by an aerial installation.

While the buried link showed a relative PMD stability, the two aerial cables presented large oscillations that we justified by the “more direct” effect of temperature variations and, supposedly, mechanical stress induced by wind.

The PMD values distributions did not show a maxwellian probability distribution; we have justified this behavior recurring to the “hinge” model and viewing the link as constituted by long stationary sections with stable PMD vector, connected by hinges which essentially rotate those larger sections.

The measured attenuation and chromatic dispersion characteristics of the links were found in accordance to the expected.

The work presented in this thesis can be further extended to completely characterize PMD behavior of the links and gain further insight. Experiments on temperature effects over PMD can be performed using a temperature chamber, in order to have control over the environment and accelerate data collection. Also, controlled mechanical stress, in an attempt to emulate aerial cable conditions, might be applied to the tested fiber/cable.

Spectral DGD behavior can be acquired and compared to the obtained PMD, in order to evaluate how different frequencies (channels) are impaired by the polarization dispersion.

The hypothesis of the presence of PMD “hot spots” along the link, and the applicability of the hinge model to our links, might be verified trying to locate such elements; a P-OTDR seems to be the ideal instrument for this experiment.



# Appendix

## A. Equipment list

Function	Vendor / Reference	Description	Main characteristics	Link
Fiber Under Test (FUT)	Corning / ClearCurve XB	Single mode fiber	Enhanced macrobend performance; compliant with ITU-T G.652.D and exceeding G.657.A1	<a href="http://www.corning.com/opticalfiber/products/clearcurve/single_mode_fiber.aspx">http://www.corning.com/opticalfiber/products/clearcurve/single_mode_fiber.aspx</a> <a href="http://www.corning.com/WorkArea/showcontent.aspx?id=41255">http://www.corning.com/WorkArea/showcontent.aspx?id=41255</a>
Laser source	Grandway / FHS2T01	Laser source	Spectral Width: 5nm Central wavelength: 1310, 1490, 1550 nm ( $\pm 20$ nm)	<a href="http://www.grandway.com.cn/UserFiles/download/catalogue/FHS2T01.pdf">www.grandway.com.cn/UserFiles/download/catalogue/FHS2T01.pdf</a>
Power meter	Grandway / FHP3P01	PON Power Meter	Wavelengths: 1310/1490/1550 nm	<a href="http://www.grandway.com.cn/UserFiles/download/catalogue/FHP3P01.pdf">www.grandway.com.cn/UserFiles/download/catalogue/FHP3P01.pdf</a>
OTDR	JDSU / E4136FCO MP-RMP	OTDR module for T-BERD/MTS4000 platform	Wavelengths: 1310/1550/1625 nm;	<a href="http://www.jdsu.com/ProductLiterature/otr20004000-ds-fop-tm-ae.pdf">www.jdsu.com/ProductLiterature/otr20004000-ds-fop-tm-ae.pdf</a>
Multifunction (AP, CD, PMD)	JDSU / E81DISPAP	AP, CD, PMD measurement	-	<a href="http://www.jdsu.com/ProductLiterature/mtsfbodmmodule_ds_fop_tm_ae.pdf">http://www.jdsu.com/ProductLiterature/mtsfbodmmodule_ds_fop_tm_ae.pdf</a>
BB Light Source	JDSU / OBS-550	Broad Band Light Source	1485-1640 nm, polarized or non-polarized, EDF amplified	<a href="http://www.jdsu.com/ProductLiterature/obs-55-500-550_ds_fop_tm_ae.pdf">http://www.jdsu.com/ProductLiterature/obs-55-500-550_ds_fop_tm_ae.pdf</a>

Table A-1: Equipment list

## **B. Fiber types (ITU-T standards)**

The International Telecommunication Union provides a set of standards that classifies single-mode fiber according to their attenuation range, chromatic dispersion values, and polarization mode dispersion coefficients.

The following summary is an excerpt from [40].

### ***Standard Single Mode Fiber (ITU-T G.652)***

*The ITU-T G.652 fiber is also known as standard SMF and is the most commonly deployed fiber. This fiber has a simple step-index structure and is optimized for operation in the 1310 nm band. It has a zero-dispersion wavelength at 1310 nm and can also operate in the 1550 nm band, but it is not optimized for this region. The typical chromatic dispersion at 1550 nm is 17 ps/nm-km. Dispersion compensation must be employed for high bit-rate applications. The attenuation parameter for G.652 fiber is typically 0.2 dB/km at 1550 nm, and the PMD parameter is less than 0.1 ps/√ km. An example of this type of fiber is Corning SMF-28.*

### ***Low Water Peak Non dispersion-Shifted Fiber (ITU-T G.652.C)***

*The legacy ITU-T G.652 standard SMFs are not optimized for WDM applications due to the high attenuation around the water peak region. ITU G.652.C-compliant fibers offer extremely low attenuation around the OH peaks. The G.652.C fiber is optimized for networks where transmission occurs across a broad range of wavelengths from 1285 nm to 1625 nm. Although G.652.C compliant fibers offer excellent capabilities for shorter, unamplified metro and access networks, they do not fully address the needs for 1550 nm transmission. The attenuation parameter for G.652 fiber is typically 0.2 dB/km at 1550 nm, and the PMD parameter is less than 0.1 ps/√ km. An example of this type of fiber is Corning SMF-28e.*

### ***Dispersion-Shifter Fiber (ITU-T G.653)***

*Conventional SMF has a zero-dispersion wavelength that falls near the 1310 nm window band. SMF shows high dispersion values over the range between 1500 nm and 1600 nm (third window band). The trend of shifting the operating transmission wavelength from 1310 nm to 1550 nm initiated the development of a fiber type called dispersion-shifted fiber (DSF). DSF exhibits a zero-dispersion value around the 1550 nm wavelength where the attenuation is minimum. The DSFs are optimized for*

operating in the region between 1500 to 1600 nm. With the introduction of WDM systems, however, channels allocated near 1550 nm in DSF are seriously affected by noise induced as a result of nonlinear effects caused by FWM. This initiated the development of NZDSF. Figure B-1 illustrates the dispersion slope of DSF with respect to SMF and NZDSF. G.653 fiber is rarely deployed any more and has been superseded by G.655.

#### **1550-nm Loss-Minimized Fiber (ITU-T G.654)**

The ITU-T G.654 fiber is optimized for operation in the 1500-nm to 1600-nm region. This fiber has a low loss in the 1550 nm band. Low loss is achieved by using a pure silica core. ITU-T G.654 fibers can handle higher power levels and have a larger core area. These fibers have a high chromatic dispersion at 1550 nm. The ITU G.654 fiber has been designed for extended long-haul undersea applications.

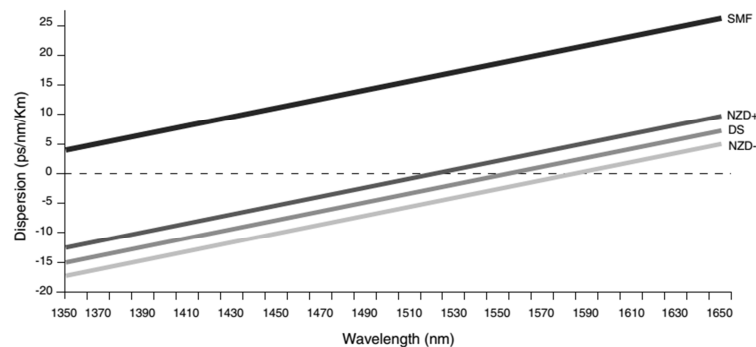


Figure B-1: Dispersion slope for various fiber types

#### **Nonzero Dispersion Shifted Fiber (ITU-T G.655)**

Using nonzero dispersion-shifted fiber (NZDSF) can mitigate nonlinear characteristics. NZDSF fiber overcomes these effects by moving the zero-dispersion wavelength outside the 1550 nm operating window. The practical effect of this is to have a small but finite amount of chromatic dispersion at 1550 nm, which minimizes nonlinear effects, such as FWM, SPM, and XPM, which are seen in the dense wavelength-division multiplexed (DWDM) systems without the need for costly dispersion compensation. There are two fiber families called nonzero dispersion (NZD+ and NZD-), in which the zero-dispersion value falls before and after the 1550 nm wavelength, respectively. The typical chromatic dispersion for G.655 fiber at 1550 nm is 4.5 ps/nm-km. The attenuation parameter for G.655 fiber is typically 0.2 dB/km at

---

*1550 nm, and the PMD parameter is less than 0.1 ps/√ km. The Corning LEAF fiber is an example of an enhanced G.655 fiber with a 32 percent larger effective area. Figure B-1 illustrates the dispersion slope of NZDSF with respect to SMF and DSF.*

## C. Optical communication standards

<b>SDH</b>	<b>SONET</b>	<b>Transmission Rate</b>	<b>Bit Time</b>	<b>PMD Limit</b>
	OC-1	51.84 Mb/s	19.29 ns	2 ns
STM-1	OC-3	155.52 Mb/s	6.43 ns	640 ps
STM-4	OC-12	622.08 Mb/s	1.61 ns	160 ps
	OC-24	1,244.16 Mb/s (1.2 Gbps)	803.76 ps	80 ps
STM-16	OC-48	2,488.32 Mb/s (2.5 Gbps)	401.88 ps	40 ps
STM-64	OC-192	9,953.28 Mb/s (10 Gbps)	100.47 ps	10 ps
STM-256	OC-768	39,318.12 Mb/s (40 Gbps)	25.12 ps	2.5 ps

Table C-6-1: Optical communications standards, corresponding bit rates and PMD limits

## D. PMD link design value

The majority of applications potentially limited by PMD require concatenation of a number of cabled fibers. A simple approach for system design might be to assume that each cabled fiber comprising the link has a PMD coefficient equal to the maximum specified value. This “worst case” assumption has been shown to produce excessively conservative system limitations.

ITU-T G.650.2 and IEC refer two methods for the PMD specification.

“Method 1” establishes an upper bound for the PMD coefficient of the concatenated link known as  $PMD_Q$  or the link design value. The parameters of the  $PMD_Q$  calculation include  $M$ , which represents the number of concatenated cabled fiber sections (considered equal to 20), and  $Q$ , which is equal to 1 minus the cumulative percentile at which the upper bound is located (i.e., 0.01% for the 99.99<sup>th</sup> percentile). Fiber manufacturers typically adopt Method 1 for the link design value specification compliance.

Number of cable sections	Probability Level Q	ITU-T SMF		PMD <sub>Q</sub> [ps/km <sup>-1/2</sup> ]
		Type	Category	
20	1 x 10 <sup>-4</sup> (0.01%)	G.652	A and B	≤ 0.5
			C and D	≤ 0.2
		G.653	A	≤ 0.5
			B	≤ 0.2
		G.654	A and B	≤ 0.5
			C, D and E	≤ 0.2
		G.656		≤ 0.2
		G.657	A	≤ 0.2
			B	n/a

Table D-2: Maximum PMD coefficient values according fiber type (adapted from [41] )

“Method 2” has a complementary approach, providing means of extrapolating the implications for system design.

This method similarly utilizes the averaging which occurs during the concatenation process to generate a large distribution of possible link PMD coefficients. To reflect the random variability in DGD over time, each link PMD coefficient comprising the

distribution is then convolved with a Maxwell distribution to determine the probability of that specific link exceeding a maximum DGD value. This is done for each link PMD coefficient, and the total probability of exceeding the maximum DGD value is normalized by the quantity of link PMD coefficients. This convolution process takes advantage of the fact that the Maxwell distribution is defined by a single parameter, and therefore by knowing the value of that parameter (that is, the PMD coefficient) one can calculate the entire distribution of possible DGD values. The maximum differential group delay ( $DGD_{max}$ ) is the typical parameter used in the design of an optical transmission system. Due to the statistical nature of PMD, a relationship between  $DGD_{max}$  and  $\langle DGD \rangle$  can be established and defined probabilistically as shown in following table.

<b>Ratio <math>DGD_{max}</math> to <math>\langle DGD \rangle</math></b>	<b>Probability of <math>\langle DGD \rangle</math> being over <math>DGD_{max}</math></b>	<b>Time per year of <math>\langle DGD \rangle</math> being over <math>DGD_{max}</math></b>
2.5	$1.5 \times 10^{-3}$	13.1 h
3.0	$4.2 \times 10^{-5}$	22 min
3.1	$2.0 \times 10^{-5}$	10.5 min
3.2	$9.2 \times 10^{-6}$	5 min
3.25	$6.19 \times 10^{-6}$	3.2 min
3.3	$4.1 \times 10^{-6}$	2.15 min
3.4	$1.8 \times 10^{-6}$	56.6 s
3.5	$7.7 \times 10^{-7}$	24 s
3.6	$3.2 \times 10^{-7}$	10.1 s
3.7	$1.3 \times 10^{-7}$	4.1 s
3.75	$8.21 \times 10^{-8}$	2.6 s
3.775	$6.5 \times 10^{-8}$	2.0 s
3.8	$5.1 \times 10^{-8}$	1.6 s
3.9	$2.0 \times 10^{-8}$	0.63 s
4.0	$7.4 \times 10^{-9}$	0.23 s
4.1	$2.7 \times 10^{-9}$	0.09 s
4.2	$9.6 \times 10^{-10}$	0.03 s
4.3	$3.3 \times 10^{-10}$	0.01 s
4.4	$1.1 \times 10^{-10}$	0.0035 s
4.5	$3.7 \times 10^{-11}$	0.0012 s
4.6	$1.2 \times 10^{-11}$	0.00038 s

Table 6-2: Probability associated to the ratio between maximum and mean DGD and corresponding outage probability (adapted from [41])

---

## E. Optical Telecom Windows

<b>Band</b>	<b>Description</b>	<b>Wavelength range</b>
O-band	original	1260–1360 nm
E-band	extended	1360–1460 nm
S-band	short wavelengths	1460–1530 nm
C-band	conventional (“erbium window”)	1530–1565 nm
L-band	long wavelengths	1565–1625 nm
U-band	ultra long wavelengths	1625–1675 nm

Table 6-3: Optical telecom windows



---

## Bibliography

- [1] R.-J. Essiambre, G. Kramer, P. J. Winzer, G. J. Foschini e B. Goebel, "Capacity Limits of Optical Fiber Networks," *Journal of Lightwave Technology*, vol. 28, n.º 4, pp. 662-701, 2010.
- [2] R.-J. Essiambre e R. W. Tkach, "Capacity Trends and Limits of Optical Communication Networks," *Proceedings of the IEEE*, vol. 100, n.º 5, pp. 1035-1055, 2012.
- [3] R.-J. Essiambre, G. J. Foschini, G. Kramer e P. J. Winzer, "Capacity Limits of Information Transport in Fiber-Optic Networks," *Physical Review Letters*, vol. 101, pp. 163901.1-4, 2008.
- [4] B. J. Shastri e D. V. Plant, "Scaling Technologies for Terabit Fiber Optic Transmission Systems," *Proc. of SPIE*, vol. 7942, pp. 794206.1-12, 2011.
- [5] Huawei, "Tata Communications, Huawei and Huawei Marine Complete First 400G Long-Haul Subsea Network Field Trial," 2014. [Online]. Available: [http://huawei.com/ilink/en/about-huawei/newsroom/press-release/HW\\_334743](http://huawei.com/ilink/en/about-huawei/newsroom/press-release/HW_334743). [Acedido em May 2014].
- [6] R. Ramaswami, K. Sivarajan e G. Sasaki, *Optical Networks: A Practical Perspective*, Elsevier Science, 2009.
- [7] F. Mitschke, *Fiber Optics - Physics and Technology*, Springer, 2009.
- [8] K. Okamoto, *Fundamentals of Optical Waveguides*, Elsevier, 2006.
- [9] J. M. Senior, *Optical Fiber Communications*, Prentice Hall, 2009.
- [10] D. Boivin, L.-A. de Montmorillon, L. Provost e P. Sillard, "Coherent Multipath Interference in Bend-Insensitive Fibers," *IEEE Photonics Technology Letters*, vol. 21, n.º 24, pp. 1891-1893, 2009.
- [11] M. Li, D. Tandon, S. Bookbinder, S. Bickham, M. McDermott, R. Desorcie, D. Nolan, J. Johnson, K. Lewis e J. Englebert, "Ultra-Low Bending Loss Single-Mode Fiber for FTTH," *Journal of Lightwave Technology*, vol. 27, n.º 3, pp. 376-382, 2009.
- [12] M.-J. Li e D. A. Nolan, "Optical Transmission Fiber Design Evolution," *Journal of Lightwave Technology*, vol. 26, n.º 9, pp. 1079-1092, 2008.

- 
- [13] Sumitomo Electric, “Application Note - G657 fibres and how to splice them,” 2011.
- [14] F. J. T. L. B. Larry Johnson, “Fiber Optic Connectors – (The bottom line is still performance.),” [Online]. Available: <http://www.lightwaveonline.com/webcasts/2013/03/fiber-optic-connectors.html>. [Acedido em 12 March 2013].
- [15] M. Kihara, “Optical Performance Analysis of Single-Mode Fiber Connections,” em *Optical Fiber Communications and Devices*, InTech, 2012, pp. 239-256.
- [16] D. R. Anderson, L. Johnson e F. G. Bell, *Troubleshooting Optical-Fiber Networks*, Elsevier, 2004.
- [17] ITU-T, G.652 - Characteristics of a single-mode optical fibre and cable, International Telecommunication Union, 2009.
- [18] G. P. Agrawal, *Nonlinear Fiber Optics*, Academic Press, 2007.
- [19] F. Mitschke, *Fiber Optics Physics and technology*, Springer, 2009.
- [20] M. O'Sullivan e R. Hui, *Fiber Optic Measurement techniques*, Elsevier, 2009.
- [21] M. Shtaif e A. Mecozzi, “Modelling of polarization mode dispersion in optical communications systems,” *Journal of Optical and Fiber Communications Reports*, vol. 1, pp. 248-265, 2004.
- [22] M. Brodsky, N. J. Frigo e M. Boroditsky, “Polarization Mode Dispersion of Installed Fibers,” *Journal of Lightwave Technology*, vol. 24, n.º 12, 2006.
- [23] M. MISHA Brodsky, M. Boroditsky, P. Magill e N. J. Frigo, “Physical Mechanism for Polarization Mode Dispersion Temporal Dynamics,” *IEEE LEOS NEWSLETTER*, pp. 4-6, June 2004.
- [24] A. Galtarossa, L. Palmieri, M. Schiano e T. Tambosso, “Measurement of birefringence correlation length in long, single-mode fibers,” *Optics Letters*, vol. 26, n.º 13, pp. 962-964, 2001.
- [25] G. J. Foschini e C. D. Poole, “Statistical Theory of Polarization Dispersion in Single Mode Fibers,” *Journal of Lightwave Technology*, vol. 9, n.º 11, pp. 1439-1456, 1991.

- 
- [26] M. Karlsson, "Probability Density Functions of the Differential Group Delay in Optical Fiber Communication Systems," *Journal of Lightwave Technology*, vol. 19, n.º 3, 2001.
- [27] J. Cameron, L. Chen, X. Bao e J. Stears, "Time Evolution of Polarization Mode Dispersion in Optical Fibers," *IEEE Photonics Technology Letters*, vol. 10, n.º 9, pp. 1265-1267, 1998.
- [28] JDS Uniphase Corporation, "Reference Guide to Fiber Optic Testing," Vol. 1 & Vol. 2, 2010.
- [29] ITU-T, G.650.1 - Definitions and test methods for linear, deterministic attributes of single-mode fibre and cable, International Telecommunication Union, 2010.
- [30] EXFO, "Chromatic Dispersion at High Bit Rates".
- [31] M. Z. Jamaludin, A. F. Abas, A. S. M. Noor e M. K. Abdullah, "Issues on Polarization Mode Dispersion (PMD) for High Speed Fiber Optics Transmission," *Suranaree J. Sci. Technol.*, vol. 12, n.º 2, pp. 98-106, 2005.
- [32] ITU-T, G.650.2 - Definitions and test methods for statistical and non-linear related attributes of single-mode fibre and cable, International Telecommunication Union, 2007.
- [33] ITU-T, Optical fibres, cables and systems, International Telecommunication Union, 2009.
- [34] Anritsu, "WP - Dispersion in Optical Fibers," 2008.
- [35] B. Huttner, B. Gisin e N. Gisin, "Distributed PMD measurement with a Polarisation-OTDR in optical fibers," Group of Applied Physics - University of Geneva, Switzerland, 1999.
- [36] ITU-T, G.695 - Optical interfaces for coarse wavelength division multiplexing applications, International Telecommunication Union, 2010.
- [37] C. De Angelis, A. Galtarossa, G. Gianello, F. Matera e M. Schiano, "Time Evolution of Polarization Mode Dispersion in Long Terrestrial Links," *Journal of Loghtwave Techniology*, vol. 10, n.º 5, pp. 552-555, 1992.

- [38] J. Li, G. Biondini, H. Kogelnik e P. J. Winzer, “Noncompliant Capacity Ratio for Systems With an Arbitrary Number of Polarization Hinges,” *Journal of Lighthwave Technology*, vol. 26, n.° 14, pp. 2110-2117, 2008.
- [39] C. Antonelli e A. Mecozzi, “Theoretical Characterization and System Impact of the Hinge Model of PMD,” *Journal of Lighthwave Technology*, vol. 24, n.° 11, pp. 4064-4074, 2006.
- [40] V. Alwayn, “Optical Network Design and Implementation,” Cisco Press, 2004.
- [41] EXFO, “PMD Issues in Advanced, Very High-Speed Networks”.